Genetically-Encoded Tools for G Protein-Coupled Receptor Ligand Detection

by

Aubrey Putansu

A dissertation submitted in partial fulfillment
of the requirements for the degree of
Doctor of Philosophy
(Chemistry)
in the University of Michigan
2026

Doctoral Committee:

Associate Professor Wenjing Wang, Chair
Professor Ryan Bailey
Professor William Birdsong
Professor Anna Mapp

Aubrey M. Putansu

aputansu@umich.edu

ORCID iD: 0009-0007-4144-3827

© Aubrey M. Putansu 2026

Dedication

This work is dedicated to my family. To the Tahoes, Mom and Mike, I couldn't have done any of this without your support. To my Maine family, Dad and Dawn, I always treasure our time together. To Mae, you will always be my favorite sister and no matter how far apart we are I know we will stay close. To Lulu, Tessie, Kipper, and Willow your emotional support cannot be understated.

Acknowledgements

It takes a village to make a PhD possible, and I am so thankful for my community that I have found during my time at University of Michigan. I have no clue if you're allowed to be this sappy

To my friend of old, fellow survivor of band camp, Ox. Thank you oh great and benevolent dungeon master for inviting me to be a part of your campaign that has now spanned my entire PhD. It has meant a lot to me.

To an even older friend, fellow volunteer librarian, wrangler of plot bunnies, fearless club wheel specialist, Blake. Thank you for always being there for me, you supported me through some huge moments in my life and I will always be so grateful. I swear (on my thesis) we are going to finish Baldur's Gate.

To a new friend, or a new old friend, fellow cat appreciator, fearless club tier list keeper, Erys. I am so happy we could reconnect and have a stronger friendship than ever these past two years. I cannot wait to see where we both will go in the future.

To my lab book club, Ola, Lexie, Isabel, Hannah, and Gwen thank you for always listening to my book critiques and more importantly thanks for sharing so many books with me (whether we'd all finished or not).

To my second D&D group Josh, Liz, and Tyler, I wanted to thank you for inviting me, we have had some great times and many laughs. Also you all always spoil me with great food and accommodating my crazy weekend schedule.

To my third D&D group Ellie, Steven, Ryan, Andrew, and Anna I was hesitant at first only because three simultaneous campaigns is a lot but I have only one regret, and its that I didn't join sooner. Thank you for welcoming me late into your campaign and it has been such a joy getting to know you all.

To my cohort, Daisy, Amelia, and Rachel I appreciate the time we've been able to make during the craziness of PhD life. Our board game nights and outings have been a happy distraction and wonderful venting avenue.

Last but not least to the person most likely to read this who may at this point be thinking, what about me? To my erstwhile roommate, you have been at every major moment within my PhD journey, you helped me join a lab that I loved, you helped me connect with my cohort, you inspired me to get back into reading with a never-ending list of great recommendations. There is no one else I would have liked to sit next to for the last 4 years. I'm really glad I met you Jen. Thank you for helping me achieve my dream of becoming a real scientist.

Table of Contents

Dedication ii

Acknowledgements iii

List of Figures viii

Abstract xvi

Chapter 1 G Protein-Coupled Receptor Signaling and Current Methods for Detecting Related Ligands 1

1.1 G Protein-Coupled Receptor Signaling 2

1.1.1 Pharmacological Significance 3

1.1.2 GPCRs' Role in Neurotransmission 3

1.2 Existing Tools for GPCR Ligand Neurotransmitter Detection 4

1.2.1 Non-genetically Encoded Methods 4

1.2.2 Genetically Encoded Real-Time Sensors 6

1.2.3 Genetically Encoded Integrator Sensors 10

1.3 Need for New Tools 16

1.4 Chapter 1 Bibliography 18

Chapter 2 Chimeric Nanobody Design, Mechanistic Study, and Directed Evolution 23

2.1 Materials and Methods 24

2.1.1 Plasmids and Cloning 24

2.1.2 Supernatant Lentivirus Preparation 24

2.1.3 B2AR-SENSIT HEK293T Library and Frozen Cell Stock Preparation 25

2.1.4 B2AR-SENSIT HEK293T Library Selection via FACS 25

2.1.5 Confocal Microscopy of HEK293T 26
2.1.6 Analysis of HEK293T Cell Images 27
2.1.7 B2AR-SENSIT Initial Testing and Engineering 28
2.1.8 Protease Based Nb39 Mechanistic Studies 28
2.2 Initial B2AR-SENSIT Chimeric Nanobody Design 28
2.2.1 Selecting the Best cpGFP Variant 30
2.3 Mechanistic Interrogation of cpGFP Maturation Inhibition 31
2.4 Mammalian Cell-based chNb80/Nb39 Directed Evolution Efforts and chNb80/Nb39 Variants Rescreening 35
2.4.1 Directed Evolution of cpGFP in SENSIT 38
2.5 Discussion of SENSIT Development and Key Insights into Nb39-cpGFP Interaction 39
2.6 Chapter 2 Bibliography 41
Chapter 3 SENSIT Characterization, Expansion to other GPCRs, and Design of Chimeric MiniG 42
3.1 Materials and Methods 42
3.1.1 B2AR-SENSIT Agonist Exposure Experiment 42
3.1.2 B2AR-SENSIT Maturation Experiment 43
3.1.3 B2AR-SENSIT pH Titration 43
3.1.4 B2AR-SENSIT Dose Response 43
3.1.5 Rat Neuronal Culture 44
3.1.6 Viral Transduction of Neuronal Cultures 44
3.1.7 B1AR- and CHRM2-SENSIT Characterization 44
3.1.8 Concentrated AAV Preparation for Stereotactic Injection 45
3.1.9 B2AR-SENSIT Mouse Testing 45
3.1.10 MiniGs-SENSIT Initial Testing and Engineering 46
3.1.11 Confocal Microscopy of HEK293T and Mouse Brain 47

3.1.12 Confocal Microscopy of Neuron Culture 47
3.1.13 Analysis of HEK293T and Neuron Cell Images..... 48
3.2 Characterization of B2AR-SENSIT1.1..... 49
3.2.1 B2AR-SENSIT Characterization in Rat Neurons and Mouse Brain 51
3.3 Characterization of B1AR-SENSIT..... 52
3.4 Characterization of CHRM2-SENSIT 53
3.5 Design of Chimeric MiniG Protein SENSIT 55
3.6 Discussion of the SENSIT platform 56
3.7 Chapter 3 Bibliography..... 58
Chapter 4 Summary and Future Directions 59
4.1 Summary of Research Results 59
4.2 Novelty and Expected Impact..... 59
4.3 Future Directions 60
4.3.1 Focusing on the GPCR..... 60
4.3.2 Focusing on the cpGFP..... 62
4.3.3 Focusing on the Chimeric Binder 62
4.3.4 Further Elucidating the Nb39 cpGFP Fluorophore Maturation Inhibition Mechanism..... 63
4.3.5 Future Applications..... 64
4.4 Chapter 4 Bibliography..... 65
Appendix 67
Bibliography 76

List of Figures

Figure 1-1: Basics of GPCR signaling. All graphics were created in BioRender. (A) An inactive receptor that has no agonist bound and is not recruiting a G-protein. G-proteins are membrane associated. (B) Upon agonist binding a conformational change allows for G protein binding. The Gα domain will interact with adenylyl cyclase, if it is stimulatory class ($G\alpha_s$) then it will lead to the increase of cAMP concentration. If it is the inhibitory class ($G\alpha_i$) then it will lead to a decrease in cAMP concentration. cAMP can activate PKA which regulates other proteins through phosphorylation. (C) Regulated by GRK a GPCR will be phosphorylated, often in the C-terminal tail region, which recruits the beta-arrestin protein leading to internalization of the receptor. Beta-arrestin binding also serves to block G-protein binding. 3

Figure 1-2: Schematic for the design of real-time sensors that modify a GPCR IL3. All graphics were created in BioRender. Showing the GPCR as a "flat" 7 transmembrane protein, it is easier to identify the third intracellular loop (IL3), and this design will remove the native IL3 residues and insert cpGFP. The conformational change induced by agonist binding will also change the conformation of cpGFP leading to increased fluorescence. 9

Figure 1-3: Schematic for the design of Tango and iTango2 integrator sensors. All graphics were created in BioRender. (A) Schematic of the Tango assay components. The Tango design use the protein-protein interaction of an activated GPCR and beta-arrestin to bring a protease (TEVp) and its cleavage site (TEVcs) in proximity. When the TEVcs is cleaved, it releases a transcription factor (tTA) that will localize to the nucleus and express a reporter gene such as a FP for fluorescent readout. Therefore fluorescence is only possible when the modified GPCR is signaling. (B) Schematic of the iTango2 assay components. To add light gating the TEVp is split into two fragments and the TEVcs is caged by a LOV domain. The LOV domain will only reveal/"uncage" the TEVcs when exposed to blue light. Then the TEVp will only be reconstituted when the GPCR beta-arrestin takes place. Therefore, both agonist stimulation and light stimulation are needed to release the transcription factor (tTA) to the nucleus and see reporter gene expression. 11

Figure 1-4: Original SPOTIT and SPOTall comparison. (A) Schematic of the design of MOR-SPOTIT and B2AR-SPOTall. In SPOTIT the Nb39 inhibits cpGFP fluorophore maturation until agonist recruits it to the active MOR. In SPOTall a second nanobody, Nb80, will sterically block Nb39-cpGFP interaction by being recruited to the active B2AR. (B) Representative fluorescence images of MOR-SPOTIT and B2AR-SPOTall in HEK293T cells. cpGFP, cpGFP fluorescence. Anti-FLAG, immunostaining. (C) Quantification of the experiment in 1-4A comparing MOR-SPOTIT2 and B2AR-SPOTall. All were stimulated with their respective agonists (10 μM fentanyl or isoproterenol) for 24 hours. The numbers above each bracket in black are the SBR between stimulated and unstimulated conditions. The number in blue is the fold-difference between B2AR-SPOTall and MOR-SPOTIT. All

significance was calculated using a two-tailed Welch's t-test. Stars indicate the degree of significance as follows *, P<0.05, **, P<0.01, ***, P<0.001, ****, P<0.0001. Dots on the plot indicate the mean of three technical replicates. n = 3. The thick horizontal bar is the mean of the three technical replicates and the error bars are the SEM. 16

Figure 2-1: Design of the chimeric nanobody-based SENSIT. (A) Schematic of the design of SENSIT. The bifunctional chimeric nanobody inhibits circularly permuted (cpGFP) fluorophore maturation until agonist binding recruits the nanobody to the active GPCR, allowing cpGFP to mature and fluoresce. (B) Crystal structure of nanobody 39 (Nb39) showing how each loop region was defined. PDB: 5C1M. (C) Crystal structure of nanobody 80 (Nb80) bound to B2AR Nb80 loop 3 position highlighted. Numbers on the expanded Nb80 view refer to the positions that were screened for replacement. PDB: 3P0G (D) Quantification of the original testing of each Nb39 loop at Nb80 position 3 in comparison to previous generation integrators mu opioid receptor (MOR)-SPOTIT and B2AR-SPOTall. All were stimulated with their respective agonists (10 µM fentanyl or isoproterenol) for 24 hours. The numbers above each bracket are the SBR between stimulated and unstimulated conditions. All significance was calculated using a two-tailed Welch's t-test. Stars indicate the degree of significance as follows *, P<0.05, **, P<0.01, ***, P<0.001, ****, P<0.0001. Dots on the plot indicate the mean of three technical replicates. n = 3. The thick horizontal bar is the mean of the three technical replicates and the error bars are the SEM. 29

Figure 2-2: Finding the best Nb80 positions to replace and the best cpGFP variant for SENSIT. (A) Quantification of an experiment replacing each Nb80 position listed in (S1A) with Nb39 loop 8 to determine the optimal insertion position. MOR-SPOTIT was stimulated with 10 µM fentanyl for 24 hours and B2AR-SPOTall and all chimeric nanobody SENSIT were stimulated with 10 µM isoproterenol for 24 hours. (B) Quantification of the MOR-SPOTIT1 with a truncated cpGFP, MOR-SPOTIT2 with an improved YNSH-cpGFP, B2AR-SPOTall with the original truncated cpGFP and B2AR-SENSIT with and without the YNSH cpGFP variant. For (A) and (B): The numbers above each bracket are the SBR between stimulated and unstimulated conditions. All significance was calculated using an unpaired two-tailed Welch's t-test. Stars indicate the degree of significance as follows *, P<0.05, **, P<0.01, ***, P<0.001, ****, P<0.0001. Dots on the plot indicate the mean of three technical replicates. n = 3. The thick horizontal bar is the mean of the three technical replicates and the error bars are the SEM. 30

Figure 2-3: Loop deletion study. (A) Schematic of the experimental design for testing Nb39 with loop deletions of 4 core residues from each loop region. (B) Defining which residues from each Nb39 were deleted in the loop deletion experiment Figure 2-3C. Red corresponds to deleted residues. (C) Loop core residue deletion study, showing fluorescence imaging quantification of the experiment described in the Figure 2-3A. All significance was calculated using a two-tailed Welch's t-test. Stars indicate the degree of significance as follows *, P<0.05, **, P<0.01, ***, P<0.001, ****, P<0.0001. Dots on the plot indicate the mean of three technical replicates. n = 3. The thick horizontal bar is the mean of the three technical replicates and the error bars are the SEM. 31

Figure 2-4: Probing the amino acid sequence of the chimeric nanobody compared to wtNb80 sequence. (A) Probing the amino acid sequence effect of the grafted Nb39 loop 7 in

chimeric Nb80/Nb39 and wtNb80 position 3 residues. Fluorescence imaging quantification. B2AR-SENSIT chimeric nanobody mutants were stimulated with 10 µM isoproterenol for 24 hours. The numbers above each bracket are the SBR between stimulated and unstimulated conditions. All significance was calculated using a two-tailed Welch's t-test. Stars indicate the degree of significance as follows *, P<0.05, **, P<0.01, ***, P<0.001, ****, P<0.0001. Dots on the plot indicate the mean of three technical replicates. n = 3. The thick horizontal bar is the mean of the three technical replicates and the error bars are the SEM. (B) Nb39 and Nb80 sequence alignment where Nb39 loops are highlighted in yellow and Nb80 loops are highlighted in gray. Labels identify each Nb39 loop and Nb80 position. The red box highlights the Nb80 point mutation from Figure 2-4A. 32

Figure 2-5: Determining if Nb39 loop sequences can function as peptides. (A) Schematic of the experimental design for testing if Nb39 loops as peptides alone can still inhibit cpGFP. (B) Fluorescence imaging quantification of the experiment described in the Figure 2-5A. All significance was calculated using a two-tailed Welch's t-test. Stars indicate the degree of significance as follows *, P<0.05, **, P<0.01, ***, P<0.001, ****, P<0.0001. Dots on the plot indicate the mean of three technical replicates. n = 3. The thick horizontal bar is the mean of the three technical replicates and the error bars are the SEM. 33

Figure 2-6: Directed evolution of the chimeric Nb80/Nb39 portion of B2AR-SENSIT. (A) Schematic for the evolution platform in HEK293T cells infected with lentivirus containing the B2AR-SENSIT library DNA (SENSIT*). FACS selection parameters are for high cpGFP from B2AR-SENSIT, and high mCherry, the expression marker. (B) Schematic for the library design with targeted mutations of the chimeric Nb80/Nb39 loop that binds to B2AR. Eight residues of the chimeric nanobody binding loop were targeted for site-saturated mutagenesis generating a library with single point mutations possible at each position. PDB: 5C1M. (C) FACS selection schematics for sorting strategy 1. Includes a round 1 with 24-hour drug stimulation sorting followed by a round 2 with 5-minute drug stimulation sorting. Representative gating mechanism is shown. (D) Quantification of the chimeric Nb80/Nb39 single mutants identified through directed evolution compared to the starting point B2AR-SENSIT1.0. The numbers above each bracket are the SBR between stimulated and unstimulated conditions. All significance was calculated using an unpaired two-tailed Student's t test. Stars indicate the degree of significance as follows *, P<0.05, **, P<0.01, ***, P<0.001, ****, P<0.0001. Dots on the plot indicate the mean of three technical replicates. n = 3. The thick horizontal bar is the mean of the three technical replicates and the error bars are the SEM. 35

Figure 2-7: Identifying the best chimeric nanobody for the final B2AR-SENSIT1.1. (A) Fluorescence imaging quantification of Nb80 position 2 replacement with each of the eight Nb39 loops. All were stimulated with their respective agonists (10 µM fentanyl or isoproterenol) for 24 hours. (B) Table summarizing the SBRs for the best chimeric Nb80/Nb39 along with MOR-SPOTIT2 and B2AR-SPOTall with 1-hour and 24-hour stimulation. Stimulation is same as described in (A). (C) Fluorescence imaging quantification of SENSIT variants using the P2L8 nanobody and its mutants, E106G, E106S and E106S/Y107R. For (A) and (C): All significance was calculated using a two-tailed Welch's t-test. Stars indicate the degree of significance as follows *, P<0.05, **, P<0.01, ***, P<0.001, ****, P<0.0001. The numbers above each bracket are the SBR between stimulated and unstimulated conditions.

Dots on the plot indicate the mean of three technical replicates. n = 3. The thick horizontal bar is the mean of the three technical replicates and the error bars are the SEM. 37

Figure 2-8: Directed evolution of the SENSIT cpGFP. (A) Schematic for the library design strategy behind cpGFP evolution. Using the cpGFP including the YNSH residues (shown in blue, yellow, orange, and pink respectively), the circled YNS residue positions were randomized for site-saturated mutagenesis. Model cpGFP is an Alphafold 3 predicted structure. (B) Representative flow cytometry plots from FACS where the upper right quadrant represents the population of interest. The number above this quadrant is the percent of the total cell population present within that quadrant. (C) Table summarizing next generation sequencing results for the cpGFP directed evolution. Column 1 is the identified amino acid sequence mutation compared to the unmutated YNSH-cpGFP. Column 2 is the fold change for number of times this sequence appears compared to the most common unmutated sequence. (D) Quantification of the comparison of new cpGFP mutants to B2AR-SENSIT1.1, as well as the B2AR-SENSIT1.0 (chimeric Nb80/Nb39 P3L7) with YNSH and B2AR-SENIST1.1 (chimeric Nb80/Nb39 P2L8 with E106S/Y107R) with YNSH. The numbers above each bracket are the SBR between stimulated and unstimulated conditions. All significance was calculated using a two-tailed Welch's t-test. Stars indicate the degree of significance as follows *, P<0.05, **, P<0.01, ***, P<0.001, ****, P<0.0001. Dots on the plot indicate the mean of three technical replicates. n = 3. The thick horizontal bar is the mean of the three technical replicates and the error bars are the SEM. 39

Figure 3-1: Characterization of B2AR-SENSIT1.1. (A) Schematic describing position 2 of Nb80 and sequence of Nb39 loop 8. The final chimeric nanobody in B2AR-SENSIT1.1 also includes the E106S/Y107R mutations in Nb80 position 4. PDB: 5C1M. (B) Representative fluorescence images of B2AR-SENSIT1.1 in HEK293T cells. Scale bar, 20 µm. Cells were stimulated with 10 µM isoproterenol. Twenty-four hours after stimulation, cells were fixed, immunostained, and imaged at pH 11. cpGFP, cpGFP fluorescence. Anti-GFP, protein expression level from immunostaining. mCherry, protein expression level. DAPI is a nuclear stain. (C) Selectivity characterization of B2AR-SENSIT1.1. The numbers above each bracket are the SBR between stimulated and unstimulated conditions. (D) Dose response characterization. EC_{50} displayed with the 95% confidence interval. (E) Temporal kinetic study of B2AR-SENSIT1.1. "s", seconds, "m", minutes, "h", hours. The numbers above each bracket are the SBRs between stimulated and unstimulated conditions. (F) Fluorophore maturation time characterization of B2AR-SENSIT1.1. After a variable stimulation time (0, 1, 3, 6, 8 and 24 hours), cells were immediately fixed and stored until imaged. For (C-F): All significance was calculated using a two-tailed Welch's t-test. Stars indicate the degree of significance as follows *, P<0.05, **, P<0.01, ***, P<0.001, ****, P<0.0001. Dots on the plot indicate the mean of three technical replicates. n = 3. The thick horizontal bar is the mean of the three technical replicates and the error bars are the SEM. (G) pKa determination for B2AR-SENSIT1.1. pKa is displayed with a 95% confidence interval. To monitor the same fluorophores over various pH ranges, we imaged one field of view at pH 6, 7, 8, 8.5, 9. 10 and 11. Dots on the plot indicate the mean of three replicates. n = 3..... 50

Figure 3-2: Application of B2AR-SENSIT1.1 *in vivo.* (A) Representative fluorescence images of B2AR-SENSIT1.1 in the rat neuronal culture cells. Scale bar indicates 100 µm. Cells were stimulated with 1 µM isoproterenol. Twenty-four hours after stimulation, cells were

fixed, and imaged at pH 11. GFP, cpGFP fluorescence. mCherry, protein expression level. (B) Quantification of B2AR-SENSIT1.1 rat neuronal culture experiment. The concentrated AAV used to infect the neurons was either undiluted (1x) or diluted by half (0.5x) or one quarter (0.25x). The numbers above each bracket are the SBR between stimulated and unstimulated conditions. All significance was calculated using a two-tailed Welch's t-test. Stars indicate the degree of significance as follows *, P<0.05, **, P<0.01, ***, P<0.001, ****, P<0.0001. Dots on the plot indicate the mean of three technical replicates. n = 3. The thick horizontal bar is the mean of the three technical replicates and the error bars are the SEM. (C) Fluorescence images of B2AR-SENSIT1.1 in mouse brain slices. Scale bar indicates 500 µm. GFP, cpGFP fluorescence. mCherry, protein expression level. Local stereotactic injection to the LHA administer either 10 mM epinephrine or saline blank. Mice were sacrificed twenty-four hours after stimulation. (D) Quantification of B2AR-SENSIT1.1 in mouse brain. The number above the bracket is the SBR between the stimulated and unstimulated condition. Each dot on the plot indicates the normalized GFP signal at a single region of interest in an expressing brain slice area. All significance was calculated using a two-tailed Welch's t-test. Stars indicate the degree of significance as follows *, P<0.05, **, P<0.01, ***, P<0.001, ****, P<0.0001. The thick horizontal bar is the mean and the error bars are the SEM. 51

Figure 3-3: Characterization of B1AR-SENSIT. (A) Schematic showing the design of B1AR-SENSIT. (B) Selectivity of B1AR-SENSIT. The numbers above each bracket are the SBRs between stimulated and unstimulated conditions. (C) Temporal kinetics study of B1AR-SENSIT. Drug was washed away after a variable incubation time, and then allowed to incubate for 24 hours before fixation. "s", seconds, "m", minutes, "h", hours. The numbers above each bracket are the SBRs between stimulated and unstimulated conditions. (D) Dose response characterization for B1AR-SENSIT. EC_{50} displayed with the 95% confidence interval. (E) Representative fluorescence images of B1AR-SENSIT in HEK293T cells. Scale bar, 20 µm. Cells were stimulated with 10 µM isoproterenol. Twenty-four hours after stimulation, cells were fixed and imaged at pH 11. GFP, cpGFP fluorescence. mCherry, protein expression level from ribosomal skip sequence P2A followed by mCherry. For (B-D): All significance was calculated using a two-tailed Welch's t-test. Stars indicate the degree of significance as follows *, P<0.05, **, P<0.01, ***, P<0.001, ****, P<0.0001. Dots on the plot indicate the mean of three technical replicates. n = 3. The thick horizontal bar is the mean of the three technical replicates and the error bars are the SEM. 53

Figure 3-4: Characterization of CHRM2-SENSIT. (A) Schematic displaying the design of Nb9-8 highlighting each loop region as well as the best site (loop 3) that was replaced with Nb39 loop 8. PDB: 4MQS. (B) Quantification of the Nb9-8 each loop replacement with Nb39 loop 8 ("L" = loop). MOR-SPOTIT was stimulated with 10 µM fentanyl for 24 hours and CHRM2-SPOTall and all chimeric nanobody SENSIT were stimulated with 10 µM iperoxo for 24 hours. (C) Representative fluorescence images of CHRM2-SENSIT in HEK293T cells. Scale bar, 20 µm. Cells were stimulated with 50 µM iperoxo. Twenty-four hours after stimulation, cells were fixed and imaged at pH 11. GFP, cpGFP fluorescence. mCherry, protein expression level from ribosomal skip sequence P2A followed by mCherry. (D) Temporal kinetics study of CHRM2-SENSIT. Drug was washed away after a variable incubation time and then allowed to incubate for 24 hours before fixation. "s", seconds, "m", minutes, "h", hours. The numbers above each bracket are the SBRs between stimulated and unstimulated conditions. (E) Fluorescence images for (D) characterizing temporal kinetics of CHRM2-

SENSIT stimulation. Each time point indicates how long drug was present before being washed away. (F) Dose response curve of iperoxo with CHRM2-SENSIT. EC_{50} displayed with the 95% confidence interval. For (B) (D) and (F): All significance was calculated using a two-tailed Welch's t-test. Stars indicate the degree of significance as follows *, P<0.05, **, P<0.01, ***, P<0.001, ****, P<0.0001. Dots on the plot indicate the mean of three technical replicates. n = 3. The thick horizontal bar is the mean of the three technical replicates and the error bars are the SEM..... 54

Figure 3-5: Design of the chimeric miniG protein B2AR-SENSIT2.0. (A) Schematic for the design strategy of miniGs based B2AR-SENSIT2.0. Three positions on miniG (A, B or C) were replaced with either Nb39 loop2 or Nb39 loop 8. PDB : 5G53. (B) Quantification of miniGs position (A, B, or C) replacement with Nb39 loop 2 or 8 in comparison to B2AR-SENSIT1.1. All sensors were stimulated with 10 µM isoproterenol for 24 hours. All significance was calculated using a two-tailed Welch's t-test. Stars indicate the degree of significance as follows *, P<0.05, **, P<0.01, ***, P<0.001, ****, P<0.0001. Dots on the plot indicate the mean of three technical replicates. n = 3. The thick horizontal bar is the mean of the three technical replicates and the error bars are the SEM. (C) Representative fluorescence images of B2AR-SENSIT2.0 from experiment described in prior figure panel (3-5B) in HEK293T cells. Scale bar, 60 µm. Cells were stimulated with 10 µM isoproterenol. Twenty-four hours after stimulation, cells were fixed, immunostained and imaged at pH 11. GFP, cpGFP fluorescence. Anti-GFP, protein expression level from immunostaining. 56

Appendix Figure A-1: Defining the amino acids of the Nb80 positions and Nb39 loops. (A) Amino acid sequence of wtNb80 used in B2AR-SPOTall and basis of design of the chimeric nanobody. Listed positions and amino acids that were replaced with Nb39 loops. (B) Amino acid sequence of wtNb39 used in MOR-SPOTIT and basis of design of the chimeric nanobody. Listed amino acid sequences for loop 1 through 8. 67

Appendix Figure A-2: Further information on the directed evolution of B2AR-SENSIT chimeric Nb80/39. (A) Gating strategy for the Strategy 1 second round of sorting. Strategy 1 involved an initial round of sorting where cells were stimulated with 10 µM isoproterenol for 24 hours then sorted. The second round of sorting using the cells from the first round were stimulated with 10 µM isoproterenol for 5 minutes then drug was washed away and cells were incubated for 24 hours before sorting. Numbers within the gate correspond to percent of total cell population present within the gate. (B) Gating strategy for the Strategy 2 sorting that was only one round. Cells were stimulated with 10 µM isoproterenol for 5 minutes then drug was washed away and cells were incubated for 24 hours before sorting. Numbers within the gate correspond to percent of total cell population present within the gate. (C) Tables summarizing next generation sequencing results for the top 10 reads from sorting Strategy 1 and 2. The first column is the percent of total reads corresponding to that base pair sequence. The second column is the amino acid sequence arising from the base pair sequence. Red corresponds to an amino acid mutation from the Nb80 position 4 sequence..... 68

Appendix Figure A-3: Images from experiments found in Figure 2-7 selecting the best chimeric nanobody. (A) Representative fluorescence images of all Nb39 loops replacing Nb80 position 2, from experiment found in Figure 2-7A. (B) Representative fluorescence images of selecting the best chimeric Nb80/Nb39 considering position 2 and 3, from

experiment found in Figure 2-7B. For (A) and (B) : 24 hours after stimulation, cells were fixed, immunostained, and imaged at pH 11. GFP, cpGFP fluorescence. Anti-GFP, protein expression level from immunostaining. Scale bar, 60 µm. 69

Appendix Figure A-4: Images from experiments found in Figure 3-1 characterizing B2AR-SENSIT1.1. (A) Fluorescence images for Figure 3C characterizing B2AR-SENSIT1.1 selectivity. Cells were stimulated with 10 µM of each indicated agonist. (B) Fluorescence images for Figure 3D characterizing B2AR-SENSIT1.1 sensitivity to epinephrine. Cells were stimulated with indicated concentration of epinephrine. (C) Fluorescence images for Figure 3D characterizing B2AR-SENSIT1.1 sensitivity to norepinephrine. Scale is same as images in (B). Cells were stimulated with indicated concentration of norepinephrine (D) Fluorescence images for Figure 3D characterizing B2AR-SENSIT1.1 sensitivity to isoproterenol. Scale is same as images in (B). Cells were stimulated with indicated concentration of norepinephrine. For (A-D): 24 hours after stimulation, cells were fixed and imaged at pH 11. GFP, cpGFP fluorescence. mCherry, protein expression level from ribosomal skip sequence P2A followed by mCherry. Scale bar, 60 µm. 70

Appendix Figure A-5: Images from experiments found in Figure 3-1 characterizing B2AR-SENSIT1.1 Continued. (A) Fluorescence images for Figure 4E characterizing temporal kinetics of B2AR-SENSIT1.1 stimulation. Each time point indicates how long drug was present before being washed away. Cells were fixed 24 hours after stimulation and imaged at pH 11. (B) Fluorescence images for Figure 4F characterizing fluorophore maturation time of B2AR-SENSIT1.1. All samples were stimulated at the same time, but the time point refers to when the sample was fixed. All were imaged at pH 11. For (A and B): GFP, cpGFP fluorescence. mCherry, protein expression level from ribosomal skip sequence P2A followed by mCherry. Scale bar, 60 µm. (C) Quantification of an experiment to show how fixation impacts fluorophore maturation. One condition was imaged twice, immediately after fixation at 8 hours and again 24 hours later and compared to a condition that was fixed and imaged after 24 hours. The numbers above each bracket are the SBR between stimulated and unstimulated conditions. All significance was calculated using a two-tailed Welch's t-test. Stars indicate the degree of significance as follows *, P<0.05, **, P<0.01, ***, P<0.001, ****, P<0.0001. Dots on the plot indicate the mean of three technical replicates. n = 3. The thick horizontal bar is the mean of the three technical replicates and the error bars are the SEM. 71

Appendix Figure A-6: B2AR-SENSIT1.1 pKa characterization images and mCherry fluorescence. (A) Fluorescence images for Figure 4G characterizing B2AR-SENSIT1.1 cpGFP pKa. Cells were fixed 24 hours after stimulation, and imaged at varying pH. GFP, cpGFP fluorescence. mCherry, protein expression level from ribosomal skip sequence P2A followed by mCherry. Scale bar, 60 µm. (B) Fluorescence of B2AR-SENSIT1.1 mCherry. To monitor the same fluorophores over various pH ranges, we imaged one field of view at pH 6, 7, 8, 8.5, 9. 10 and 11. Dots on the plot indicate the mean of three replicates. n = 3, and the error bars are the SEM. 72

Appendix Figure A-7: Images from Figure 3-3 characterizing B1AR-SENSIT. (A) Fluorescence images for Figure 5B characterizing B1AR-SENSIT selectivity. Each time point indicates how long drug was present before being washed away. (B) Fluorescence images for Figure 5D characterizing B1AR-SENSIT sensitivity to norepinephrine. For (A) and (B): 24

hours after stimulation, cells were fixed and imaged at pH 11. GFP, cpGFP fluorescence. mCherry, protein expression level from ribosomal skip sequence P2A followed by mCherry. Scale bar, 60 µm. 73

Appendix Figure A-8: Expanded characterization of CHRM2-SENSIT. (A) Fluorescence images for Figure S10F characterizing CHRM2-SENSIT sensitivity to iperoxo. 24 hours after stimulation, cells were fixed and imaged at pH 11. GFP, cpGFP fluorescence. mCherry, protein expression level from ribosomal skip sequence P2A followed by mCherry. Scale bar, 60 µm. (B) Selectivity characterization of CHRM2-SENSIT. The numbers above each bracket are the SBRs between stimulated and unstimulated conditions. (C) Acetylcholine dose response characterization for CHRM2-SENSIT. EC_{50} displayed with the 95% confidence interval. For (B) and (C): All significance was calculated using a two-tailed Welch's t-test. Stars indicate the degree of significance as follows *, P<0.05, **, P<0.01, ***, P<0.001, ****, P<0.0001. Dots on the plot indicate the mean of three technical replicates. n = 3. The thick horizontal bar is the mean of the three technical replicates and the error bars are the SEM. 74

Appendix Figure A-9: Annotated amino acid sequences for B2AR-, B1AR-, and CHRM2-SENSIT. (A) Key for color annotation on amino acid sequences. (B) B2AR-SENSIT1.1 amino acid sequence. (C) B1AR-SENSIT amino acid sequence. (D) CHRM2-SENSIT amino acid sequence. 75

Abstract

Studying neurotransmitter localization at cellular resolution at large brain volumes still remains challenging with the current available genetically encoded tools. Integrator sensors based on G protein-coupled receptors (GPCRs) offer one genetically encoded design approach to address this limitation. Based on the SPOTIT motif this thesis will focus on the development of Single-chain Expressing Neurotransmitter Sensing Integrator Tool (SENSIT). This required the development of conformation specific GPCR binders that also could inhibit circularly permuted GFP (cpGFP) fluorophore maturation.

I achieved this by grafting loop regions from nanobody 39 (Nb39) into other nanobody or protein scaffolds, calling these chimeric nanobodies or chimeric GPCR binders. Based on the beta-2 adrenergic receptor (B2AR)-based SENSIT design, I studied the Nb39 loop regions to determine what portion of the amino acid sequence was most vital for cpGFP fluorophore maturation inhibition. Then I performed mammalian cell directed evolution of the chimeric nanobody to improve the original B2AR-SENSIT design. With the evolved nanobody for B2AR-SENSIT, I characterized sensors for epinephrine with B2AR-SENSIT and norepinephrine with beta-1 adrenergic receptor (B1AR)-SENSIT. To test the generalizability of the SENSIT design, I next engineered a chimeric nanobody based on a conformation specific nanbobody, Nb9-8, for the muscarinic acetylcholine receptor M2 (CHRM2) to develop an acetylcholine sensor CHRM2-SENSIT. Finally, I further demonstrated the generalizability of the SENSIT strategy by creating a chimeric miniGs to design B2AR-SENSIT2.0.

Overall, this thesis outlines a new generalizable integrator sensor design strategy that will allow for the development of sensors for diverse neurotransmitters. In addition, this work establishes a mammalian cell-based directed evolution platform to improve SENSIT and analogous sensors. With further optimization of the fluorophore maturation time, SENSIT offers the potential for studying and mapping complex neural circuits across large brain volumes and in deep tissue.

Chapter 1 G Protein-Coupled Receptor Signaling and Current Methods for Detecting Related Ligands

Multicellular organisms require chemical means for cells to communicate with other cells and regulate individual internal processes in response to their environment. This regulation is often achieved by cellular receptor proteins that transduce an extracellular chemical signal into an internal response. The largest family of receptor proteins are known as G protein-coupled receptors (GPCRs), which generally bind a ligand, causing a conformational change and allowing a G protein to bind.[1] Then, the G protein carries out varying downstream signaling effects. Due to their prevalence and importance in the body, GPCRs constitute a large percent of drug targets.[2] Therefore, understanding GPCR signaling is critical for unraveling the effects in physiological processes and successfully targeting related disease states.

Many approaches have been applied to studying GPCR ligands, signaling, and activity. Pharmacological approaches add a drug to a system and study its effect, but this method lacks specificity to understand which cell types, and further which receptors, were perturbed. Other traditional physiological or electrochemical approaches such as microdialysis or cyclic voltammetry can help identify ligands that are present, and even fluctuations in concentration, but cannot link ligand presence back to a particular cell or GPCR.[3] In response to the limitations of these approaches, researchers developed genetically encoded tools which offer much desired cellular specificity and cellular resolution when paired with powerful imaging techniques.[3] These methods can provide detail about how, when or where an endogenous ligand or potential drug affects a particular GPCR.

This introduction will encompass the function of GPCRs, their relevance, traditional methods for GPCR ligand detection, and finally the design of GPCR-based genetically encoded tools. Many genetically encoded tools have been developed and applied extensively, so this introduction chooses to focus on representative examples that demonstrate current protein engineering principles for designing tools to study GPCR ligands.

1.1 G Protein-Coupled Receptor Signaling

GPCRs are seven-transmembrane domain receptors with an extracellular ligand binding pocket and an intracellular G-protein binding pocket. GPCR signaling starts when a ligand, also known as an agonist, binds and induces a conformational change (Figure 1-1A and 1-1B). This active state conformational change reveals a binding pocket for the heterotrimeric G protein complex, composed of an α, β, and γ subunit each of which can uniquely contribute to signaling.[4] In the classical GPCR signaling pathway the Gα subunit of the stimulatory or inhibitory family ($G\alpha_s$ or $G\alpha_i$ respectively) interact with adenyl cyclase which converts ATP to a second messenger molecule known as cyclic AMP (cAMP).[5] The second messenger cAMP then activates protein kinase A (PKA) which regulates other proteins through phosphorylation.[6] This process, from agonist binding down to final effects of the signaling, is also known as a signaling cascade due to the amplification inherent in taking one ligand and producing many second messengers which then can each activate/deactivate many proteins within the cell.

Additionally, there are two other major Gα subunit families, $G\alpha_{q/11}$ and $G\alpha_{12/13}$, which have unique signaling pathways relying on other second messengers or protein interactions. $G\alpha_q$/11 signaling activates phospholipase-Cβ that produces diacylglycerol and inositol 1,4,5-trisphospate (IP_3).[7] Second messenger IP_3 stimulates local Ca^{2+} release that together with diacylglycerol activates protein kinase C-alpha (PKC-a).[8] Dissimilarly, $G\alpha_{12/13}$ activates a GTPase RhoA which regulates downstream kinases.[9] It is also worth mentioning that the Gβ and Gγ subunits are involved in their own signaling pathways that lead to different downstream effects.[10]

GPCR signaling is regulated through GPCR kinases (GRKs) that phosphorylate intracellular loops or the C-terminal tail of the GPCR.[11] GRK activity may lead to the recruitment of β-arrestins that sterically block G-protein binding or lead to receptor internalization (Figure 1-1C).[12] This process is known as desensitization, as the available population of receptors on the cell membrane is depleted reducing the signaling effect. Desensitization makes a cell "less sensitive" toward a GPCR ligand as there are less GPCRs available to bind and activate a signaling cascade. Many of the tools I will discuss in this work rely on these basic signaling properties of GPCRs.

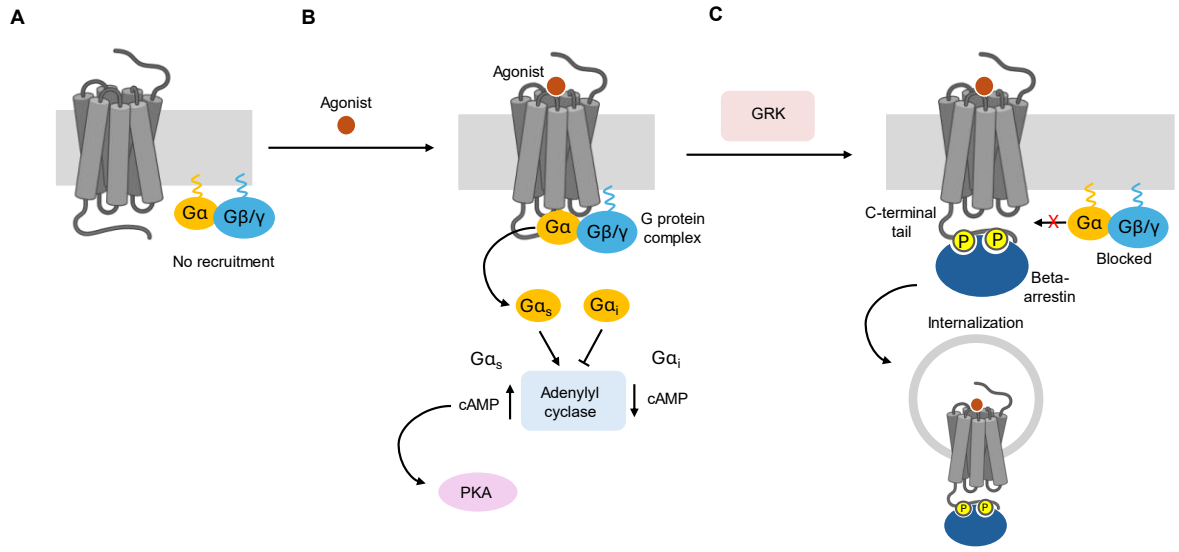


Figure 1-1: Basics of GPCR signaling. All graphics were created in BioRender. (A) An inactive receptor that has no agonist bound and is not recruiting a G-protein. G-proteins are membrane associated. (B) Upon agonist binding a conformational change allows for G protein binding. The Gα domain will interact with adenylyl cyclase, if it is stimulatory class ($G\alpha_s$) then it will lead to the increase of cAMP concentration. If it is the inhibitory class ($G\alpha_i$) then it will lead to a decrease in cAMP concentration. cAMP can activate PKA which regulates other proteins through phosphorylation. (C) Regulated by GRK a GPCR will be phosphorylated, often in the C-terminal tail region, which recruits the beta-arrestin protein leading to internalization of the receptor. Beta-arrestin binding also serves to block G-protein binding.

1.1.1 Pharmacological Significance

GPCRs are the largest membrane receptor family in the human genome and consequently control a vast array of processes in the body. Therefore, modulating GPCR signaling has massive potential for therapeutic benefits.[13] Currently, GPCRs are the most frequently targeted protein family for approved drugs.[2] Some of the most extensively studied GPCRs, the beta-adrenergic receptor family, are targets for many common medications such as albuterol for asthma, and beta-blockers (beta-adrenergic receptor partial agonists or antagonists) such as carvedilol and propranolol to treat high blood pressure and many heart-related conditions.[5, 14, 15]

1.1.2 GPCRs' Role in Neurotransmission

GPCRs are expressed nearly ubiquitously in the body, including in the brain.[16] In the brain, nerve cells communicate to each other at a cellular junction known as a synapse.[17] Chemicals released into the synapse must travel from the pre-synaptic neuron to interact with a receptor protein on the post-synaptic neuron, and such chemicals are known as

neurotransmitters.[17] A more specific type of neurotransmitter is a neuromodulator, which can be released at a synapse, but may diffuse to further targets and may use less direct signaling to modulate neurotransmission.[18] Some neurochemicals fall under both definitions, but neurotransmitter is a broader term. Many neurotransmitters interact with GPCRs in the synapse, therefore understanding neurotransmission requires an understanding of which neurotransmitters may interact with a GPCR and what resulting activity occurs within the neuron. Many of the genetically encoded tools I will discuss have been applied to neuroscience research efforts. Indeed, the final application of my work aims to help elucidate the localization of various neurotransmitters, primarily adrenergic receptor agonists epinephrine and norepinephrine (also known as adrenaline and noradrenaline).

Epinephrine is a neurotransmitter released from the brainstem, as well as a neurohormone (a neurochemical that acts on distant peripheral targets) produced at the adrenal medulla.[19] Norepinephrine is a common neurotransmitter produced primarily in the locus coeruleus that diffuses broadly and can interact with both neuronal and glial cells.[20] Norepinephrine also serves as a neurohormone produced at the adrenal medulla, with recent efforts to elucidate its role in neurodegenerative disease.[21] Both epinephrine and norepinephrine are part of the "stress axis" and chronic or long-term elevated stress levels have been linked to a variety of illnesses such as cardiovascular disease, immune dysregulation, cancer, and psychiatric disorders.[22-25]

1.2 Existing Tools for GPCR Ligand Neurotransmitter Detection

Though GPCR ligand detection tools are not limited to studying neurotransmitters, I will focus on this application as it is a major focus for my own work. This section will cover some of the traditional detection methods and highlight why genetically encoded tools were developed as alternative and complementary methods. Then, I will discuss protein engineering efforts towards two classes of genetically encoded fluorescent GPCR ligand detection tools, separated by their readout, being either transient "real-time" sensors or permanent marking "integrator" sensors. This introduction will not be fully inclusive of each of these existing methods, as the goal is to focus on methodologies widely employed in the field. Further, in order to increase relevance, I will highlight examples relevant to epinephrine and norepinephrine where possible.

1.2.1 Non-genetically Encoded Methods

Non-genetically encoded methods are extremely established within neuroscience research and there is a vast body of work that has iterated on these methodologies. Here, I will focus on some of the most broadly applied for in vivo neurotransmitter detection: microdialysis and fast-scan cyclic voltammetry (FSCV). Method development for neurotransmitter detection often focuses on the need for spatial resolution, referring to how accurately the method can pinpoint the area of localization, and temporal resolution, or how accurately the method can determine when that neurotransmitter was present, particularly in relation to a neuronal signaling event or behavior. Therefore, I will discuss the advantages and disadvantages of microdialysis and FSCV in relation to their spatial and temporal resolution, as well as molecular specificity, sensitivity, and in vivo applicability.

1.2.1.1 Microdialysis

Microdialysis mimics the natural activity of capillaries by using a semipermeable membrane across which neurotransmitters can selectively diffuse. Once the dialysate is collected, it can be paired with liquid chromatography or mass spectrometry for simultaneous sampling of many soluble chemicals with highly sensitive and specific identification.[26, 27] Microdialysis is not limited to studying endogenous molecules and has even been applied for delivery of compounds.[28] This technique remains widely applied for studying neurotransmitters in vivo because of the modularity, where any neurotransmitter may be detected determined by region of probe insertion and the sample analysis method.[29-32] This gives researchers a wealth and breadth of information about many neurochemical interactions when compared to highly specific sensors such as will be described in the following sections.

This method remains limited by its low spatial and temporal resolution. The microdialysis probe samples a local tissue environment and lacks cellular resolution, and the sampling time to collect enough dialysate for further analysis is on the scale of minutes. Lastly, the procedure for installing the probe is quite invasive, since the probes are often large, and probe insertion can compromise the affected area.[33]

1.2.1.2 Fast-Scan Cyclic Voltammetry

Voltammetry is a technique that can measure electrically active chemicals by detecting their oxidation and reduction at a fixed voltage, and cyclic voltammetry applies linearly cycled potential. FSCV boasts the ability to rapidly oxidize and reduce electroactive chemicals at the

electrode providing it with sub-second temporal resolution.[34] Comparatively, FSCV probes are smaller and therefore less invasive than microdialysis probes.[35] With the ability to monitor neurotransmitter dynamics in vivo while also distinguishing between the neurotransmitters present, FSCV remains a key technique for studying neurotransmission.[36-38]

Being reliant on a probe FSCV still suffers from lack of cellular or subcellular resolution. In addition, it cannot easily distinguish between structurally similar chemicals that have similar redox potentials, such as dopamine and norepinephrine, and the method cannot be expanded to many important neurotransmitters that are not electroactive, such as acetylcholine.[39]

1.2.2 Genetically Encoded Real-Time Sensors

Genetically encoded sensors offer many advantages to address needs left by non-genetically encoded methods. First, they offer cellular or subcellular spatial resolution and through tailored delivery methods and the use of promoters can target specific cell types. Second, they can be expressed for days or months which increases the options for experimental design. Third, by taking advantage of the natural biochemical toolkit protein engineers can create highly specific sensors for particular neurotransmitters or neuromodulators of interest. This section discusses real-time sensors, which provide high temporal resolution by directly reporting on signaling dynamics.

1.2.2.1 Fluorescence Resonance Energy Transfer Sensors

Fluorescence (also known as Förster) Resonance Energy Transfer (FRET) is a distance-dependent process by which an excited donor molecule transfers energy to an acceptor group leading to fluorescence emission. FRET partners can be any two chromophores that have a sufficient overlap between the donor emission and acceptor absorption, and the need for proximity allows for the design of sensors that will only fluoresce when the chromophores are brought into proximity, which can be induced through protein-protein interactions or conformational changes within the protein.

One such FRET design used the parathyroid hormone receptor (PTHR) as well as alpha-2A adrenergic receptor (α_{2A}AR) and modified them by adding a CFP to the intracellular loop 3 (IL3) and a yellow FP (YFP) at the C-terminus. The best FRET sensors generated were referred to as PTHR-cam and α_{2A}AR-cam, and both reported a decrease in FRET signal upon agonist binding, proposed to be due to the movement of IL3 away from the C-terminus. In the same

study, to determine the order of β-arrestin2 binding compared to agonist binding, they also generated a PTHR-CFP C-terminal and a β-arrestin2-YFP.[40]

To study the conformational change of the beta-2 adrenergic receptor (B2AR), one group introduced a tetracysteine motif (CCXXCC) into the IL3 of B2AR as well as cyan fluorescent protein (CFP) to the B2AR C-terminus. A membrane-permeable biarsenical fluorophore called FlAsH (fluorescein with As(III) substituents on the 4'- and 5'- positions) was then added to cell culture and interacted with the tetracysteine motif, setting up a FRET donor-acceptor pair related to the conformational change undergone by IL3 when B2AR binds an agonist.[41]

FRET sensors are highly modular, as moving the position of the acceptor-donor pair gives spatial information about the molecular interactions taking place either within a GPCR or between the GPCR and its binding partners, such as β-arrestin. These sensors also have high spatial and temporal resolution and can report on the kinetics of agonist induced conformational change. However, the norepinephrine sensors discussed above lack in vivo characterization or struggle in vivo due to low signal-to-noise ratio (SNR) and narrow dynamic range, meaning there is only a small difference between the agonist-bound signal and the no agonist-bound signal.

1.2.2.2 Cell-based Neurotransmitter Fluorescent Engineered Reporters

To distinguish between dopamine and norepinephrine during neuronal signaling, the cell-based neurotransmitter fluorescent engineered reporters (CNiFERs) were developed.[42] In this system, a HEK293 cell stably expresses a GPCR of interest and a genetically encoded FRET-based Ca^{2+} indicator called TN-XXL. For the sensor to function, the GPCR of interest must bind to G_q proteins, as a downstream consequence of that signaling is calcium release. To detect dopamine, the D2 dopaminergic receptor (D2DR) was selected, alongside a chimeric G_{qi5}. This chimeric G protein has a $G\alpha_q$ sequence with the five C-terminal residues changed to $G\alpha_i$, allowing D2DR coupling. To detect norepinephrine, the α_{1A} adrenergic receptor (α_{1A}AR) was selected as it already binds G_q proteins.

The D2-CNiFER and α_{1A}-CNiFER were characterized in vivo by injecting the cells into the substantia nigra (SN) and locus coeruleus (LC) and then stimulating the regions with implanted electrodes. Reporting high sensitivity and temporal resolution, CNiFERs were applied to behavioral studies in mice to simultaneously track dopamine and norepinephrine, where they also developed a murine receptor-based acetylcholine CNiFER (M1-CNiFER).[42, 43] However,

because CNiFERs are part of an exogenous cell line, they can only report on volume transmission, when the neurotransmitter diffuses into the extracellular space losing spatial resolution. Additionally, the in vivo procedures are quite invasive, requiring CNiFER injection as the system relies on stably expressing cell lines to incorporate all components.

1.2.2.3 Bioluminescence Resonance Energy Transfer and Split Protein NanoLuc Sensors

Some sensors rely on bioluminescence as opposed to fluorescence, and luciferases are enzymes that provide bioluminescence. Bioluminescence offers the advantage of needing no light excitation making it less invasive and often have excellent SNR because of the extremely low to completely negligible background.[44] An engineered deep sea shrimp luciferase named NanoLuc was introduced to GRK3 as an energy donor to the fluorescence acceptor Venus (a YFP) added to the $G\beta_1\gamma_2$ complex leading to bioluminescence resonance energy transfer (BRET).[45, 46] This system was deemed NanoBRET, and can study downstream GPCR signaling rather than direct ligand binding or localization. Downstream effects are reliant on ligand binding. NanoBRET was applied to study muscarinic acetylcholine receptors, noting biased G protein signaling differences between acetylcholine and two strong synthetic agonists.

In a different study, NanoLuc was modified to make the split protein NanoLuc Binary Technology (NanoBiT).[47] In this system NanoLuc is split into two components with low affinity for each other, large BiT (LgBiT) and small BiT (SmBiT), and requires induced proximity to reconstitute NanoLuc. To track agonist binding, the SmBiT was added to the C-terminus of various GPCRs and LgBiT was attached to various Gα proteins, so bioluminescence only occurs when the GPCR becomes activated by an agonist. This assay has been reported for use in high-throughput screening, where it could distinguish between full and partial agonism, identify biased agonists, and de-orphanize uncharacterized GPCRs.

These highly sensitive assays were designed primarily for in vitro work, but they have high spatial resolution afforded by being genetically encoded. Additionally, they are highly modular for many GPCRs. In the case of split NanoLuc the native GPCR structure is only minorly perturbed as SmBiT is a short peptide sequence. The temporal resolution is controlled by NanoLuc enzyme turnover, mainly consumption of exogenously added substrate that will run out before the enzyme is degraded. NanoBRET reports millisecond resolution, but split NanoLuc does not initially characterize sensor kinetics. Applying these systems in vivo requires NanoLuc

substrate addition where bioluminescence readout has lower spatial resolution but deeper tissue penetration.

1.2.2.4 GPCR Conformational Change Paired to Circularly Permuted GFP Sensors

One class of real-time sensors modifies IL3 of a GPCR introducing a circularly permuted GFP (cpGFP) so that agonist binding induces conformational changes in the GPCR, resulting in a change in the chromophore environment of cpGFP (Figure 1-2). This directly pairs agonist binding to the level of fluorescence hence these sensors report on the increase of fluorescence upon agonist binding denoted as $\Delta F/F_{max}$ (F=fluorescence).

The first example is dLight1, named for its ability to detect dopamine. In the same paper, the general design strategy was expanded to the beta-2 (B2AR), beta-1 (B1AR), and alpha-2 adrenergic receptors (A2AR) for norepinephrine, the mu (MOR) and kappa opioid receptors (KOR) for opioid peptides, 5-hydroxytryptamine receptor-2A (5HT2A) for serotonin, and melatonin type-2 receptor (MT2) for melatonin.[48] This demonstrates the generalizability of the design strategy due to the conserved conformational change position among GPCRs. Pairing dLight1 with red-shifted calcium indicators allowed for linking dopamine release dynamics with neuronal activity. The same IL3 replacement strategy was also applied for the GPCR activation-based (GRAB) sensors. Following the design of $GRAB_{DA}$ for dopamine detection, the $GRAB_{NE}$ for norepinephrine detection was also reported.[49] Light and GRAB sensors have both reported detecting optogenetically stimulated neurotransmitter concentrations as well as endogenous release concentrations.

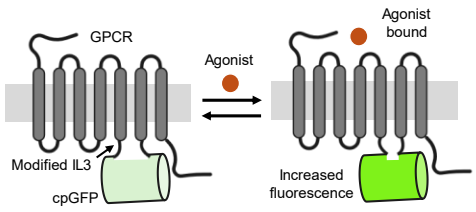


Figure 1-2: Schematic for the design of real-time sensors that modify a GPCR IL3. All graphics were created in BioRender. Showing the GPCR as a "flat" 7 transmembrane protein, it is easier to identify the third intracellular loop (IL3), and this design will remove the native IL3 residues and insert cpGFP. The conformational change induced by agonist binding will also change the conformation of cpGFP leading to increased fluorescence.

The Light and GRAB sensors have been heavily characterized in vivo where they report rapid kinetics capable of reporting on highly specific neurotransmitter dynamics at cellular resolution. One of the major limitations remains the huge engineering effort required for each sensor, and consequently each neurotransmitter. Although the design is generalizable, not every

receptor immediately creates an applicable sensor. Additionally, monitoring the sensor dynamics still requires the installation of an imaging probe, which is both invasive and limits the area of imaging to a very targeted region determined by the probe.

1.2.3 Genetically Encoded Integrator Sensors

Though real-time sensors provide high temporal resolution and can report on GPCR system dynamics, additional information can be gained by sensors capable of permanently labeling a cell. Such a permanent label could be explained as "integrating signal over time", hence the term integrator sensors. Being genetically encoded, they offer many of the same advantages outlined in the prior section 1.2.2., such as high spatial resolution, cell-type specificity, as well as specificity and sensitivity encoded by the modified GPCRs. This section will discuss relevant integrator sensors applied for studying GPCR ligand interaction.

1.2.3.1 Tango and iTango Assays

The Tango assay is named for "dance" between two protein interaction partners, such as the GPCR and arrestin.[50] The Tango system has three main components. First is the modified GPCR with a C-terminal tobacco etch virus cleavage site (TEVcs) and transcriptional activator tTA (tetracycline-controlled transcriptional activator TetR-VP16). Second is a β-arrestin2 protein linked to the TEV protease (TEVp) which will recognize and cleave the TEVcs when brought into proximity to the GPCR C-terminus by β-arrestin2. Third the reporter gene gives the assay its readout, when the tTA is released by TEVcs cleavage it will localize to the nucleus and interact with a tTA dependent gene for expression of a luciferase (Figure 1-3A). Though the initial design started with the arginine vasopressin receptor 2 (AVPR2) it was expanded to over 89 GPCRs including D2DR and KOR, which normally have weak arrestin recruitment but were further modified with AVPR2 C-terminal tail residues, as well as the adrenergic receptor family such as α_{2A}AR, B1AR, and B2AR. The design modularity also allowed for Tango assays for receptor tyrosine kinases and steroid hormone receptors, relying on unique protein-protein interactions.

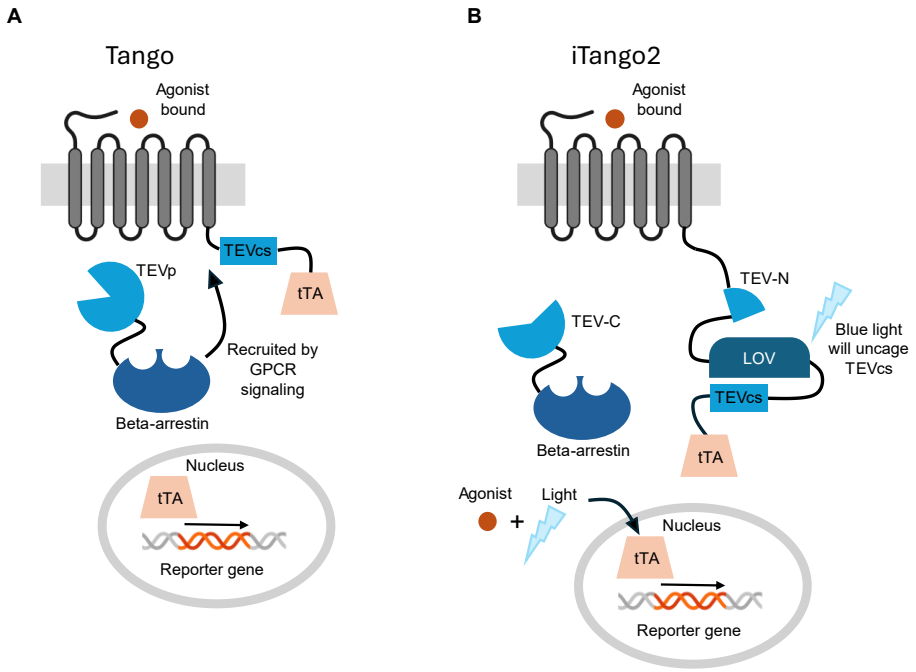


Figure 1-3: Schematic for the design of Tango and iTango2 integrator sensors. All graphics were created in BioRender. (A) Schematic of the Tango assay components. The Tango design use the protein-protein interaction of an activated GPCR and beta-arrestin to bring a protease (TEVp) and its cleavage site (TEVcs) in proximity. When the TEVcs is cleaved, it releases a transcription factor (tTA) that will localize to the nucleus and express a reporter gene such as a FP for fluorescent readout. Therefore fluorescence is only possible when the modified GPCR is signaling. (B) Schematic of the iTango2 assay components. To add light gating the TEVp is split into two fragments and the TEVcs is caged by a LOV domain. The LOV domain will only reveal/"uncage" the TEVcs when exposed to blue light. Then the TEVp will only be reconstituted when the GPCR beta-arrestin takes place. Therefore, both agonist stimulation and light stimulation are needed to release the transcription factor (tTA) to the nucleus and see reporter gene expression.

To adapt Tango for the study of neurotransmission, neural circuitry, and animal behavior the inducible Tango (iTango) system was developed, adding temporal control through light-activated domains and used split TEVp for protein interaction-dependence.[51] The first iTango design expanded to four necessary components. The modified GPCR C-terminus includes CIBN (a truncated cryptochrome-interacting basic-helix-loop-helix1), AsLOV2 (*Avena sativa* phototropin1 light-oxygen-voltage 2 domains) with a modified Jα-helix sterically blocking TEVcs access, and finally tTA. Then β-arrestin2 is attached to a split N-terminal TEVp fragment called TEV-N. In order to reconstitute TEVp, the C-terminal TEV-C is attached to CRY2PHR (cryptochrome 2 photolyase homology region). The final component is the reporter gene, which can express secreted alkaline phosphatase (SEAP) or EGFP. CRY2PHR and CIBN dimerize with blue light stimulation, and AsLOV2 undergoes a conformational change with blue light

stimulation to allow access to the TEVcs. iTango2 simplifies the initial design reducing it to 3 components by excluding CIBN and CRY2PHR, where TEV-N is included in the GPCR component and β-arrestin2 is linked to TEV-C (Figure 1-3B). The blue light control or "gating" adds some temporal resolution to the Tango system. Now iTango2 is only "on" and expressing reporter gene during the period of light irradiation. iTango2 also has high sensitivity for GPCR ligands of interest as it takes advantage of the signal amplification from the signaling cascade. Altogether, iTango2 marked an improvement in the spatial and temporal resolution of Tango as well as improving the SNR which allowed for extensive in vivo applications primarily detecting dopamine. However, due to the reliance on translation of the reporter gene, the timescale for initial readout still requires hours.

1.2.3.2 Specific Protein Association Tool Giving Transcriptional Readout with Rapid Kinetics

In SPARK (Specific Protein Association tool giving transcriptional Readout with rapid Kinetics), a protein-protein interaction (PPI) is light gated with the use of the eLOV (evolved LOV) domain blocking or "caging" TEVcs access attached to a transcription factor, Gal4, all linked to protein A while protein B is linked to the TEVp.[52] In this system both PPI and blue light stimulation are needed to release the transcription factor which can activate a reporter gene. The first PPI pair tested was B2AR as protein A and β-arrestin2 as protein B while the reporter gene expressed a Citrine FP or a luciferase. The initial publication demonstrates the versatility of SPARK by swapping out protein A and B for 12 total PPI pairs. Studying arrestin recruitment, SPARK reported on PPI dynamics by controlling the window in which light was applied, noting a temporal resolution of 5 minutes, and noting different strengths of arrestin recruitment between Class A and Class B GPCRs. One of the unique advantages SPARK highlights is for directed evolution of PPI through fluorescence activated cell sorting (FACS), something only possible with the persistent fluorescent labeling of an integrator sensor.

SPARK was benchmarked against iTango2 reporting a higher SNR potentially due to the background from iTango2's split TEVp fragments' natural affinity as well as slow reversibility. SPARK uses a truncated TEVp, to reduce its background activity. A strength of any reporter gene-based system that I did not address is that it can be changed from a readout focused protein (FP or luciferase) to a protein for effecting the cell, such as for rescue or further investigation. The need for three different genetically encoded components to be introduced does present a

challenge for application in vivo as it requires achieving the right ratios of each protein component to the other for high SNR.

1.2.3.3 Cleavage of Leucine Zipper-caged APEX for Protease Detection

The integrators I have discussed so far all detect PPI, which can be applied to measure GPCR ligand interactions by measuring PPI between the downstream signaling cascade partners, primarily β-arrestin. As the name Cleavage of Leucine zipper-caged APEX for Protease detection (CLAPon) implies, this system was designed initially for protease activity detection but was also adapted to detect PPI.[53] CLAPon is a single protein chain sensor that relies on the evolved split enhanced ascorbate peroxidase (APEX) which when reconstituted can catalyze the reaction of Amplex UltraRed to fluorescent resorufin or label proximal proteins with biotin.[54] The smaller half of APEX, termed EX, was sterically blocked from the larger half, AP, using acid-base coils (the leucine zipper-caging) that block the favored reconstitution surface. EX and the acid-base coils are connected at a critical junction by TEVcs so that in the presence of TEVp the APEX can reconstitute and turnover. In addition to track the expression of the construct AP is connected to acid-base coils by a linker containing EGFP.

To adapt CLAPon for PPI detection, the single-chain CLAPon was attached to the C-terminus of B2AR, D1 dopamine receptor (D1DR), fly leucokinin receptor (LKR), and MOR. Then β-arrestin was linked to truncated TEVp. The final version was named PPI-CLAPon1.1. To introduce light gating the LOV domain was added at the TEVcs location, and this tool was named LiPPI-CLAPon (Light and PPI-CLAPon). There are temporal resolution concerns due to the reconstitution of split APEX and the kinetics of TEVp and TEVcs cleavage, also limiting this to the minute time scale for readout. However, that is still a vast improvement on the timescale requirements of transcriptional readout systems. The different types of substrates for labeling also offer different spatial resolution, with Amplex UltraRed being more sensitive for ligand (in the case of B2AR based PPI-CLAPon) but only having cellular resolution while biotin paired to streptavidin-647 could show subcellular resolution overlapping with internalized B2AR-CLAPon expression marker EGFP. APEX-based labeling will continue to be challenging to apply in vivo due to reliance on peroxide which is toxic to living cells, and availability of the heme cofactor, which varies across cellular compartments.

1.2.3.4 Bimolecular Fluorescence Complementation and Self-Labelling Enzymes

Above, iTango2 and CLAPon could be categorized as complementation methods as they rely on the reconstitution (or complementation) of protein fragments to reform a functional protein. Bimolecular fluorescence complementation (BiFC) takes place when the non-fluorescent protein fragments reconstitute and become fluorescent upon protein assembly. It is a simple method capable of detecting PPI by fusing the non-fluorescent components to interacting proteins of interest. This allows for subcellular resolution of the PPI but it has minute to hour long temporal resolution due to the speed of the fluorophore assembly chemical reaction. It is important to know that formation of the fluorophore is irreversible, giving BiFC the integrator permanent fluorescence as opposed to FRET reporting on dynamics.

In comparison to FRET, BiFC can detect lower concentrations of protein complexes and has more multiplexing potential since one BiFC is reliant on only one fluorophore. Additionally, BiFC could be more flexible for protein orientation, and protein fragments should be less perturbative to the fusion partner proteins of interest than entire FPs.[55] An example is the development of split superfolder GFP, into the two fragments GFP 1-10 (amino acids 1-214) and GFP 11 (amino acids 215-230).[56] GFP 1-10 was initially insoluble and through directed evolution an optimized version with 12 mutations in comparison to superfolder GFP, called GFP1 -10 OPT. One group developed a tool called GRASP (GFP reconstitution across synaptic partners) based on the split superfolder GFP to label synaptic contacts demonstrated in *C. elegans*.[57]

A related design is the development of TagBiFC which rather than applying a split FP uses a split self-labelling enzyme, HaloTag, to conjugate fluorescent HaloTag ligand dyes which allows for single-molecule imaging in live cells.[58] Another split HaloTag system using a different split site was applied to studying GPCR ligand interactions through GPCR C-terminal linked to the circularly permuted HaloTag (cpHalo) and β-arrestin linked to the HaloTag peptide fragment (Hpep), while also developing a calcium indicator version applied in vivo (called Caprola for "Calcium dependent protein labeling").[59]

1.2.3.5 Single-Chain Protein-Based Opioid Transmission Indicator Tool and Related Designs

The final integrator design I will discuss is the foundation of my thesis work, a single-chain protein-based opioid transmission indicator tool (SPOTIT). Rather than relying on intermolecular interactions with a GPCR and arrestin as in many of the prior sections, SPOTIT's

function primarily relies on the addition of nanobody 39 (Nb39), an active conformation specific G-protein mimetic for the MOR.[60] The MOR C-terminus is modified to link cpGFP and Nb39, where Nb39 has two functions. In the inactive state, Nb39 interacts with cpGFP and stops fluorophore maturation from occurring, but in the presence of ligand, Nb39 is recruited to the active receptor, allowing cpGFP to mature (Figure 1-4A). The integrator nature of SPOTIT arises from the irreversibility of fluorophore maturation. SPOTIT fluorescence relies on the speed of fluorophore maturation which has been found to take many hours in the SPOTIT system. SPOTIT could be applied to whole-brain mapping of neural circuitry, as it can be widely expressed and analyzed ex vivo. As a single genetic construct it increases the robustness and scalability in vivo.

To address the need for better temporal control, MAturation-based Protease-gated Indicator Tool (MAPIT) was developed, using a second redundant Nb39 attached to the first Nb39 by a linker containing a TEVcs.[61] Then protease expression is controlled by small molecule addition of either rapamycin to reconstitute a split TEVp or doxycycline which controls transcription of the TEVp through the TetOn system.

Another major limitation of SPOTIT is the lack of generalizability because Nb39 is specific to MOR and has only successfully been applied to develop a KOR-SPOTIT and DOR-SPOTIT. The first method to expand SPOTIT for detecting other neurotransmitters was SPOTall (SPOTIT for all GPCRs) which adds a second active conformation specific nanobody, Nb80, that binds to active B2AR.[62] In this system the cpGFP Nb39 interaction is interrupted in the active state by steric hindrance, but this mechanism proved to result in lower signal and smaller SBR (Figure 1-4A, 1-4B, and 1-4C)..

This led to the development of Single-chain Protein-based Ligand Indication through a Chimerically Engineered Integrator Tool (SPLICEIT) which creates chimeric GPCRs that have the MOR intracellular surface for binding to Nb39 and the membrane and extracellular regions of the GPCR of interest for binding to a different neurotransmitter.[63] SPLICEIT was best demonstrated for dopamine detection in the DRD3-SPLICEIT, relying on the dopamine receptor

D3. This strategy still requires extensive protein engineering design for each new chimeric receptor, which serves as a key limitation.

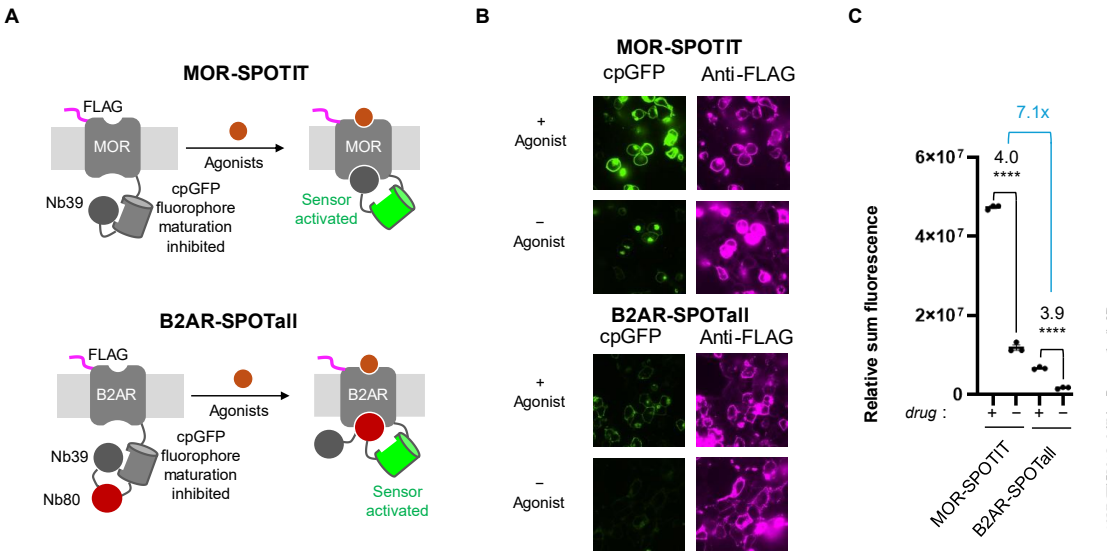


Figure 1-4: Original SPOTIT and SPOTall comparison. (A) Schematic of the design of MOR-SPOTIT and B2AR-SPOTall. In SPOTIT the Nb39 inhibits cpGFP fluorophore maturation until agonist recruits it to the active MOR. In SPOTall a second nanobody, Nb80, will sterically block Nb39-cpGFP interaction by being recruited to the active B2AR. (B) Representative fluorescence images of MOR-SPOTIT and B2AR-SPOTall in HEK293T cells. cpGFP, cpGFP fluorescence. Anti-FLAG, immunostaining. (C) Quantification of the experiment in 1-4A comparing MOR-SPOTIT2 and B2AR-SPOTall. All were stimulated with their respective agonists (10 µM fentanyl or isoproterenol) for 24 hours. The numbers above each bracket in black are the SBR between stimulated and unstimulated conditions. The number in blue is the fold-difference between B2AR-SPOTall and MOR-SPOTIT. All significance was calculated using a two-tailed Welch's t-test. Stars indicate the degree of significance as follows *, P<0.05, **, P<0.01, ***, P<0.001, ****, P<0.0001. Dots on the plot indicate the mean of three technical replicates. n = 3. The thick horizontal bar is the mean of the three technical replicates and the error bars are the SEM.

1.3 Need for New Tools

There is currently a need for sensors that can study neurotransmitters across large brain volumes. An ideal sensor for this application will be modular, sensitive, and robust in vivo with appropriate spatial and temporal resolution. SPOTIT's single-chain design limits complications of balancing multiple genetic component expression. For modularity, SPOTall and SPLICEIT offer options to expand the SPOTIT sensor toolkit for more GPCR ligand detection, to epinephrine, acetylcholine, and dopamine primarily, however, these require time-intensive design for each new sensor.

My thesis work focuses on the design of chimeric G protein mimetics to generalize SPOTIT further. First, I needed to better understand the mechanism by which Nb39 inhibits cpGFP fluorophore maturation so I developed a panel of experiments to home in on what regions of Nb39, but not structurally similar Nb80, could inhibit cpGFP. This led to the first chimeric nanobody design, where a singular loop region of Nb39 replaces a single Nb80 loop position. The resulting platform I named Single-chain Expressing Neurotransmitter Sensing Integrator Tool (SENSIT) and focuses on the design of chimeric nanobodies, reporting the improved B2AR-SENSIT, in comparison to B2AR-SPOTall, that can specifically detect epinephrine. Then I used directed evolution of the chimeric nanobody to improve B2AR-SENSIT further.

In my third chapter I will show the work done in characterizing B2AR-SENSIT1.1, that incorporates the evolved chimeric nanobody variant. I used the same evolved chimeric nanobody to develop B1AR-SENSIT for specific detection of norepinephrine. Then generalizability of chimeric nanobody design was applied to nanobody9-8 for the muscarinic acetylcholine receptor 2 (CHRM2), and further expanded to generate chimeric miniG proteins that could be highly modular.

In my last chapter I will focus on future work that could improve SENSIT for in vivo applications. I separated my discussion into ways that we could target each component of SENSIT the receptor, the cpGFP, and the chimeric GPCR binder. I propose many directed evolution strategies based on my directed evolution platform in mammalian cell. I

1.4 Chapter 1 Bibliography

(1) Yang, D.; Zhou, Q.; Labroska, V.; Qin, S.; Darbalaei, S.; Wu, Y.; Yuliantie, E.; Xie, L.; Tao, H.; Cheng, J.; et al. G protein-coupled receptors: structure- and function-based drug discovery. *Signal Transduct Target Ther* **2021**, *6* (1), 7. DOI: 10.1038/s41392-020-00435-w From NLM Medline.
(2) Sriram, K.; Insel, P. A. G Protein-Coupled Receptors as Targets for Approved Drugs: How Many Targets and How Many Drugs? *Mol Pharmacol* **2018**, *93* (4), 251-258. DOI: 10.1124/mol.117.111062 From NLM Medline.
(3) Wu, Z.; Lin, D.; Li, Y. Pushing the frontiers: tools for monitoring neurotransmitters and neuromodulators. *Nat Rev Neurosci* **2022**, *23* (5), 257-274. DOI: 10.1038/s41583-022-00577-6 From NLM Medline.
(4) Jiang, H.; Galtes, D.; Wang, J.; Rockman, H. A. G protein-coupled receptor signaling: transducers and effectors. *Am J Physiol Cell Physiol* **2022**, *323* (3), C731-C748. DOI: 10.1152/ajpcell.00210.2022 From NLM Medline.
(5) Liu, S.; Anderson, P. J.; Rajagopal, S.; Lefkowitz, R. J.; Rockman, H. A. G Protein-Coupled Receptors: A Century of Research and Discovery. *Circ Res* **2024**, *135* (1), 174-197. DOI: 10.1161/CIRCRESAHA.124.323067 From NLM Medline.
(6) Gilman, A. G. G proteins and dual control of adenylate cyclase. *Cell* **1984**, *36* (3), 577-579. DOI: 10.1016/0092-8674(84)90336-2 From NLM Medline.
(7) Simon, M. I.; Strathmann, M. P.; Gautam, N. Diversity of G proteins in signal transduction. *Science* **1991**, *252* (5007), 802-808. DOI: 10.1126/science.1902986 From NLM Medline.
(8) Berridge, M. J. The Inositol Trisphosphate/Calcium Signaling Pathway in Health and Disease. *Physiol Rev* **2016**, *96* (4), 1261-1296. DOI: 10.1152/physrev.00006.2016 From NLM Medline.
(9) Chen, Z.; Singer, W. D.; Sternweis, P. C.; Sprang, S. R. Structure of the p115RhoGEF rgRGS domain-Galpha13/i1 chimera complex suggests convergent evolution of a GTPase activator. *Nat Struct Mol Biol* **2005**, *12* (2), 191-197. DOI: 10.1038/nsmb888 From NLM Medline.
(10) Ford, C. E.; Skiba, N. P.; Bae, H.; Daaka, Y.; Reuveny, E.; Shekter, L. R.; Rosal, R.; Weng, G.; Yang, C. S.; Iyengar, R.; et al. Molecular basis for interactions of G protein betagamma subunits with effectors. *Science* **1998**, *280* (5367), 1271-1274. DOI: 10.1126/science.280.5367.1271 From NLM Medline.
(11) Benovic, J. L.; Strasser, R. H.; Caron, M. G.; Lefkowitz, R. J. Beta-adrenergic receptor kinase: identification of a novel protein kinase that phosphorylates the agonist-occupied form of the receptor. *Proc Natl Acad Sci U S A* **1986**, *83* (9), 2797-2801. DOI: 10.1073/pnas.83.9.2797 From NLM Medline.
(12) Lohse, M. J.; Benovic, J. L.; Codina, J.; Caron, M. G.; Lefkowitz, R. J. beta-Arrestin: a protein that regulates beta-adrenergic receptor function. *Science* **1990**, *248* (4962), 1547-1550. DOI: 10.1126/science.2163110 From NLM Medline.
(13) Zhang, M.; Chen, T.; Lu, X.; Lan, X.; Chen, Z.; Lu, S. G protein-coupled receptors (GPCRs): advances in structures, mechanisms, and drug discovery. *Signal Transduct Target Ther* **2024**, *9* (1), 88. DOI: 10.1038/s41392-024-01803-6 From NLM Medline.
(14) Hikino, K.; Kobayashi, S.; Ota, E.; Mushiroda, T.; Kobayashi, T. The Influence of Beta-2 Adrenergic Receptor Gene Polymorphisms on Albuterol Therapy for Patients With Asthma: Protocol for a Systematic Review and Meta-Analysis. *JMIR Res Protoc* **2019**, *8* (9), e14759. DOI: 10.2196/14759 From NLM PubMed-not-MEDLINE.

(15) Frishman, W. H. Cardiology patient page. Beta-adrenergic blockers. *Circulation* **2003**, *107* (18), e117-119. DOI: 10.1161/01.CIR.0000070983.15903.A2 From NLM Medline.
(16) Azam, S.; Haque, M. E.; Jakaria, M.; Jo, S. H.; Kim, I. S.; Choi, D. K. G-Protein-Coupled Receptors in CNS: A Potential Therapeutic Target for Intervention in Neurodegenerative Disorders and Associated Cognitive Deficits. *Cells* **2020**, *9* (2). DOI: 10.3390/cells9020506 From NLM Medline.
(17) Sudhof, T. C.; Malenka, R. C. Understanding synapses: past, present, and future. *Neuron* **2008**, *60* (3), 469-476. DOI: 10.1016/j.neuron.2008.10.011 From NLM Medline.
(18) Burrows, M. Neurotransmitters, neuromodulators and neurohormones. In *The Neurobiology of an Insect Brain*, Oxford University Press, 1996; pp 168-228.
(19) Fuller, R. W. Pharmacology of brain epinephrine neurons. *Annu Rev Pharmacol Toxicol* **1982**, *22*, 31-55. DOI: 10.1146/annurev.pa.22.040182.000335 From NLM Medline.
(20) O'Donnell, J.; Zeppenfeld, D.; McConnell, E.; Pena, S.; Nedergaard, M. Norepinephrine: a neuromodulator that boosts the function of multiple cell types to optimize CNS performance. *Neurochem Res* **2012**, *37* (11), 2496-2512. DOI: 10.1007/s11064-012-0818-x From NLM Medline.
(21) Holland, N.; Robbins, T. W.; Rowe, J. B. The role of noradrenaline in cognition and cognitive disorders. *Brain* **2021**, *144* (8), 2243-2256. DOI: 10.1093/brain/awab111 From NLM Medline.
(22) Wong, D. L.; Tai, T. C.; Wong-Faull, D. C.; Claycomb, R.; Meloni, E. G.; Myers, K. M.; Carlezon, W. A., Jr.; Kvetnansky, R. Epinephrine: a short- and long-term regulator of stress and development of illness : a potential new role for epinephrine in stress. *Cell Mol Neurobiol* **2012**, *32* (5), 737-748. DOI: 10.1007/s10571-011-9768-0 From NLM Medline.
(23) Kim, M. H.; Gorouhi, F.; Ramirez, S.; Granick, J. L.; Byrne, B. A.; Soulika, A. M.; Simon, S. I.; Isseroff, R. R. Catecholamine stress alters neutrophil trafficking and impairs wound healing by beta2-adrenergic receptor-mediated upregulation of IL-6. *J Invest Dermatol* **2014**, *134* (3), 809-817. DOI: 10.1038/jid.2013.415 From NLM Medline.
(24) Wood, S. K.; Valentino, R. J. The brain norepinephrine system, stress and cardiovascular vulnerability. *Neurosci Biobehav Rev* **2017**, *74* (Pt B), 393-400. DOI: 10.1016/j.neubiorev.2016.04.018 From NLM Medline.
(25) Chandley, M. J.; Ordway, G. A. Noradrenergic Dysfunction in Depression and Suicide. In *The Neurobiological Basis of Suicide*, Dwivedi, Y. Ed.; Frontiers in Neuroscience, 2012.
(26) Buck, K.; Voehringer, P.; Ferger, B. Rapid analysis of GABA and glutamate in microdialysis samples using high performance liquid chromatography and tandem mass spectrometry. *J Neurosci Methods* **2009**, *182* (1), 78-84. DOI: 10.1016/j.jneumeth.2009.05.018 From NLM Medline.
(27) Kao, C. Y.; Anderzhanova, E.; Asara, J. M.; Wotjak, C. T.; Turck, C. W. NextGen Brain Microdialysis: Applying Modern Metabolomics Technology to the Analysis of Extracellular Fluid in the Central Nervous System. *Mol Neuropsychiatry* **2015**, *1* (1), 60-67. DOI: 10.1159/000381855 From NLM PubMed-not-MEDLINE.
(28) Westerhout, J.; Ploeger, B.; Smeets, J.; Danhof, M.; de Lange, E. C. Physiologically based pharmacokinetic modeling to investigate regional brain distribution kinetics in rats. *AAPS J* **2012**, *14* (3), 543-553. DOI: 10.1208/s12248-012-9366-1 From NLM Medline.
(29) Flik, G.; Folgering, J. H.; Cremers, T. I.; Westerink, B. H.; Dremencov, E. Interaction Between Brain Histamine and Serotonin, Norepinephrine, and Dopamine Systems: In Vivo

Microdialysis and Electrophysiology Study. *J Mol Neurosci* **2015**, *56* (2), 320-328. DOI: 10.1007/s12031-015-0536-3 From NLM Medline.
(30) Yoshitake, T.; Kehr, J.; Todoroki, K.; Nohta, H.; Yamaguchi, M. Derivatization chemistries for determination of serotonin, norepinephrine and dopamine in brain microdialysis samples by liquid chromatography with fluorescence detection. *Biomed Chromatogr* **2006**, *20* (3), 267-281. DOI: 10.1002/bmc.560 From NLM Medline.
(31) Folkesson, K. T.; Samuelsson, A.; Tesselaar, E.; Dahlstrom, B.; Sjoberg, F. A human vascular model based on microdialysis for the assessment of the vasoconstrictive dose-response effects of norepinephrine and vasopressin in skin. *Microcirculation* **2012**, *19* (4), 352-359. DOI: 10.1111/j.1549-8719.2012.00170.x From NLM Medline.
(32) Devoto, P.; Sagheddu, C.; Santoni, M.; Flore, G.; Saba, P.; Pistis, M.; Gessa, G. L. Noradrenergic Source of Dopamine Assessed by Microdialysis in the Medial Prefrontal Cortex. *Front Pharmacol* **2020**, *11*, 588160. DOI: 10.3389/fphar.2020.588160 From NLM PubMed-not-MEDLINE.
(33) Hascup, E. R.; af Bjerken, S.; Hascup, K. N.; Pomerleau, F.; Huettl, P.; Stromberg, I.; Gerhardt, G. A. Histological studies of the effects of chronic implantation of ceramic-based microelectrode arrays and microdialysis probes in rat prefrontal cortex. *Brain Res* **2009**, *1291*, 12-20. DOI: 10.1016/j.brainres.2009.06.084 From NLM Medline.
(34) Puthongkham, P.; Venton, B. J. Recent advances in fast-scan cyclic voltammetry. *Analyst* **2020**, *145* (4), 1087-1102. DOI: 10.1039/c9an01925a From NLM Medline.
(35) Vickrey, T. L.; Condron, B.; Venton, B. J. Detection of endogenous dopamine changes in Drosophila melanogaster using fast-scan cyclic voltammetry. *Anal Chem* **2009**, *81* (22), 9306-9313. DOI: 10.1021/ac901638z From NLM Medline.
(36) Nicolai, E. N.; Trevathan, J. K.; Ross, E. K.; Lujan, J. L.; Blaha, C. D.; Bennet, K. E.; Lee, K. H.; Ludwig, K. A. Detection of Norepinephrine in Whole Blood via Fast Scan Cyclic Voltammetry. *IEEE Int Symp Med Meas Appl* **2017**, *2017*, 111-116. DOI: 10.1109/MeMeA.2017.7985859 From NLM PubMed-not-MEDLINE.
(37) Park, J.; Takmakov, P.; Wightman, R. M. In vivo comparison of norepinephrine and dopamine release in rat brain by simultaneous measurements with fast-scan cyclic voltammetry. *J Neurochem* **2011**, *119* (5), 932-944. DOI: 10.1111/j.1471-4159.2011.07494.x From NLM Medline.
(38) Samels, S. B., Yuksel, P., Espana, R.A. Monoamine Transporters in Drugs of Abuse : Insights from Fast Scan Cyclic Voltammetry. In *Monoamine Transporters, Advances in Neurobiology*, Mortensen, O. V. Ed.; Vol. 46; Springer, Cham, 2025.
(39) Ou, Y.; Buchanan, A. M.; Witt, C. E.; Hashemi, P. Frontiers in Electrochemical Sensors for Neurotransmitter Detection: Towards Measuring Neurotransmitters as Chemical Diagnostics for Brain Disorders. *Anal Methods* **2019**, *11* (21), 2738-2755. DOI: 10.1039/c9ay00055k From NLM PubMed-not-MEDLINE.
(40) Vilardaga, J. P.; Bunemann, M.; Krasel, C.; Castro, M.; Lohse, M. J. Measurement of the millisecond activation switch of G protein-coupled receptors in living cells. *Nat Biotechnol* **2003**, *21* (7), 807-812. DOI: 10.1038/nbt838 From NLM Medline.
(41) Nakanishi, J.; Takarada, T.; Yunoki, S.; Kikuchi, Y.; Maeda, M. FRET-based monitoring of conformational change of the beta2 adrenergic receptor in living cells. *Biochem Biophys Res Commun* **2006**, *343* (4), 1191-1196. DOI: 10.1016/j.bbrc.2006.03.064 From NLM Medline.

(42) Muller, A.; Joseph, V.; Slesinger, P. A.; Kleinfeld, D. Cell-based reporters reveal in vivo dynamics of dopamine and norepinephrine release in murine cortex. *Nat Methods* **2014**, *11* (12), 1245-1252. DOI: 10.1038/nmeth.3151 From NLM Medline.
(43) Nguyen, Q. T.; Schroeder, L. F.; Mank, M.; Muller, A.; Taylor, P.; Griesbeck, O.; Kleinfeld, D. An in vivo biosensor for neurotransmitter release and in situ receptor activity. *Nat Neurosci* **2010**, *13* (1), 127-132. DOI: 10.1038/nn.2469 From NLM Medline.
(44) Martin, J. R. In vivo brain imaging: fluorescence or bioluminescence, which to choose? *J Neurogenet* **2008**, *22* (3), 285-307. DOI: 10.1080/01677060802298517 From NLM Medline.
(45) Masuho, I.; Ostrovskaya, O.; Kramer, G. M.; Jones, C. D.; Xie, K.; Martemyanov, K. A. Distinct profiles of functional discrimination among G proteins determine the actions of G protein-coupled receptors. *Sci Signal* **2015**, *8* (405), ra123. DOI: 10.1126/scisignal.aab4068 From NLM Medline.
(46) Hall, M. P.; Unch, J.; Binkowski, B. F.; Valley, M. P.; Butler, B. L.; Wood, M. G.; Otto, P.; Zimmerman, K.; Vidugiris, G.; Machleidt, T.; et al. Engineered luciferase reporter from a deep sea shrimp utilizing a novel imidazopyrazinone substrate. *ACS Chem Biol* **2012**, *7* (11), 1848-1857. DOI: 10.1021/cb3002478 From NLM Medline.
(47) Laschet, C.; Dupuis, N.; Hanson, J. A dynamic and screening-compatible nanoluciferase-based complementation assay enables profiling of individual GPCR-G protein interactions. *J Biol Chem* **2019**, *294* (11), 4079-4090. DOI: 10.1074/jbc.RA118.006231 From NLM Medline.
(48) Patriarchi, T.; Cho, J. R.; Merten, K.; Howe, M. W.; Marley, A.; Xiong, W. H.; Folk, R. W.; Broussard, G. J.; Liang, R.; Jang, M. J.; et al. Ultrafast neuronal imaging of dopamine dynamics with designed genetically encoded sensors. *Science* **2018**, *360* (6396). DOI: 10.1126/science.aat4422 From NLM Medline.
(49) Feng, J.; Zhang, C.; Lischinsky, J. E.; Jing, M.; Zhou, J.; Wang, H.; Zhang, Y.; Dong, A.; Wu, Z.; Wu, H.; et al. A Genetically Encoded Fluorescent Sensor for Rapid and Specific In Vivo Detection of Norepinephrine. *Neuron* **2019**, *102* (4), 745-761 e748. DOI: 10.1016/j.neuron.2019.02.037 From NLM Medline.
(50) Barnea, G.; Strapps, W.; Herrada, G.; Berman, Y.; Ong, J.; Kloss, B.; Axel, R.; Lee, K. J. The genetic design of signaling cascades to record receptor activation. *Proc Natl Acad Sci U S A* **2008**, *105* (1), 64-69. DOI: 10.1073/pnas.0710487105 From NLM Medline.
(51) Lee, D.; Creed, M.; Jung, K.; Stefanelli, T.; Wendler, D. J.; Oh, W. C.; Mignocchi, N. L.; Lüscher, C.; Kwon, H. B. Temporally precise labeling and control of neuromodulatory circuits in the mammalian brain. *Nature Methods* **2017**, *14* (5), 495-+. DOI: 10.1038/Nmeth.4234.
(52) Kim, M. W.; Wang, W.; Sanchez, M. I.; Coukos, R.; von Zastrow, M.; Ting, A. Y. Time-gated detection of protein-protein interactions with transcriptional readout. *Elife* **2017**, *6*. DOI: 10.7554/eLife.30233 From NLM Medline.
(53) Zhou, G.; Wan, W. W.; Wang, W. Modular Peroxidase-Based Reporters for Detecting Protease Activity and Protein Interactions with Temporal Gating. *J Am Chem Soc* **2022**, *144* (50), 22933-22940. DOI: 10.1021/jacs.2c08280 From NLM Medline.
(54) Han, Y.; Branon, T. C.; Martell, J. D.; Boassa, D.; Shechner, D.; Ellisman, M. H.; Ting, A. Directed Evolution of Split APEX2 Peroxidase. *ACS Chem Biol* **2019**, *14* (4), 619-635. DOI: 10.1021/acschembio.8b00919 From NLM Medline.
(55) Kerppola, T. K. Bimolecular fluorescence complementation (BiFC) analysis as a probe of protein interactions in living cells. *Annu Rev Biophys* **2008**, *37*, 465-487. DOI: 10.1146/annurev.biophys.37.032807.125842 From NLM Medline.

(56) Cabantous, S.; Terwilliger, T. C.; Waldo, G. S. Protein tagging and detection with engineered self-assembling fragments of green fluorescent protein. *Nat Biotechnol* **2005**, *23* (1), 102-107. DOI: 10.1038/nbt1044 From NLM Medline.
(57) Feinberg, E. H.; Vanhoven, M. K.; Bendesky, A.; Wang, G.; Fetter, R. D.; Shen, K.; Bargmann, C. I. GFP Reconstitution Across Synaptic Partners (GRASP) defines cell contacts and synapses in living nervous systems. *Neuron* **2008**, *57* (3), 353-363. DOI: 10.1016/j.neuron.2007.11.030 From NLM Medline.
(58) Shao, S.; Zhang, H.; Zeng, Y.; Li, Y.; Sun, C.; Sun, Y. TagBiFC technique allows long-term single-molecule tracking of protein-protein interactions in living cells. *Commun Biol* **2021**, *4* (1), 378. DOI: 10.1038/s42003-021-01896-7 From NLM Medline.
(59) Huppertz, M. C.; Wilhelm, J.; Grenier, V.; Schneider, M. W.; Falt, T.; Porzberg, N.; Hausmann, D.; Hoffmann, D. C.; Hai, L.; Tarnawski, M.; et al. Recording physiological history of cells with chemical labeling. *Science* **2024**, *383* (6685), 890-897. DOI: 10.1126/science.adg0812 From NLM Medline.
(60) Kroning, K. E.; Li, M.; Shen, J.; Fiel, H.; Nassar, M.; Wang, W. A Modular Fluorescent Sensor Motif Used to Detect Opioids, Protein-Protein Interactions, and Protease Activity. *ACS Chem Biol* **2022**, *17* (8), 2212-2220. DOI: 10.1021/acschembio.2c00364 From NLM Medline.
(61) Sescil, J.; Fiel, H.; Havens, S. M.; Fu, E.; Li, X.; Kroning, K. E.; Solowiej, I.; Li, P.; Wang, W. Functionalization of a versatile fluorescent sensor for detecting protease activity and temporally gated opioid sensing. *RSC Chem Biol* **2025**, *6* (4), 555-562. DOI: 10.1039/d4cb00276h From NLM PubMed-not-MEDLINE.
(62) Kroning, K.; Gannot, N.; Li, X.; Putansu, A.; Zhou, G.; Sescil, J.; Shen, J.; Wilson, A.; Fiel, H.; Li, P.; et al. Single-chain fluorescent integrators for mapping G-protein-coupled receptor agonists. *Proc Natl Acad Sci U S A* **2024**, *121* (18), e2307090121. DOI: 10.1073/pnas.2307090121 From NLM Medline.
(63) Havens, S. M.; Georgis, B.; Weng, J.; Rodriguez, J.; Rivett, H.; Alrawi, S.; Li, P.; Wang, W. SPLICEIT Fluorescent Sensor for Integrating Dopamine Release with Cellular Resolution. *Angew Chem Int Ed Engl* **2025**, *64* (33), e202511186. DOI: 10.1002/anie.202511186 From NLM Medline.

Chapter 2 Chimeric Nanobody Design, Mechanistic Study, and Directed Evolution

SPOTIT was originally intended to be a real-time sensor design where rather than modulating cpGFP conformation with IL3 insertion, cpGFP conformation would be controlled by an active state specific nanobody. However, it was discovered that on the same protein chain Nb39 was capable of inhibiting cpGFP fluorophore maturation, creating the integrator sensor motif discussed in my introduction. The specifics of the Nb39-cpGFP interaction have remained elusive, as finding a molecular scale explanation would likely require structural studies and the applications of the motif remain limited to sensor design.

The two primary nanobodies I discuss in my work, Nb39 and Nb80, were developed as crystallization chaperones for structural studies, and were produced through immunization of llamas using purified GPCRs.[64, 65] Therefore, development of new conformation specific nanobodies remains challenging and there is a limited pool of available nanobodies to work with. Another limitation with nanobodies such as Nb39 and Nb80 is that they are highly specific for the receptor used in the immunization, MOR and B2AR respectively. Though we have demonstrated that Nb39 shows some interaction with the KOR and DOR as well, these nanobodies are still highly specific to structurally similar receptors in the same family. With both the development difficulty and high specificity of Nb39, the SPOTIT motif is limited to application based on opioid receptors.

To expand the generalizability of the fluorescent integrator sensor platform, the idea of chimeric nanobodies arose.[1] Though still limited by receptor specificity and lack of conformation

[1] Chapter 2 was largely adapted from the following publication:

Putansu, A., Soloweij, I., Rivett-Trznadel, H., Lakkanasirorat, B., Moran, L., Kroning, K., Liu, J., Li, X., Li, P., and Wang, W. "SENSIT, a modular single-chain fluorescent integrator platform for GPCR ligands." (Manuscript under revision).

specific scaffolds, they could be an interesting platform to discover more about the Nb39-cpGFP interaction. An ideal chimeric nanobody needs to maintain the cpGFP fluorophore maturation inhibition property, but be able to bind preferentially to the active conformation of the GPCR of interest. This led to the first chimeric nanobody designs of the chimeric Nb80/Nb39, also referred to by shorthand chNb80/39. From here I used this design to determine which Nb39 loop regions could contribute to cpGFP fluorophore maturation inhibition as well as which regions of Nb80 served as the best positions for replacement. Then I tried to determine what parts of the sequence and structure of these loop regions contributed to cpGFP inhibition using a TEV protease based system such as in the design of SPOTon.[62] Finally, to address limitations with the initial chNb80/39 I performed directed evolution in HEK293T cells and identified a mutant with improved signal to background ratios (SBRs) at shorter agonist stimulation times, an important improvement for animal experiment application.

2.1 Materials and Methods

2.1.1 Plasmids and Cloning

Constructs were cloned into an ampicillin-resistant adeno-associated viral vector or lentiviral vector with a CAG promoter. Standard cloning procedures were employed, using a Q5 polymerase PCR amplification, NEB restriction enzyme digest, and Gibson assembly. DNA was transformed via heat shock transformation into XL-1 blue competent cells.

2.1.2 Supernatant Lentivirus Preparation

To prepare lentivirus, 2.5 µg viral construct DNA, 0.25 µg pVSVG, and 2.25 µg Δ8.9 were incubated with serum free DMEM and mixed before adding PEI max solution and incubating for at least 10 minutes at RT before addition of complete media. Complete media

---

Aubrey Putansu wrote the entirety of the above article, with editing from Isabel Soloweij, Hannah Rivett-Trznadel, Benya Lakkanasirorat, Lexie Moran, Kayla Kroning, Gwen Shingles, Jiahui Ding, Professor Peng Li, and Professor Wenjing Wang. The loop deletion experiment was conceptualized by Jiying Liu. I was assisted in all flow cytometry experiments by Benya Lakkanasirorat. Hannah Rivett-Trznadel conducted all the of cpGFP directed evolution experiments.

contains 450 mL DMEM (Invitrogen), 450 mL MEM (Invitrogen), 100 mL FBS, 20 mL 1M HEPES buffer (Invitrogen), 10 mL penicillin/streptomycin (Invitrogen). One T25 of HEK293T cells at approximately 60-80% confluence was then incubated with the viral DNA transfection mixture for 48 hours. Then media was collected and aliquoted into 500 µL, flash frozen in liquid nitrogen, and then stored at -80°C.

2.1.3 B2AR-SENSIT HEK293T Library and Frozen Cell Stock Preparation

Targeted mutagenesis was carried out using primers with mixed bases (IDT) at specified codon positions. Each separate codon position mutation was transformed into XL-1 blue competent cells and then all colonies that grew were harvested and miniprepped. The DNA from each miniprep was then combined to constitute the library DNA which would be prepared as described above in lentivirus preparation. A T75 of HEK293T cells at 25% confluence were incubated for 48 hours with an appropriate volume of supernatant lentivirus to achieve a multiplicity of infection of ~30% ensuring cells only took up a single plasmid. Following infection the cells were split for library selection while some were split for long term storage. To prepare long term frozen HEK293T cell stocks a T150 of library infected cells were lifted with 0.25% trypsin (Invitrogen) and then quenched with 30mL complete media (prepared as described above). Cells were then centrifuged at 1200xg for 3min and media aspirated. The cell pellet was resuspended in 15mL of 10% v/v DMSO in FBS and aliquoted into 1mL cryotubes and frozen slowly using Mr. Frosty Freezing Container (ThermoFisher) kept at -80°C overnight. Samples are then moved to a liquid nitrogen dewar next day.

2.1.4 B2AR-SENSIT HEK293T Library Selection via FACS

Library size for B2AR-SENSIT chimeric Nb80/39 mutants is 160 variants (20 AA x 8 positions) as each construct is a single mutant. Single HEK293T cells were selected by consecutive gates according to Supplementary Figure 3. Library samples were analyzed and sorted with a BD FACSDiscover S8 Cell Sorter (BD Biosciences) equipped with 488 nm excitation and 561 nm excitation and algorithmically optimized filter bandwidths as follows Blue 488-nm laser – 16 Blue detectors, covering 495–860 nm and Y/G 561-nm laser – 12 Yellow-green detectors, covering 570–860 nm. All HEK293T cells were collected into 5 mL complete media. Immediately after sorting, cells were grown at 37 ℃ approximately 7-10 d. Number of cells collects for each round was as follows:

Strategy 1 Round 1 twenty-four-hour stimulation:
5,155 cells sorted out of 7,315,878 events total
Strategy 1 Round 2 five-minute stimulation:
6,557 cells sorted out of 6,569,966 events total
Strategy 2 Round 1 five-minute stimulation:
3,214 cells sorted out of 10,155,373 events total

Library size for B2AR-SENSIT cpGFP evolution is 20^3 (8000) variants due to 20 AA at 3 simultaneous mutation positions. Single HEK293T cells were selected by consecutive gates according to [Supplementary Figure 4]. Library samples were analyzed and sorted with a BD FACSDiscover S8 Cell Sorter (BD Biosciences) equipped with 488 nm excitation and 561 nm excitation and algorithmically optimized filter bandwidths as follows Blue 488-nm laser – 16 Blue detectors, covering 495–860 nm and Y/G 561-nm laser – 12 Yellow-green detectors, covering 570–860 nm. All HEK293T cells were collected into 5 mL complete media. Immediately after sorting, cells were grown at 37 °C approximately 7-10 d. Number of cells collected for the single sorting round was as follows:

Sorted 43,584 cells and 10,022,153 events total

The total number of cells far sorted and collected each round far exceeds library size, because it is important for HEK cell health to collect a sufficient amount to grow well after sorting. The number of rounds was also kept limited to improve cell health and avoid inconsistencies due to poor cell health.

2.1.5 Confocal Microscopy of HEK293T

All images were fixed cells in 100 mM CAPS 100 mM NaCl buffer kept at pH 11, except for images taken in the pH titration. Confocal imaging was performed on a Nikon inverted confocal microscope with 20× air objective and 60× oil immersion objective, outfitted with a Yokogawa CSU-X1 5000RPM spinning disk confocal head, and Ti2-ND-P perfect focus system 4, a compact 4-line laser source: 405 nm (100 mW) 488 nm (100 mW), 561 nm (100mW), and 640-nm (75 mW) lasers. The following combinations of laser excitation and emission filters were used for various fluorophores: EGFP/Alexa Fluor 488 (488 nm excitation; 525/36

emission), mCherry (568 nm excitation; 605/52 emission), Alexa Fluor 647 (647 nm excitation; 705/72 emission), and differential interference contrast (DIC). The acquisition time was 500ms at 30% laser intensity. The camera unit is an ORCA-Flash 4.0 LT + sCMOS camera. All images were taken with either the 20× or 60× objectives. To interface with the microscope and take images we used the Nikon NIS-Elements hardware control software and images were processed with NIS-Elements General Analysis 3 software.

2.1.6 Analysis of HEK293T Cell Images

All HEK293T cell experiments were done with three technical replicates meaning three wells per condition. Then ten images were taken per well, and the fluorescence mean intensity value was measured and taken from the NIS-Elements General Analysis 3 software. To determine the optimal threshold value for counting true signal above autofluorescence of the cells, we chose ten points devoid of cells on the plate and multiplied this background autofluorescence by 2. The same threshold is used for all conditions in a single experiment. Two values were taken from the cell images that have fluorescence values above the threshold, the mean intensity value and the total object area. The total object area is defined as the area of cells that are within the threshold value. Then the mean intensity is the count of fluorescence intensity from cells within the total object area. If the system did not use a co-expression of mCherry we then would multiply the total object area by the mean intensity value to calculate the sum intensity. Background subtraction for HEK293T experiments used the mean intensity of the plate without any cells present and multiplied by the total object area within the threshold, and then subtracted this from the sum intensity.

If the system did use a co-expression of mCherry we chose to normalize the fluorescent signal of the sensor cpGFP to the mCherry to account for differences in expression between wells and conditions. For this calculation we took the mean intensity and subtracted the background mean intensity, then multiplied by the total object area for each channel separately. To get the normalized signal we divided the cpGFP sum intensity with background subtraction by the mCherry sum intensity with background subtraction.

For HEK293T, the sum intensity of the 10 images from each technical replicate were averaged and plotted as one point on the graph. All images were included in analysis, unless they were blurry, had autofluorescent artifacts, or were primarily devoid of cells.

For all experiments, Prism GraphPah software was used for plotting, as well as performing unpaired Welch's *t* tests to calculate significance.

2.1.7 B2AR-SENSIT Initial Testing and Engineering

Twenty to twenty-four hours after transfection with 100 ng B2AR-SENSIT DNA, HEK293T cells were stimulated with 100 µL of isoproterenol diluted in complete media, for a final concentration of 10 µM within the well. No drug conditions had an equal volume of only complete media. Twenty-four hours after stimulation cells were fixed, immunostained, and imaged with a CAPS pH 11 buffer. These images were taken with #1.5 glass bottom plates (Cellvis) at 60× objective.

Immunostaining was done with 1mg/mL antibody/dye diluted 1000× in 1% w/v BSA in PBS. The first antibody incubation was 60 minutes on a shaker with chicken anti-GFP (Abcam), and the second antibody incubation was 60 minutes on a shaker with goat anti-chicken Alexa Fluor 647 (Abcam) and DAPI nuclear stain (Bio-Rad). Immunostaining was not done for following experiments that have mCherry co-expression.

2.1.8 Protease Based Nb39 Mechanistic Studies

Some constructs described in Figure 2-3 and 2-5 no longer contain a GPCR domain and therefore do not require stimulation. Therefore, twenty to twenty-four hours after transfection with protease cpGFP-mutant Nb39 or cpGFP-Nb39 loop peptides DNA, HEK293T cells were fixed, immunostained, and imaged at 20× with a CAPS pH 11 buffer.

2.2 Initial B2AR-SENSIT Chimeric Nanobody Design

The SENSIT approach utilizes native GPCRs, ensuring proper receptor trafficking and enabling the detection of a range of neuromodulators. Additionally, SENSIT employs bifunctional chimeric binder proteins engineered to maintain high selectivity for activated GPCRs while simultaneously modulating the fluorophore maturation of cpGFP. Mechanistically, agonist binding induces a conformational change in the GPCR that competitively recruits the chimeric binder, thereby relieving the inhibition of the cpGFP fluorophore maturation (Figure 2-1A).

To develop the SENSIT platform, we selected the beta-2 adrenergic receptor (B2AR) as a proof-of-concept, leveraging the availability of Nb80, a nanobody that specifically targets the receptor's active conformation. [65] We sought to design chimeric Nb80 by grafting a cpGFP fluorophore maturation inhibition motif from Nb39 into Nb80. Since it was unknown how

nanobody 39 (Nb39) inhibits fluorophore maturation, we focused on Nb39's loop regions, where most of the sequence variability among nanobodies arises from as opposed to the more conserved structural beta-sheets (Figure 2-1B).[66] Additionally, to preserve binding affinity and conformational specificity of Nb80 for the activated B2AR, it was important to only slightly alter Nb80. Therefore, we chose to substitute one loop region of Nb80 with each of the eight Nb39 loops (Figure 2-1B and 2-1C). The specific residues for Nb80 positions and Nb39 loops are defined in Appendix Figure A-1.

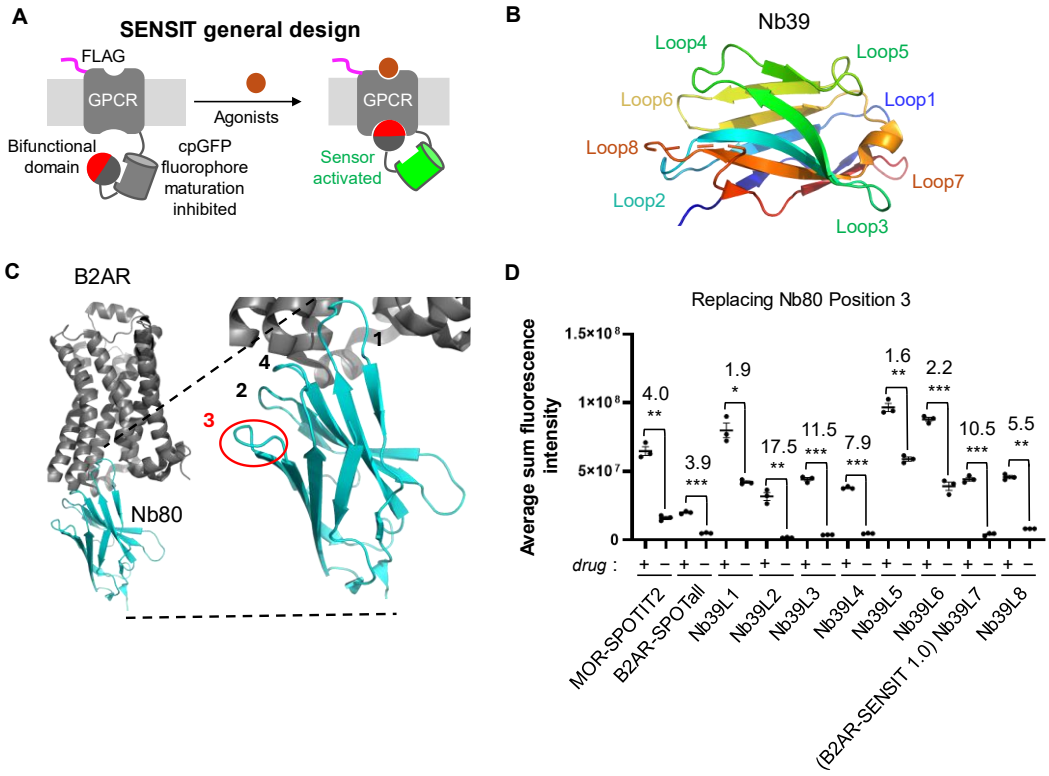


Figure 2-1: Design of the chimeric nanobody-based SENSIT. (A) Schematic of the design of SENSIT. The bifunctional chimeric nanobody inhibits circularly permuted (cpGFP) fluorophore maturation until agonist binding recruits the nanobody to the active GPCR, allowing cpGFP to mature and fluoresce. (B) Crystal structure of nanobody 39 (Nb39) showing how each loop region was defined. PDB: 5C1M. (C) Crystal structure of nanobody 80 (Nb80) bound to B2AR Nb80 loop 3 position highlighted. Numbers on the expanded Nb80 view refer to the positions that were screened for replacement. PDB: 3P0G (D) Quantification of the original testing of each Nb39 loop at Nb80 position 3 in comparison to previous generation integrators mu opioid receptor (MOR)-SPOTIT and B2AR-SPOTall. All were stimulated with their respective agonists (10 µM fentanyl or isoproterenol) for 24 hours. The numbers above each bracket are the SBR between stimulated and unstimulated conditions. All significance was calculated using a two-tailed Welch's t-test. Stars indicate the degree of significance as follows *, P<0.05, **, P<0.01, ***, P<0.001, ****, P<0.0001. Dots on the plot indicate the mean of three technical replicates. n = 3. The thick horizontal bar is the mean of the three technical replicates and the error bars are the SEM.

We screened several positions within Nb80 for Nb39 loop replacement and found that grafting at positions 2 and 3 yielded favorable SBRs and the highest activation (Figure 2-2A). These replacements were likely successful due to their location at the B2AR–Nb80 interface. We hypothesize steric hindrance occurs upon receptor activation preventing the chimeric nanobody from interacting with the cpGFP, allowing the fluorophore to mature.

Nb80 Position 3 appeared the most promising in initial screening, so we focused on position 3 for more extensive screening. Among the eight B2AR-SENSIT designs with Nb39 loop grafting at Nb80 position 3, five exhibited B2AR agonist dependent fluorescence activation (Figure 2-1D). For further characterization and optimization, we selected the chimeric Nb80 position 3 replaced with Nb39 loop 7 (P3L7). P3L7 has comparable brightness to MOR-SPOTIT2 and a robust signal to background ratio (SBR) of 10.5, calculated as activation signal divided by background signal (Figure 2-1D). This sensor was named B2AR-SENSIT1.0. Because evaluating subsequent optimization strategies required only a single representative sensor, we selected B2AR-SENSIT1.0 for further development, recognizing that P3L2 and P3L3 (Figure 2-1D) remain promising candidates with comparable or better SBRs.

2.2.1 Selecting the Best cpGFP Variant

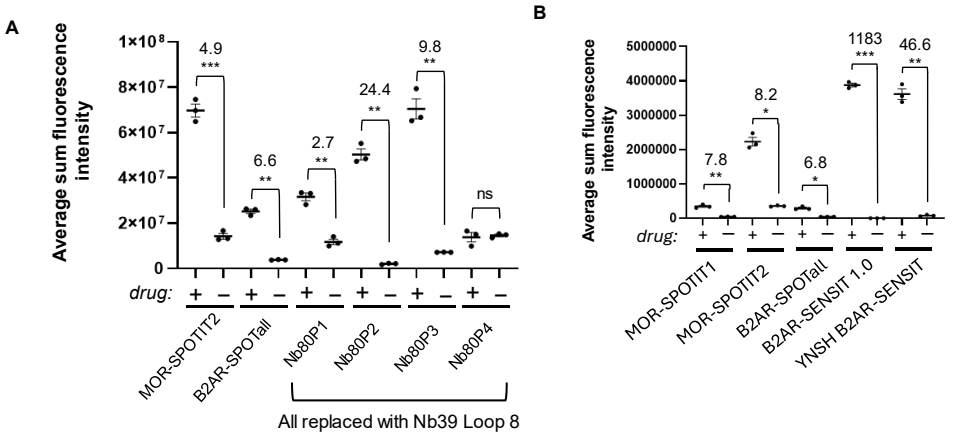


Figure 2-2: Finding the best Nb80 positions to replace and the best cpGFP variant for SENSIT. (A) Quantification of an experiment replacing each Nb80 position listed in (S1A) with Nb39 loop 8 to determine the optimal insertion position. MOR-SPOTIT was stimulated with 10 µM fentanyl for 24 hours and B2AR-SPOTall and all chimeric nanobody SENSIT were stimulated with 10 µM isoproterenol for 24 hours. (B) Quantification of the MOR-SPOTIT1 with a truncated cpGFP, MOR-SPOTIT2 with an improved YNSH-cpGFP, B2AR-SPOTall with the original truncated cpGFP and B2AR-SENSIT with and without the YNSH cpGFP variant. For (A) and (B): The numbers above each bracket are the SBR between stimulated and unstimulated conditions. All significance was calculated using an unpaired two-tailed Welch's t-test. Stars indicate the degree of significance as follows *, P<0.05,

**, P<0.01, ***, P<0.001, ****, P<0.0001. Dots on the plot indicate the mean of three technical replicates. n = 3. The thick horizontal bar is the mean of the three technical replicates and the error bars are the SEM.

During the initial design of MOR-SPOTIT we found that adding back four residues (YNSH) from EGFP to the N-terminus of cpGFP greatly improved the maximum signal, so MOR-SPOTIT2 cpGFP contains YNSH.10 We probed the effect of adding back the YNSH residues on the N-terminus of cpGFP for SENSIT, believing it could increase the brightness of B2AR-SENSIT1.0. However, adding YNSH increased background without increasing maximum brightness in B2AR-SENSIT (Figure 2-2B). We believe this could be because cpGFP folds differently in MOR-SPOTIT than in B2AR-SENSIT. The cpGFP's fluorophore is sensitive to its immediate environment as a result of circular permutation, so even slight differences in the structural environment between MOR-SPOTIT's and B2AR-SENSIT's cpGFP could lead to this difference. Therefore, we continued with B2AR-SENSIT1.0, without YNSH in cpGFP.

2.3 Mechanistic Interrogation of cpGFP Maturation Inhibition

While the mechanism by which Nb39 inhibits cpGFP fluorophore maturation remained elusive, the design of chimeric nanobodies provides a new platform to interrogate this process. We investigated the Nb39 and cpGFP interaction in a simplified GPCR-free system that still allows for controlled removal of Nb39 from cpGFP. This was achieved by fusing Nb39 and cpGFP via a linker containing the tobacco etch virus protease (TEVp) cleavage site (TEVcs) based on the SPOTon design (Figure 2-3A).[62] In the absence of TEVp, the tethered Nb39 inhibits cpGFP fluorophore maturation. When TEVp is coexpressed, the TEVcs is cleaved and the weakly bound Nb39 dissociates, allowing the cpGFP fluorophore to mature.



Figure 2-3: Loop deletion study. (A) Schematic of the experimental design for testing Nb39 with loop deletions of 4 core residues from each loop region. (B) Defining which residues from each Nb39 were deleted in the loop

deletion experiment Figure 2-3C. Red corresponds to deleted residues. (C) Loop core residue deletion study, showing fluorescence imaging quantification of the experiment described in the Figure 2-3A. All significance was calculated using a two-tailed Welch's t-test. Stars indicate the degree of significance as follows *, P<0.05, **, P<0.01, ***, P<0.001, ****, P<0.0001. Dots on the plot indicate the mean of three technical replicates. n = 3. The thick horizontal bar is the mean of the three technical replicates and the error bars are the SEM.

The results from replacing Nb80 position 3 with single Nb39 loops showed that multiple Nb39 loops were capable of fluorophore maturation inhibition. To further investigate the effect of Nb39 loops, we deleted three to four residues from each Nb39 loop region to fully disrupt the structure of these loop regions (Figure 2-3B). We hypothesized that if any loop deletion mutant abolished the capability of Nb39 to inhibit cpGFP fluorophore maturation, that construct would always be fluorescent, even if TEVp did not remove the Nb39 variant. Interestingly, none of the loop deletion mutants increased the background fluorescence in the no TEVp condition, indicating a single loop deletion is not sufficient to disrupt Nb39's fluorophore maturation inhibition capability (Figure 2-3C). This is consistent with our previous Nb39 loop grafting experiment (Figure 2-1D), in which multiple Nb39 loops grafted alone into Nb80 exhibit cpGFP fluorophore inhibition abilities. Therefore, deleting one loop at a time in Nb39 did not abolish fluorophore maturation inhibition abilities, because other Nb39 loops are able to compensate and still inhibit the fluorescence.

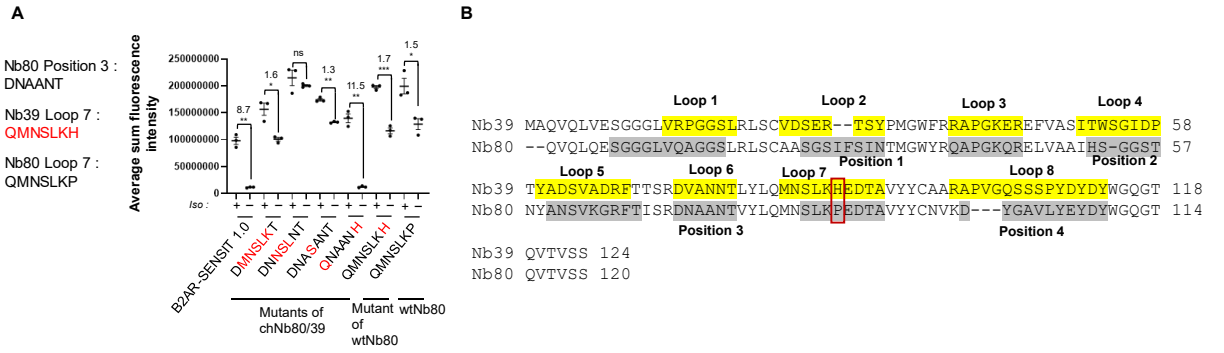


Figure 2-4: Probing the amino acid sequence of the chimeric nanobody compared to wtNb80 sequence. (A) Probing the amino acid sequence effect of the grafted Nb39 loop 7 in chimeric Nb80/Nb39 and wtNb80 position 3 residues. Fluorescence imaging quantification. B2AR-SENSIT chimeric nanobody mutants were stimulated with 10 µM isoproterenol for 24 hours. The numbers above each bracket are the SBR between stimulated and unstimulated conditions. All significance was calculated using a two-tailed Welch's t-test. Stars indicate the degree of significance as follows *, P<0.05, **, P<0.01, ***, P<0.001, ****, P<0.0001. Dots on the plot indicate the mean of three technical replicates. n = 3. The thick horizontal bar is the mean of the three technical replicates and the error bars are the SEM. (B) Nb39 and Nb80 sequence alignment where Nb39 loops are highlighted in yellow and Nb80 loops are highlighted in gray. Labels identify each Nb39 loop and Nb80 position. The red box highlights the Nb80 point mutation from Figure 2-4A.

The chNb80/39 in B2AR-SENSIT1.0 enables the probing of individual loops to study their specific roles in inhibiting cpGFP fluorophore maturation. We next examined the role of chNb80/39 P3L7 loop composition. We designed a series of B2AR-SENSIT1.0 mutants by systematically reverting chNb80/39 back to the wild type Nb80 (wtNb80) counterpart, as shown in Figure 2-4A. The chimeric Nb80/Nb39 (chNb80/39) mutant with only 2 amino acids at the two ends of the loop reverted to wtNb80 residues already exhibited high background without stimulation (Figure 2-4A, first mutant), suggestive of a weakened ability for inhibiting cpGFP fluorophore maturation. Further mutations resulted in even higher background. Notably, the chNb80/39 mutant with only the first and last residue of P3L7 showed low background fluorescence without stimulation (Figure 2-4A). This result suggests that the first and last residue of Nb39 loop 7 likely play a role in the cpGFP fluorophore maturation inhibition.

In addition, sequence alignment of Nb80 and Nb39 showed a highly conserved loop sequence differing by only one amino acid (Figure 2-4B). This led us to include a wtNb80 mutant that had this P87H single point mutation to resemble Nb39 loop 7 (Figure 2-4A). This mutant exhibited high background with an SBR of ~ 2 (Figure 2-4A, last mutant), suggesting weak inhibition. As a control for the Nb80 P87H mutant we also compared to wtNb80 in the SENSIT system. Intriguingly, we found that wtNb80 also exhibits weak inhibition fairly similar to the P87H mutant (Figure 2-4A). A nanobody such as Nb80 may already contribute to cpGFP fluorophore maturation inhibition, although Nb39 and chimeric nanobodies with Nb39 loops clearly have a stronger influence. This finding indicates that the cpGFP inhibition is dependent on the loop composition as well as position in the nanobody.

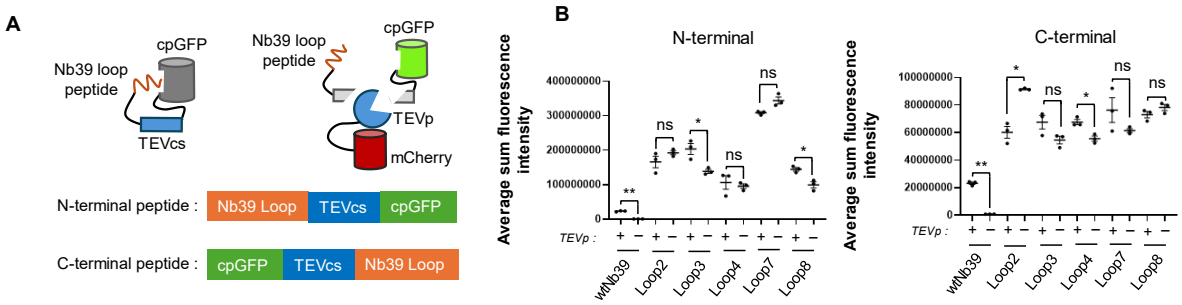


Figure 2-5: Determining if Nb39 loop sequences can function as peptides. (A) Schematic of the experimental design for testing if Nb39 loops as peptides alone can still inhibit cpGFP. (B) Fluorescence imaging quantification of the experiment described in the Figure 2-5A. All significance was calculated using a two-tailed Welch's t-test. Stars indicate the degree of significance as follows *, P<0.05, **, P<0.01, ***, P<0.001, ****, P<0.0001. Dots on

the plot indicate the mean of three technical replicates. n = 3. The thick horizontal bar is the mean of the three technical replicates and the error bars are the SEM.

Since loop positioning is critical, we next investigated whether the nanobody scaffold itself is essential for inhibiting cpGFP fluorophore maturation. Using the TEVcs fusion system, we replaced the chimeric nanobody with the Nb39 loop residues expressed as an unstructured peptide (Figure 2-5A). As expected, these constructs exhibited high background fluorescence (Figure 2-5B), suggesting the peptide sequence without the structural constraints of the nanobody scaffold could no longer inhibit cpGFP fluorophore maturation.

In summary, these mechanistic studies suggested the critical importance of the loop positioning, structure, and sequence for inhibition of cpGFP fluorophore maturation.

2.4 Mammalian Cell-based chNb80/Nb39 Directed Evolution Efforts and chNb80/Nb39 Variants Rescreening

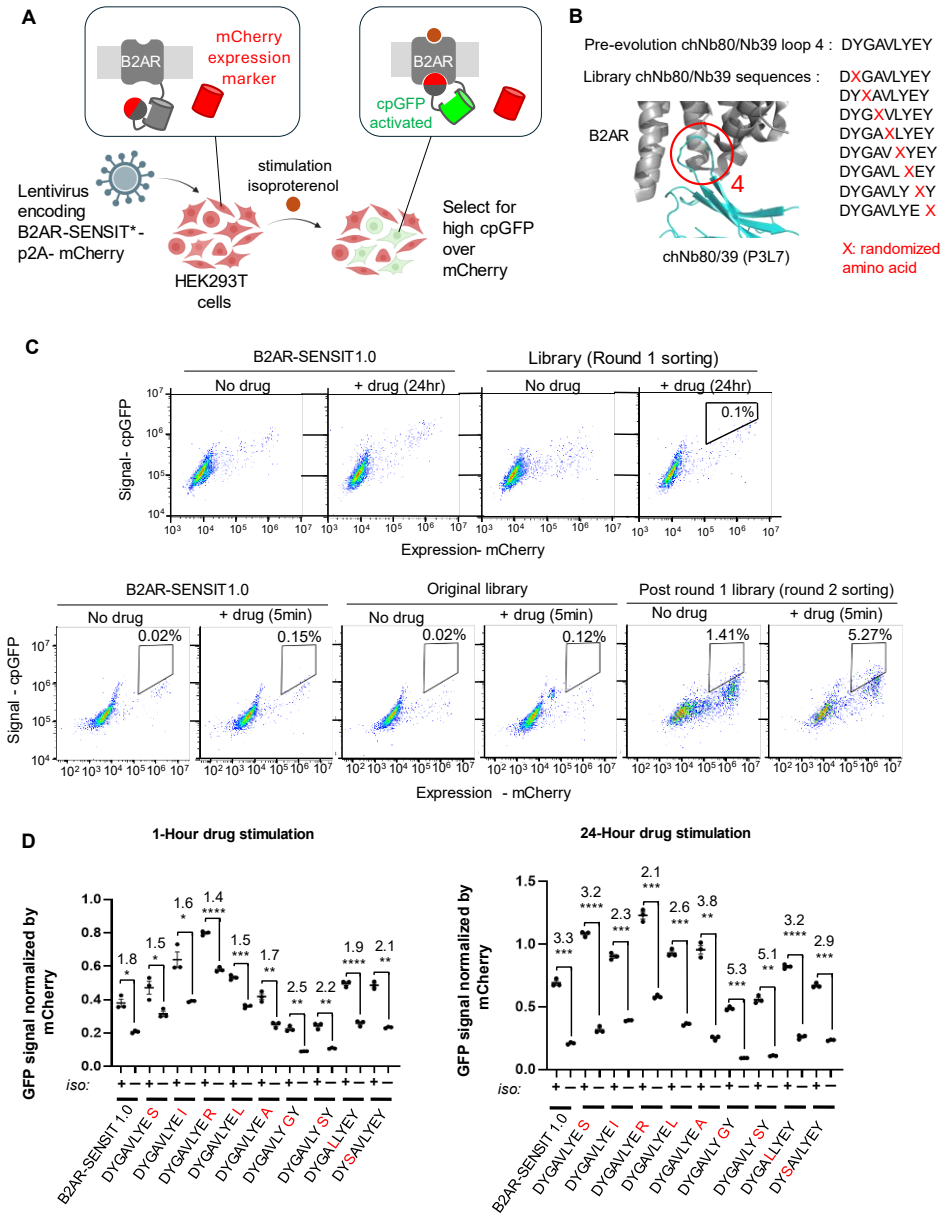


Figure 2-6: Directed evolution of the chimeric Nb80/Nb39 portion of B2AR-SENSIT. (A) Schematic for the evolution platform in HEK293T cells infected with lentivirus containing the B2AR-SENSIT library DNA (SENSIT*). FACS selection parameters are for high cpGFP from B2AR-SENSIT, and high mCherry, the expression marker. (B) Schematic for the library design with targeted mutations of the chimeric Nb80/Nb39 loop that binds to B2AR. Eight residues of the chimeric nanobody binding loop were targeted for site-saturated mutagenesis generating a library with single point mutations possible at each position. PDB: 5C1M. (C) FACS selection schematics for sorting strategy 1. Includes a round 1 with 24-hour drug stimulation sorting followed by a round 2 with 5-minute drug stimulation sorting. Representative gating mechanism is shown. (D) Quantification of the chimeric Nb80/Nb39 single mutants identified through directed evolution compared to the starting point B2AR-

SENSIT1.0. The numbers above each bracket are the SBR between stimulated and unstimulated conditions. All significance was calculated using an unpaired two-tailed Student's t test. Stars indicate the degree of significance as follows *, P<0.05, **, P<0.01, ***, P<0.001, ****, P<0.0001. Dots on the plot indicate the mean of three technical replicates. n = 3. The thick horizontal bar is the mean of the three technical replicates and the error bars are the SEM.

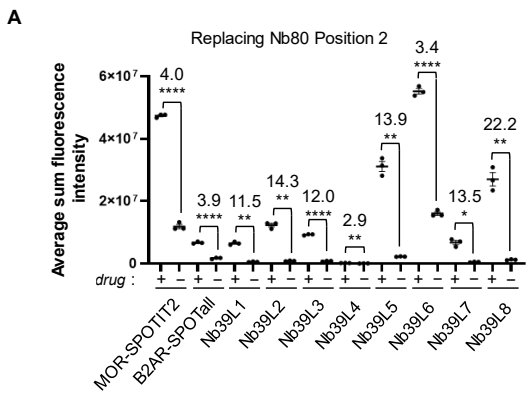
We previously observed that B2AR-SENSIT1.0 requires one day (24-hours) of agonist stimulation to achieve high SBRs, while 1 hour of drug stimulation leads to low activation and SBRs. This long stimulation time requirement would greatly limit B2AR-SENSIT's applications in animal models, as epinephrine release is transient. To address this limitation, we employed directed evolution to further improve B2AR-SENSIT's response time to agonist stimulation.

We opted to use mammalian cell-based directed evolution methods (Figure 2-6A) to ensure efficient membrane trafficking of B2AR-SENSIT and introduced a P2A sequence followed by mCherry to monitor sensor expression. For the library design, we sought to improve the binding between B2AR and chNb80/39 by targeting the loop that directly binds B2AR's intracellular G-protein binding pocket. We used site-saturation random mutagenesis to generate a library of single mutants for each residue of chNb80/39 loop 4 (Figure 2-6B). A B2AR-SENSIT library was then prepared in lentivirus for infection in HEK293T cells, with subsequent agonist stimulation and fluorescence-activated cell sorting (FACS) (Figure 2-6A).

In the first round of sorting, we stimulated the cells expressing the library of SENSIT mutants with agonists for 24 hours and then selected the population with the highest GFP/mCherry ratios, about 0.1% of the total population (Figure 2-6C, top row). In the second round, we stimulated the cells with agonists for only 5 minutes for an additional round of positive selection (Figure 2-6C, bottom row). The gating strategy for the second round can be found in Appendix Figure A-2A. A stricter strategy was also implemented, in which the original library was stimulated for 5 minutes only followed by positive sorting (Appendix Figure A-2B). Both sorted libraries were analyzed using next generation sequencing to identify enriched mutants (Appendix Figure A-2C).

We characterized nine of the highest enriched mutants with 1 hour and 24 hour stimulation with isoproterenol. Compared to B2AR-SENSIT1.0, most of these mutants exhibited simultaneous increases or decreases in both background and activation signal (Figure 2-6D). Notably, two mutants, E106G and E106S, showed 1 hour stimulation SBRs of 2.5 and 2.2, respectively, a notable increase from the 1.8 SBR observed with B2AR-SENSIT1.0 (Figure 2-6D). Another variant, Y107R, showed the largest increase in activation signal but also a

significant increase in background signal (Figure 2-6D). We hypothesized a combination of E106G or E106S and Y107R could enhance the activation signal while retaining a good SBR.



B

Construct	1hr	24hr
MOR-SPOTIT2	3.4 ± 0.2	5.5 ± 0.5
B2AR-SPOTall	1.4 ± 0.1	1.8 ± 0.2
Position 2 Loop 5	3.7 ± 0.3	18.9 ± 1.8
Position 2 Loop 8	3.3 ± 0.3	26.8 ± 2.1
Position 3 Loop 2	2.8 ± 0.3	12.3 ± 1.2
Position 3 Loop 3	2.5 ± 0.2	5.6 ± 0.4
Position 3 Loop 7	2.0 ± 0.2	5.6 ± 0.4

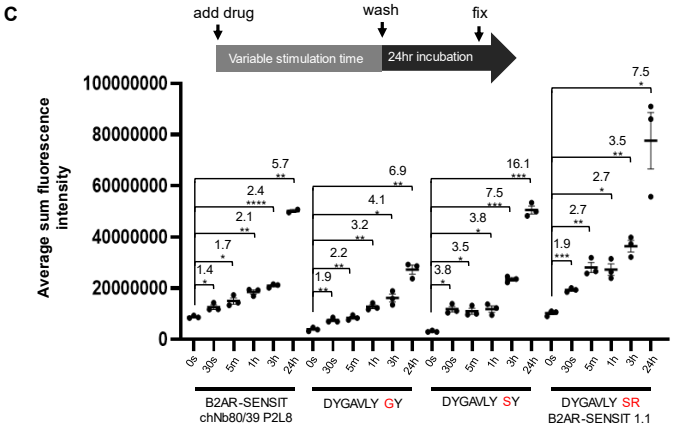


Figure 2-7: Identifying the best chimeric nanobody for the final B2AR-SENSIT1.1. (A) Fluorescence imaging quantification of Nb80 position 2 replacement with each of the eight Nb39 loops. All were stimulated with their respective agonists (10 µM fentanyl or isoproterenol) for 24 hours. (B) Table summarizing the SBRs for the best chimeric Nb80/Nb39 along with MOR-SPOTIT2 and B2AR-SPOTall with 1-hour and 24-hour stimulation. Stimulation is same as described in (A). (C) Fluorescence imaging quantification of SENSIT variants using the P2L8 nanobody and its mutants, E106G, E106S and E106S/Y107R. For (A) and (C): All significance was calculated using a two-tailed Welch's t-test. Stars indicate the degree of significance as follows *, P<0.05, **, P<0.01, ***, P<0.001, ****, P<0.0001. The numbers above each bracket are the SBR between stimulated and unstimulated conditions. Dots on the plot indicate the mean of three technical replicates. n = 3. The thick horizontal bar is the mean of the three technical replicates and the error bars are the SEM.

In parallel to the mammalian cell-based directed evolution, we rescreened chNb80/39 designs by replacing Nb80 position 2 with each Nb39 loop (Figure 2-7A and Appendix Figure A-3A). Notably, Nb39 loop 5 at Nb80 position 2 exhibited a SBR of 13.9, much higher than the SBR of 1.6 when at Nb80 position 3 (Figure 2-1D and 2-7A). This underscores that the position of Nb39 loop insertion is critical for inhibiting fluorophore maturation. Insertion of Nb39 loops 7

and 8 at Nb80 position 2 and 3 all yielded high SBRs, with the best SBR of 22.2 resulting from Nb80 position 2 with Nb39 loop 8 insertion (P2L8) (Figure 2-7A).

To select the chNb80/39 with the best sensitivity to agonist stimulation time, we characterized the top five chNb80/39 variants from both position 2 and 3, using 1-hour and 24-hour agonist stimulation (Figure 2-7B and Appendix Figure A-3B). Among these variants, P2L8 exhibited a high SBR of 3.27 after 1 hour of drug stimulation compared to the SBR of 2.0 for B2AR-SENSIT 1.0 P3L7 insertion. P2L8 also showed the highest overall SBR of 26.7 with 24-hour agonist stimulation (Figure 2-7B).

Building on the chimeric nanobody rescreening and the directed evolution results, we introduced the single mutations E106G and E106S, as well as the double mutation E106S and Y107R into the P2L8-SENSIT variant. We characterized their SBRs across a series of agonist stimulation times ranging from 30 seconds to 24 hours (Figure 2-7C). The E106S/Y107R double mutant exhibited the highest activation signal with 5 minutes of stimulation and a strong SBR of 7.5 with 24 hour stimulation (Figure 2-7C). We designated this improved variant as B2AR-SENSIT1.1.

2.4.1 Directed Evolution of cpGFP in SENSIT

In addition to evolving the chNb80/39 we utilized another approach for increasing the SBR at lower agonist stimulation times, by evolving the cpGFP with YNSH simultaneously targeting the first 3 residues (YNS) for site-saturated mutagenesis (Figure 2-8A). We hypothesized that YNSH were at a critical position for effecting cpGFP's fluorophore, but that a different amino acid sequence than YNSH could improve the SBR. After one round of sorting, a greater difference in the no drug versus plus drug library was observed, so we analyzed these cells using next-generation sequencing (Figure 2-8B and 2-8C). Among the mutants we chose to focus on the GHA and ENG sequences, from initial screening of the top variants. We tested these mutants in B2AR-SENSIT 1.1 (which does not contain YNSH residues) compared to SENSIT variants with YNSH-cpGFP and B2AR-SENSIT1.0 P3L7 chimeric nanobody or the B2AR-SENSIT1.1 P2L8 chimeric nanobody. Neither sequence improved the SBR at 1 hour in comparison to B2AR-SENSIT1.1 (Figure 2-8D). Therefore, we proceeded with characterization of B2AR-SENSIT1.1.

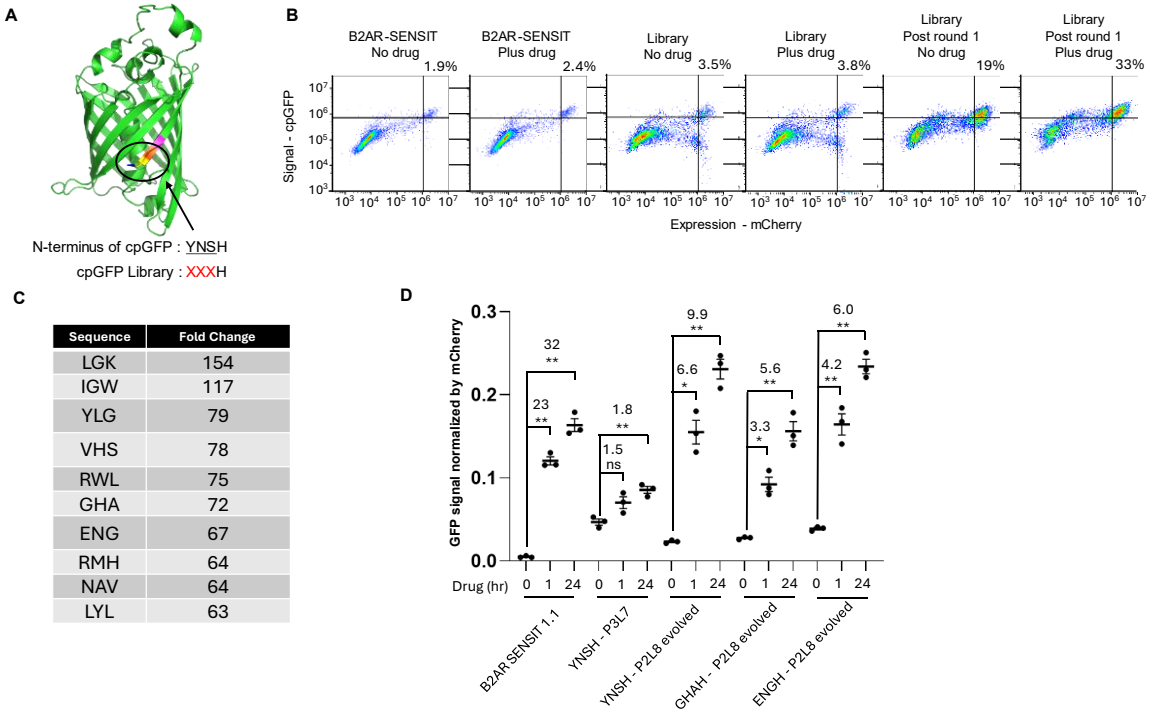


Figure 2-8: Directed evolution of the SENSIT cpGFP. (A) Schematic for the library design strategy behind cpGFP evolution. Using the cpGFP including the YNSH residues (shown in blue, yellow, orange, and pink respectively), the circled YNS residue positions were randomized for site-saturated mutagenesis. Model cpGFP is an Alphafold 3 predicted structure. (B) Representative flow cytometry plots from FACS where the upper right quadrant represents the population of interest. The number above this quadrant is the percent of the total cell population present within that quadrant. (C) Table summarizing next generation sequencing results for the cpGFP directed evolution. Column 1 is the identified amino acid sequence mutation compared to the unmutated YNSH-cpGFP. Column 2 is the fold change for number of times this sequence appears compared to the most common unmutated sequence. (D) Quantification of the comparison of new cpGFP mutants to B2AR-SENSIT1.1, as well as the B2AR-SENSIT1.0 (chimeric Nb80/Nb39 P3L7) with YNSH and B2AR-SENIST1.1 (chimeric Nb80/Nb39 P2L8 with E106S/Y107R) with YNSH. The numbers above each bracket are the SBR between stimulated and unstimulated conditions. All significance was calculated using a two-tailed Welch's t-test. Stars indicate the degree of significance as follows *, P<0.05, **, P<0.01, ***, P<0.001, ****, P<0.0001. Dots on the plot indicate the mean of three technical replicates. n = 3. The thick horizontal bar is the mean of the three technical replicates and the error bars are the SEM.

2.5 Discussion of SENSIT Development and Key Insights into Nb39-cpGFP Interaction

In this chapter, I introduce SENSIT, a highly modular single-chain fluorescent integrator platform that establishes a new design paradigm for genetically encoded neuromodulator sensing. The key innovation is a bifunctional, conformation-specific binding protein in which ligand recognition and fluorescent signal integration are unified by grafting a cpGFP fluorophore maturation–inhibitory motif into a defined structural loop. This architecture encodes the sensing

logic directly within a modular binding scaffold, eliminating the need for additional conformation specific nanobodies (as in SPOTall) or chimeric receptor design (as in SPLICEIT).

Beyond tool development, the SENSIT platform enabled mechanistic interrogation of cpGFP fluorophore maturation inhibition, revealing that both the amino acid composition of the inhibitory loop and its structural context within the grafted protein critically influence sensor function. These findings establish design rules for engineering fluorophore maturation–based integrators and inform future optimization strategies.

Finally, I established a protocol for direct directed evolution of the entire sensor in mammalian cell, a challenging system due to limitations of library size and also the time required to passage after sorting and prepare for further sorting and analysis. To increase the applicability of the SENSIT platform, directed evolution will be required.

2.6 Chapter 2 Bibliography

(62) Kroning, K.; Gannot, N.; Li, X.; Putansu, A.; Zhou, G.; Sescil, J.; Shen, J.; Wilson, A.; Fiel, H.; Li, P.; et al. Single-chain fluorescent integrators for mapping G-protein-coupled receptor agonists. *Proc Natl Acad Sci U S A* **2024**, *121* (18), e2307090121. DOI: 10.1073/pnas.2307090121 From NLM Medline.
(64) Huang, W.; Manglik, A.; Venkatakrishnan, A. J.; Laeremans, T.; Feinberg, E. N.; Sanborn, A. L.; Kato, H. E.; Livingston, K. E.; Thorsen, T. S.; Kling, R. C.; et al. Structural insights into mu-opioid receptor activation. *Nature* **2015**, *524* (7565), 315-321. DOI: 10.1038/nature14886 From NLM Medline.
(65) Rasmussen, S. G.; Choi, H. J.; Fung, J. J.; Pardon, E.; Casarosa, P.; Chae, P. S.; Devree, B. T.; Rosenbaum, D. M.; Thian, F. S.; Kobilka, T. S.; et al. Structure of a nanobody-stabilized active state of the beta(2) adrenoceptor. *Nature* **2011**, *469* (7329), 175-180. DOI: 10.1038/nature09648 From NLM Medline.
(66) Mitchell, L. S.; Colwell, L. J. Comparative analysis of nanobody sequence and structure data. *Proteins* **2018**, *86* (7), 697-706. DOI: 10.1002/prot.25497 From NLM Medline.

Chapter 3 SENSIT Characterization, Expansion to other GPCRs, and Design of Chimeric MiniG

In this chapter I will discuss my work in characterizing the best experimental parameters for B2AR-SENSIT1.1 application, from HEK cell culture to rat neuronal culture, to mouse brain. Then, I will demonstrate the generalizability through design and characterization of B1AR-SENSIT, CHRM2-SENSIT, and B2AR-SENSIT2.0 which relies on a unique chimeric G protein mimetic, the engineered miniG protein.[2] This shows that the chimeric nanobody design principle can be expanded beyond nanobody scaffolds, and that one Nb39 loop region is sufficient for cpGFP inhibition even in a larger protein than a nanobody.

3.1 Materials and Methods

3.1.1 B2AR-SENSIT Agonist Exposure Experiment

Twenty to twenty-four hours after transfection with B2AR-SENSIT DNA, HEK293T cells were stimulated with 100 uL of isoproterenol diluted in complete media, for a final concentration of 10 µM within the well. Cells were incubated for 30s, 5 min, 1 h, 3 h, 6 h, and 24

[2] Chapter 3 was largely adapted from the following publication:

Putansu, A., Soloweij, I., Rivett-Trznadel, H., Lakkanasirorat, B., Moran, L., Kroning, K., Liu, J., Li, X., Li, P., and Wang, W. "SENSIT, a modular single-chain fluorescent integrator platform for GPCR ligands." (Manuscript under revision).

Aubrey Putansu wrote the entirety of the above article, with editing from Isabel Soloweij, Hannah Rivett-Trznadel, Benya Lakkanasirorat, Lexie Moran, Kayla Kroning, Gwen Shingles, Jiahui Ding, Professor Peng Li, and Professor Wenjing Wang. Isabel Solowiej conducted the neuron and animal experiments for B2AR-SENSIT1.1. Xiaoyan Li did all the cloning of the miniG constructs. Lexie Moran completed the B2AR-SENSIT2.0 miniG cell culture experiment.

h. After the incubation time cells were washed twice with complete media and left in media for 24 hours. The cells were then fixed and imaged at 20× with a CAPS pH 11 buffer.

3.1.2 B2AR-SENSIT Maturation Experiment

Twenty to twenty-four hours after transfection with B2AR-SENSIT DNA, HEK293T cells were stimulated with 100 uL of isoproterenol diluted in complete media, for a final concentration of 10 µM within the well. Then cells were fixed after stimulation at each time point 1 h, 3 h, 6 h, 8 h, and 24 h to capture fluorophore maturation progress. For the 0 h time point the cells were never stimulated but fixed at the same time as the 24 h condition. After fixation, plates were stored in PBS buffer until the day of imaging awaiting the 24 h condition. The cells were then imaged at 20× with a CAPS pH 11 buffer.

3.1.3 B2AR-SENSIT pH Titration

Twenty to twenty-four hours after transfection with B2AR-SENSIT DNA, HEK293T cells were stimulated with 100 uL of isoproterenol diluted in complete media, for a final concentration of 10 µM within the well. Twenty-four hours after stimulation cells were fixed and imaged in a range of buffers to cover distinct pH ranges; 1× PBS for pH 6 and 7, 100 mM Tris for pH 7.5, 8, and 9, and 100 mM CAPS for pH 10 and 11.

B2AR-SENSIT Selectivity

Twenty to twenty-four hours after transfection with B2AR-SENSIT DNA, HEK293T cells were stimulated with 100 uL of selected drug for panel which included isoproterenol, epinephrine, norepinephrine, dopamine, serotonin, and butoxamine and each was diluted in complete media. The final well concentration was 10 µM for each. Twenty-four hours after stimulation cells were fixed and imaged with a CAPS pH 11 buffer.

3.1.4 B2AR-SENSIT Dose Response

Twenty to twenty-four hours after transfection with B2AR-SENSIT DNA, HEK293T cells were stimulated with varying concentrations of epinephrine or norepinephrine to achieve the following final well concentrations; 500 pM, 1 nM, 5 nM, 10 nM, 50 nM, 100 nM, 500 nM, 1 µM, 5 µM, 10 µM, 50 µM, 100 µM, 500 µM, and 1 mM. Due to the sensitivity for isoproterenol the final well concentrations were adjusted to the following; 50 pM, 100 pM, 500 pM, 1 nM, 5 nM, 10 nM, 50 nM, 100 nM, 500 nM, 1 µM, 5 µM, 10 µM, 50 µM, and 100 µM. All

preparations were diluted in complete media. Twenty-four hours after stimulation cells were fixed and imaged with a CAPS pH 11 buffer.

3.1.5 Rat Neuronal Culture

E18 Sprague-Dawley Rat Whole Brain (TransnetYX, Cat no. SDEWB) was dissociated with L-Cys-activated papain solution pH 6.5 containing 2 mL of L-Cysteine (Sigma, Cat no. 30089) and 100 µL papain (Sigma, Cat no. P3125). After dissociation, 1x105 neuronal cells were plated into each well of a 48 well plate precoated with 400 µL of poly-D-lysine (0.1 mg/mL, Sigma, Cat no. P7280) and laminin (3 ug/mL, Sigma, Cat no. L2020) premixed solution. Neuronal cells were cultured at 37 C under 5% CO2 in plating medium and maintained by replacing 300 µL of old media with 500 µL of fresh neurobasal medium (NGM) every 4 days. The plating medium contained Neurobasal Plus Medium (Gibco), 2 % B27 supplement (Thermo Fisher Scientific), 1% GlutaMAX (Gibco), and 24% complete growth media. The NGM contained Neurobasal Plus Medium, 2% B27 supplement, and 1% GlutaMAX.

3.1.6 Viral Transduction of Neuronal Cultures

At DIV6, neuronal cultures were transduced with the addition of up to 1 µL concentrated B2AR and B1AR SENSIT AAV per well. The plate was returned to incubate at 37 C under 5% CO2.

Neuronal Culture Stimulation and Fixation

At DIV13 (7 days post transduction), neurons were stimulated by 1 µM isoproterenol (Sigma, Cat no. I6504) or equivalent volume of NGM and allowed to incubate for 24 hours at 37 C under 5% CO2. Following the incubation, neuronal cells were fixed for 30 minutes on ice with fixation solution comprised of 4% paraformaldehyde, 25 mM HEPES, 10 mM EGTA, 2 mM MgCl2, and 0.12 M sucrose at pH 7.3. Wells were washed once with PBS prior to addition of 200 µL pH 11.0 CAPS buffer and imaging.

3.1.7 B1AR- and CHRM2-SENSIT Characterization

B1AR-SENSIT characterization followed an identical procedure to B2AR-SENSIT, transfecting with 100 ng DNA and using 10 µM isoproterenol to stimulate for agonist exposure time experiment. Selectivity panel drug concentrations were 10 µM. All dose response curves ranged from 500 pM to 1 mM with the same intervals as described above for B2AR-SENSIT dose response.

CHRM2-SENSIT characterization followed an identical procedure, transfecting with 100 ng DNA but instead stimulating with 50 µM iperoxo for agonist exposure time experiment. Selectivity panel drug concentrations were 100 µM. All dose response curves ranged from 500 pM to 1 mM with the same intervals as described above for B2AR-SENSIT dose response. All images were fixed and taken at 20× with a CAPS pH 11 buffer.

3.1.8 Concentrated AAV Preparation for Stereotactic Injection

To prepare AAV1/2 concentrated virus, 5.2 µg viral construct DNA, 4.35 µg AAV1, 4.35 µg AAV2, 10.4 µg DF6 were incubated with serum free DMEM and mixed before adding PEI max solution and incubating for at least 10 minutes at RT before addition of DMEM, MEM, and FBS media. Four T150 flasks of HEK293T cells at approximately 80% confluence were then incubated with the viral DNA transfection mixture for 48 hours. Media was aspirated and the cell pellet was collected via cell scraping, collecting in DPBS, and centrifugation at 1,200 rpm. The DPBS is aspirated and the pellet is resuspended in 20 mL tris buffer containing 20 mM Tris 100 mM NaCl pH = 8.0. Freshly made 10% w/v sodium deoxycholate (Sigma-aldrich) in H2O was added to a final concentration of 0.5%, then benzonase nuclease (Sigma-aldrich) to a final concentration of 50 units per mL. This solution was incubated for 1 hour at 37 oC and cleared of cellular debris via centrifugation at 10,000 rpm for 10 minutes. The supernatant was loaded onto a pre-equilibrated, with 10 mL 150 mM NaCl, 20 mM Tris, pH=8.0 solution, HiTrap heparin column via peristaltic pump. The column was washed with 20 mM Tris pH 8.0 buffer with the following salt gradient of with 1 mL 200 mM NaCl then 1 mL 300 mM NaCl. The virus was eluted with 20 mM Tris pH 8.0 buffer and a salt gradient of 1.5 mL 400 mM NaCl, 3 mL 450 mM NaCl, and 1.5 mL 500 mM NaCl . Eluted virus was concentrated down with Amicon ultra centrifugal units at 6,000 rpm. 1mL of sterile DPBS, 35 mM NaCl, 5% glycerol was added to the centrifugal filter unit and centrifuged at 8,000 rpm until a final volume of 100-200 µL was achieved. The concentrated AAV was aliquoted into 10 µL and stored at -80 oC.

Viral titer was determined using SYBR Green quantitative PCR master mix protocol (Fisher Scientific) with measurements taken on an Applied Biosystems StepOnePlus Real-Time PCR System Thermal Cycling Block.

3.1.9 B2AR-SENSIT Mouse Testing

3.1.9.1 Mouse lines:

All procedures were conducted in accordance with NIH guidelines for the care and use of laboratory animals and were approved by the University of Michigan University Committee on the Use and Care of Animals. Mice were housed on a 12-h light/dark cycle with ad libitum access to food and water. All mouse strains used were on a C57BL/6J genetic background, and both male and female animals were included in the study.

3.1.9.2 Stereotactic injection:

Adult mice were anesthetized with isoflurane (3% for induction, 1.5% for maintenance) for bilateral stereotactic injection. Animals received 5 mg/kg of preemptive analgesic carprofen prior to placement in the stereotactic frame (David Kopf Instruments) and body temperature was maintained at 35 to 37 ℃ using a feedback-controlled heating pad (Physitemp, TCAT-2LV). The following coordinates were used for injections; LHA: 0.95 mm from midline, −1.40 mm posterior to bregma, and −5.25 mm ventral from bregma. Then, 1000 nL of the AAV1/2-CAG-B2AR SENSIT virus was injected into the LHA at a rate of 60 nL/min. After injection, the pipette was left in the brain for 10 min to allow for pressure to equalize.

3.1.9.3 Drug administration and histology:

Seven days post intracerebral viral vector delivery, 1000 nL of 10 mM of epinephrine drug or a saline control was injected locally into the LHA via stereotactic injection at 80 nL/min. After drug injection, the pipette was left in the brain for 5 minutes to allow for pressure to equalize. Twenty-four hours following drug injection, the mice were deeply anesthetized and transcardially perfused with 10 mL PBS followed by 10 mL 4% paraformaldehyde (PFA, Electron Microscopy Science, 15713). The brain tissue was extracted and postfixed in 4% PFA overnight. The tissue was cryopreserved in 30% sucrose for 48 hours and then embedded into optimum cutting temperature compound (OCT). The brain was sectioned into serial slices through the LHA at 40 microns with a Leica cryostat CM3050 S.

3.1.10 MiniGs-SENSIT Initial Testing and Engineering

Twenty to twenty-four hours after transfection with 100 ng Mini-Gs variant DNA, HEK293T cells were stimulated with 100 uL of isoproterenol diluted in complete media, for a final concentration of 10 µM within the well. No drug conditions had an equal volume of only

complete media. Twenty-four hours after stimulation cells were fixed, immunostained, and imaged at 20× with a CAPS pH 11 buffer.

Immunostaining procedure is identical to B2AR-SENSIT characterization.

3.1.11 Confocal Microscopy of HEK293T and Mouse Brain

All images were fixed cells in 100 mM CAPS 100 mM NaCl buffer kept at pH 11, except for images taken in the pH titration. Confocal imaging was performed on a Nikon inverted confocal microscope with 20× air objective and 60× oil immersion objective, outfitted with a Yokogawa CSU-X1 5000RPM spinning disk confocal head, and Ti2-ND-P perfect focus system 4, a compact 4-line laser source: 405 nm (100 mW) 488 nm (100 mW), 561 nm (100mW), and 640-nm (75 mW) lasers. The following combinations of laser excitation and emission filters were used for various fluorophores: EGFP/Alexa Fluor 488 (488 nm excitation; 525/36 emission), mCherry (568 nm excitation; 605/52 emission), Alexa Fluor 647 (647 nm excitation; 705/72 emission), and differential interference contrast (DIC). The acquisition time was 500ms at 30% laser intensity. The camera unit is an ORCA-Flash 4.0 LT + sCMOS camera. All images were taken with either the 20× or 60× objectives. To interface with the microscope and take images we used the Nikon NIS-Elements hardware control software and images were processed with NIS-Elements General Analysis 3 software.

For the mouse brain slices, sections were washed in 0.1% PBS Tween 20 three times before staining with DAPI dihydrochloride (Invitrogen) diluted 1:5,000 in PBS. After washing in 0.1% PBS Tween 20 three times, sections were then imaged as described above at 10×, with pH 11 buffer.

3.1.12 Confocal Microscopy of Neuron Culture

Neuronal cells were imaged with a Nikon inverted confocal microscope with the 10x air objective outfitted with a Yokogawa CSU-X1 5000RPM spinning disk confocal head, and Ti2-ND-P perfect focus system 4, a compact 4-line laser source: 405 nm (100 mW) 488 nm (100 mW), 561 nm (100mW), and 640-nm (75 mW) lasers. The combinations of laser excitation and emission filters were used as follows: EGFP (488 nm excitation; 525/36 emission), mCherry (568 nm excitation; 605/52 emission), and differential interference contrast (DIC). All images were taken with a 500 ms acquisition time, 50% laser intensity, and an ORCA-Flash 4.0 LT +

sCMOS camera. All images were collected and processed using the Nikon NIS-Elements software.

3.1.13 Analysis of HEK293T and Neuron Cell Images

All HEK293T cell experiments were done with three technical replicates meaning three wells per condition. Then ten images were taken per well, and the fluorescence mean intensity value was measured and taken from the NIS-Elements General Analysis 3 software. To determine the optimal threshold value for counting true signal above autofluorescence of the cells, we chose ten points devoid of cells on the plate and multiplied this background autofluorescence by 2. The same threshold is used for all conditions in a single experiment. Two values were taken from the cell images that have fluorescence values above the threshold, the mean intensity value and the total object area. The total object area is defined as the area of cells that are within the threshold value. Then the mean intensity is the count of fluorescence intensity from cells within the total object area. If the system did not use a co-expression of mCherry we then would multiply the total object area by the mean intensity value to calculate the sum intensity. Background subtraction for HEK293T experiments used the mean intensity of the plate without any cells present and multiplied by the total object area within the threshold, and then subtracted this from the sum intensity.

If the system did use a co-expression of mCherry we chose to normalize the fluorescent signal of the sensor cpGFP to the mCherry to account for differences in expression between wells and conditions. For this calculation we took the mean intensity and subtracted the background mean intensity, then multiplied by the total object area for each channel separately. To get the normalized signal we divided the cpGFP sum intensity with background subtraction by the mCherry sum intensity with background subtraction.

For HEK293T and rat neuronal culture experiments, the sum intensity of the 10 images from each technical replicate were averaged and plotted as one point on the graph. All images were included in analysis, unless they were blurry, had autofluorescent artifacts, or were primarily devoid of cells.

For mouse brain slice analysis, we manually defined 4 regions of interest (ROI) per injection site for 3 brain slices per mouse giving a total of 24 ROI per mouse. We then pulled the ROI statistics focusing on the mean intensity and area of each ROI per channel. Background was calculated from taking the mean fluorescence intensity per channel from 5 random non-

expressing brain slice regions. The background value was then multiplied by area and subtracted from the ROI mean intensity times area to give the average sum fluorescence intensity. Because the mCherry expression marker was present we calculated the normalized signal as described prior. We plotted all normalized signal values for each condition.

For all experiments, Prism GraphPah software was used for plotting, as well as performing unpaired Welch's *t* tests to calculate significance.

3.2 Characterization of B2AR-SENSIT1.1

B2AR-SENSIT1.1 contains the P2L8 chNb80/39 with the E106S/Y107R mutation (Figure 3-1A). To characterize the membrane-trafficking of B2AR-SENSIT1.1 we performed immunostaining of the sensor expressed in HEK cells. B2AR-SENSIT1.1 exhibited efficient membrane-trafficking (Figure 3-1B).

Next, we characterized the selectivity of B2AR-SENSIT1.1 by screening a panel of ligands, including isoproterenol (a strong synthetic agonist), epinephrine (the native agonist), norepinephrine (another native but weaker agonist), the antagonist butoxamine and several non-activating molecules. As expected, B2AR-SENSIT1.1 showed selective activity similar to B2AR (Figure 3-1C and Appendix Figure A-4A).[67]

To evaluate the sensitivity of B2AR-SENSIT1.1 to various agonists, we generated dose response curves for isoproterenol, epinephrine, and norepinephrine. Agonist was present for a full 24 hours in every concentration condition. B2AR-SENSIT1.1 preferentially detected epinephrine (EC50 = 225 nM) with 19-fold higher sensitivity than norepinephrine (EC50 = 4.45 µM) (Figure 3-1D, and Appendix Figure A-4B and A-4C). As expected, the sensor was most sensitive to the potent synthetic agonist isoproterenol with an EC50 of 45.5 nM (Figure 3-1D and Appendix Figure A-4D).

To characterize the temporal kinetics of B2AR-SENSIT1.1, we conducted a time-course experiment by exposing the sensor to agonist for varying durations, while agonist concentration was held constant. While B2AR-SENSIT1.1 exhibited the expected positive correlation between exposure time and activation signal, it notably achieved a robust SBR of 2.5 after only 5 minutes of isoproterenol stimulation (Figure 3-1E and Appendix Figure A-5A).

We next characterized the fluorophore maturation time for B2AR-SENSIT1.1. In this study, all samples were stimulated at the same time, and isoproterenol was present for the entirety of the experiment, but we varied the time at which the cells are fixed to terminate further

maturation. We tried 1, 3, 6, and 8 hours as well as the standard timepoint for fixation of 24 hours post stimulation. Higher activation signals were observed at longer stimulation times, mirroring the trends of previously published SPOTIT sensors (Figure 3-1F and Appendix Figure A-5B).

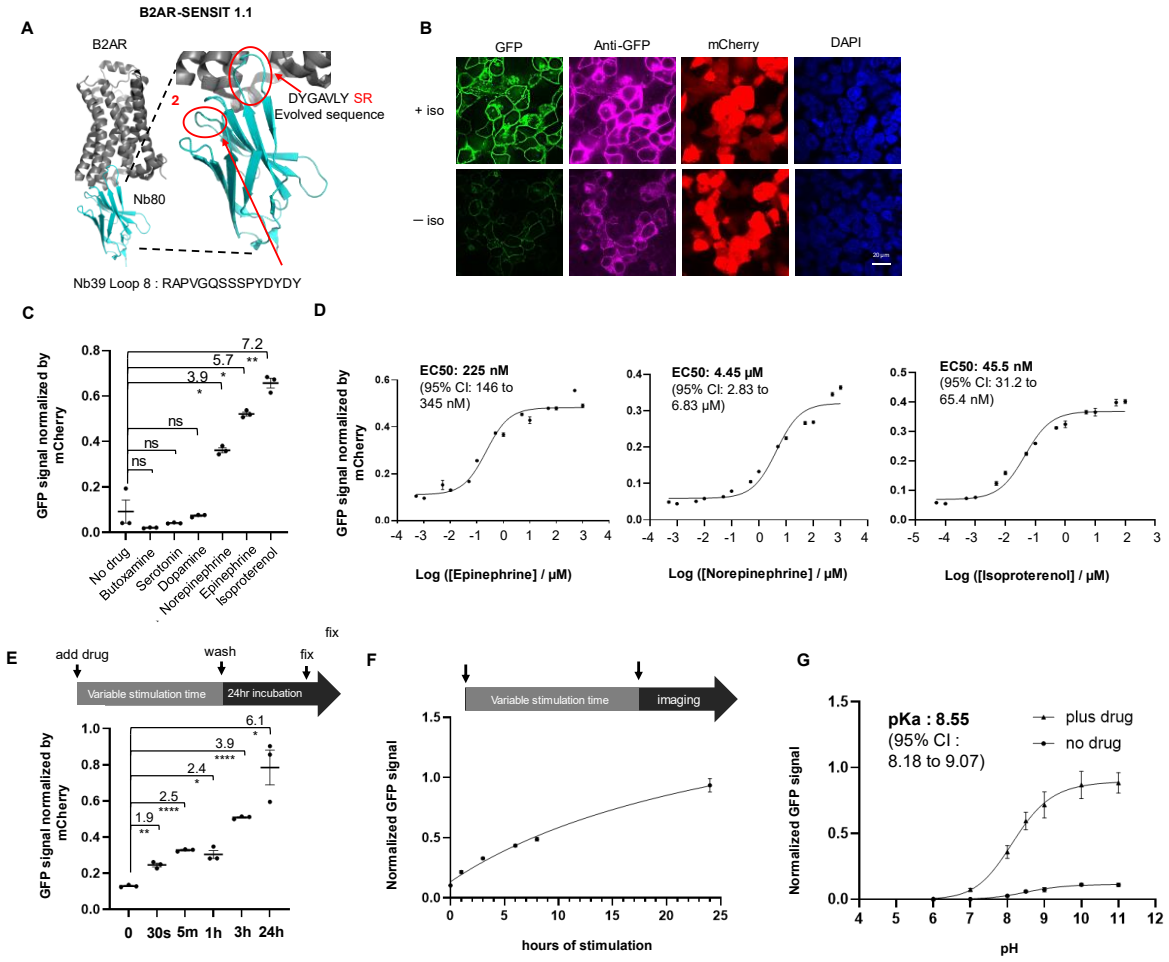


Figure 3-1: Characterization of B2AR-SENSIT1.1. (A) Schematic describing position 2 of Nb80 and sequence of Nb39 loop 8. The final chimeric nanobody in B2AR-SENSIT1.1 also includes the E106S/Y107R mutations in Nb80 position 4. PDB: 5C1M. (B) Representative fluorescence images of B2AR-SENSIT1.1 in HEK293T cells. Scale bar, 20 µm. Cells were stimulated with 10 µM isoproterenol. Twenty-four hours after stimulation, cells were fixed, immunostained, and imaged at pH 11. cpGFP, cpGFP fluorescence. Anti-GFP, protein expression level from immunostaining. mCherry, protein expression level. DAPI is a nuclear stain. (C) Selectivity characterization of B2AR-SENSIT1.1. The numbers above each bracket are the SBR between stimulated and unstimulated conditions. (D) Dose response characterization. EC_{50} displayed with the 95% confidence interval. (E) Temporal kinetic study of B2AR-SENSIT1.1. "s", seconds, "m", minutes, "h", hours. The numbers above each bracket are the SBRs between stimulated and unstimulated conditions. (F) Fluorophore maturation time characterization of B2AR-SENSIT1.1. After a variable stimulation time (0, 1, 3, 6, 8 and 24 hours), cells were immediately fixed and stored until imaged. For (C-F): All significance was calculated using a two-tailed Welch's t-test. Stars indicate the degree of significance as follows *, P<0.05, **, P<0.01, ***, P<0.001, ****, P<0.0001. Dots on the plot indicate the mean of three technical replicates. n = 3. The thick horizontal bar is the mean of the three technical replicates and the error bars are the SEM. (G) pKa determination for B2AR-SENSIT1.1. pKa is displayed with a 95% confidence interval. To

monitor the same fluorophores over various pH ranges, we imaged one field of view at pH 6, 7, 8, 8.5, 9. 10 and 11. Dots on the plot indicate the mean of three replicates. n = 3.

The pKa for the cpGFP in SPOTIT sensors was found to be higher than EGFP, necessitating imaging of the fixed cells and tissues at higher pH. Therefore, we performed pH titrations of B2AR-SENSIT1.1 from pH 6 to 11 using fluorescence imaging of fixed cells. B2AR SENSIT1.1 showed a pKa of 8.6, and consequently, SENSIT imaging should be done at pH 11 to ensure all fluorophores are deprotonated for the maximum fluorescence intensity (Figure 3-1H and Appendix Figure A-6A). In addition, mCherry fluorescence is also increased at pH 11 as shown in Appendix Figure A-6B.

3.2.1 B2AR-SENSIT Characterization in Rat Neurons and Mouse Brain

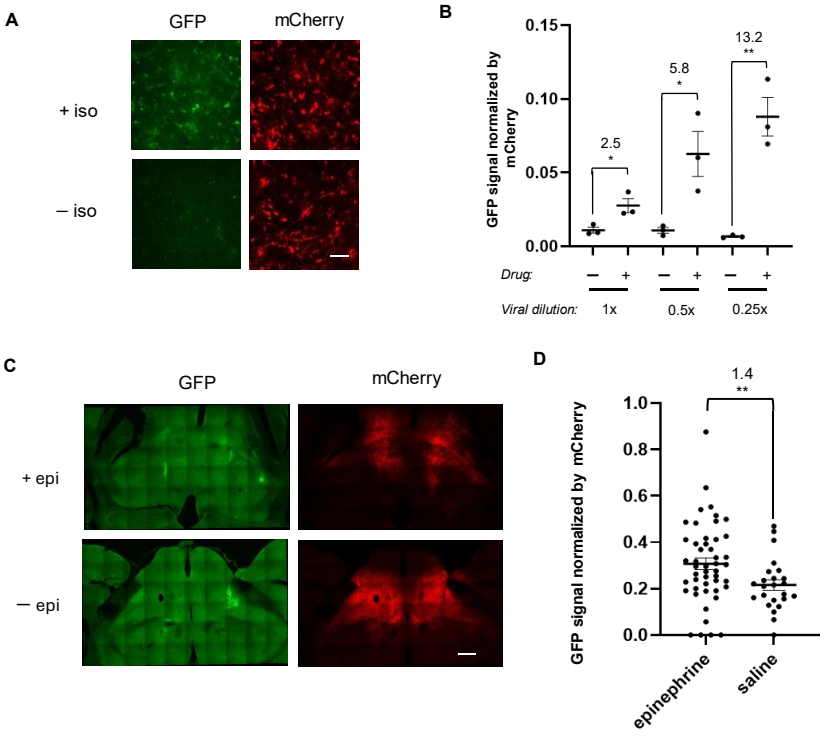


Figure 3-2: Application of B2AR-SENSIT1.1 *in vivo.* (A) Representative fluorescence images of B2AR-SENSIT1.1 in the rat neuronal culture cells. Scale bar indicates 100 µm. Cells were stimulated with 1 µM isoproterenol. Twenty-four hours after stimulation, cells were fixed, and imaged at pH 11. GFP, cpGFP fluorescence. mCherry, protein expression level. (B) Quantification of B2AR-SENSIT1.1 rat neuronal culture experiment. The concentrated AAV used to infect the neurons was either undiluted (1x) or diluted by half (0.5x) or one quarter (0.25x). The numbers above each bracket are the SBR between stimulated and unstimulated conditions. All significance was calculated using a two-tailed Welch's t-test. Stars indicate the degree of significance as follows *, P<0.05, **, P<0.01, ***, P<0.001, ****, P<0.0001. Dots on the plot indicate the mean of three technical replicates. n = 3. The thick horizontal bar is the mean of the three technical replicates and the error bars are the

SEM. (C) Fluorescence images of B2AR-SENSIT1.1 in mouse brain slices. Scale bar indicates 500 μm. GFP, cpGFP fluorescence. mCherry, protein expression level. Local stereotactic injection to the LHA administer either 10 mM epinephrine or saline blank. Mice were sacrificed twenty-four hours after stimulation. (D) Quantification of B2AR-SENSIT1.1 in mouse brain. The number above the bracket is the SBR between the stimulated and unstimulated condition. Each dot on the plot indicates the normalized GFP signal at a single region of interest in an expressing brain slice area. All significance was calculated using a two-tailed Welch's t-test. Stars indicate the degree of significance as follows *, P<0.05, **, P<0.01, ***, P<0.001, ****, P<0.0001. The thick horizontal bar is the mean and the error bars are the SEM.

Prior to conducting animal experiments, B2AR-SENSIT1.1 was tested in rat neuronal cultures with different dilutions of concentrated adeno-associated virus (AAV) 1/2 mixed serotype. We chose to use the chicken beta-actin promoter (CAG) for expression of B2AR-SENSIT1.1 in both neuron and glial cells to maximize sensor expression. Interestingly, the 0.25x dilution (1:4) viral infection condition showed the best SBR of 13.2 (Figure 3-2A and 3-2B).

With the success of B2AR-SENSIT1.1 in neurons we proceeded to application in mouse brain. AAV containing B2AR-SENSIT1.1-p2a-mCherry was injected bilaterally into the lateral hypothalamic area (LHA) and allowed to express for seven days. Epinephrine was administered by stereotactic injection to the LHA and mice were anesthetized 24 hours after stimulation for brain removal. B2AR-SENSIT exhibited a SBR of 1.4, showing a fluorescence increase in the presence of epinephrine stimulation (Figure 3-2C and 3-2D). This demonstrates that B2AR-SENSIT1.1 can be applied to detect epinephrine at large brain volumes. However, the SBR is low likely because the brief agonist exposure in the brain, due to rapid epinephrine clearance, limits sensor activation. Further directed evolution efforts as well as experimental optimization could improve B2AR-SENSIT1.1 for this application.

3.3 Characterization of B1AR-SENSIT

Given the importance of norepinephrine as a neuromodulator, we adapted the SENSIT platform for norepinephrine detection by leveraging the high-affinity binding of Nb80 for beta-1 adrenergic receptor (B1AR). We generated B1AR-SENSIT by replacing the B2AR in B2AR-SENSIT1.1 with B1AR (Figure 3-3A), and evaluated its activity and selectivity. We screened a panel of ligands, including known agonists for B1AR (norepinephrine, epinephrine, and isoproterenol) and non-activating compounds (dopamine and serotonin) (Figure 3-3B). As expected, the sensor responded exclusively to the known agonists.

We next characterized the temporal kinetics of B1AR-SENSIT. Similar to B2AR-SENSIT1.1, the sensor showed increasing SBRs with longer agonist stimulation time. Notably,

B1AR-SENSIT achieved an SBR of 4.6 after only 30 seconds of isoproterenol exposure (Figure 3-3C and Appendix Figure A-7A). Dose response curve characterization revealed that B1AR-SENSIT exhibits a 5-fold preference for norepinephrine (EC50 of 959 nM) over epinephrine (EC50 of 5.65 µM) (Figure 3-3D and Appendix Figure A-7B). Finally, we assessed the membrane trafficking for B1AR-SENSIT, confirming that it localizes to the membrane efficiently (Figure 3-3E).

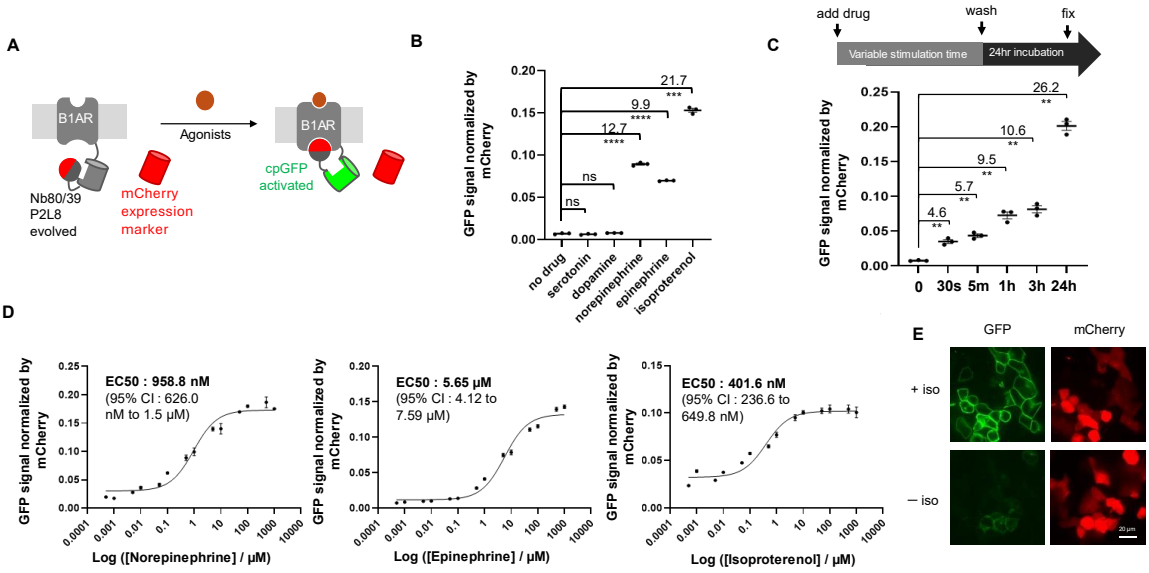


Figure 3-3: Characterization of B1AR-SENSIT. (A) Schematic showing the design of B1AR-SENSIT. (B) Selectivity of B1AR-SENSIT. The numbers above each bracket are the SBRs between stimulated and unstimulated conditions. (C) Temporal kinetics study of B1AR-SENSIT. Drug was washed away after a variable incubation time, and then allowed to incubate for 24 hours before fixation. "s", seconds, "m", minutes, "h", hours. The numbers above each bracket are the SBRs between stimulated and unstimulated conditions. (D) Dose response characterization for B1AR-SENSIT. EC_{50} displayed with the 95% confidence interval. (E) Representative fluorescence images of B1AR-SENSIT in HEK293T cells. Scale bar, 20 µm. Cells were stimulated with 10 µM isoproterenol. Twenty-four hours after stimulation, cells were fixed and imaged at pH 11. GFP, cpGFP fluorescence. mCherry, protein expression level from ribosomal skip sequence P2A followed by mCherry. For (B-D): All significance was calculated using a two-tailed Welch's t-test. Stars indicate the degree of significance as follows *, P<0.05, **, P<0.01, ***, P<0.001, ****, P<0.0001. Dots on the plot indicate the mean of three technical replicates. n = 3. The thick horizontal bar is the mean of the three technical replicates and the error bars are the SEM.

3.4 Characterization of CHRM2-SENSIT

To adapt the SENSIT platform to other neuromodulators, we designed another chimeric nanobody based on Nb9-8, a nanobody for muscarinic acetylcholine receptor 2 (CHRM2).[68] The Nb39 loop 8 was grafted to various loop positions of Nb9-8. The Nb9-8 loop 8 was specifically excluded as it is essential for CHRM2 binding (Figure 3-4A). Among these variants, the loop 3

replacement yielded the highest SBR of 12.5 when stimulated with iperoxo, exhibiting significantly higher fluorescence than our previous CHRM2-SPOTall (Figure 3-4B and 3-4C).[62] This sensor version was designated CHRM2-SENSIT.

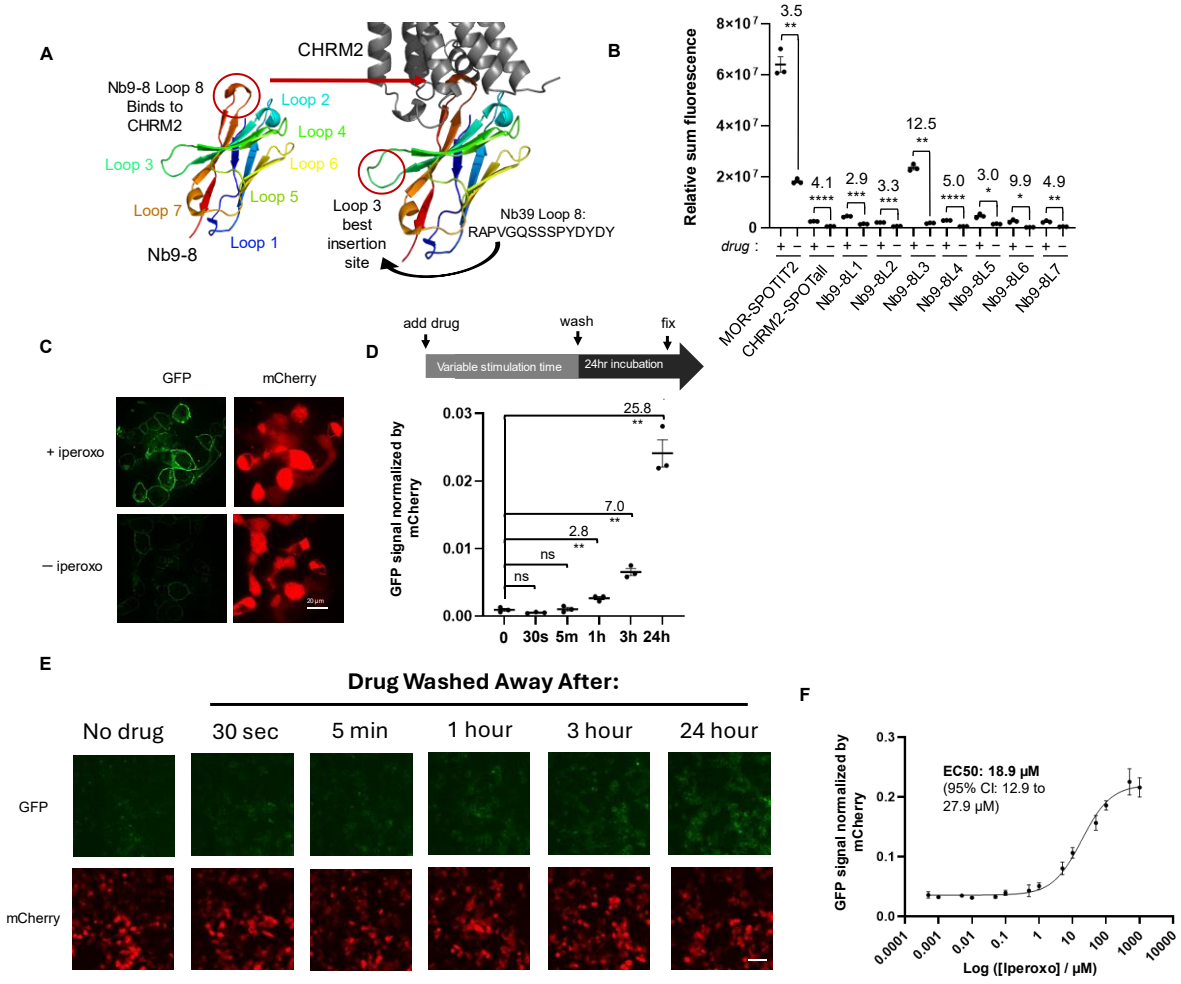


Figure 3-4: Characterization of CHRM2-SENSIT. (A) Schematic displaying the design of Nb9-8 highlighting each loop region as well as the best site (loop 3) that was replaced with Nb39 loop 8. PDB: 4MQS. (B) Quantification of the Nb9-8 each loop replacement with Nb39 loop 8 ("L" = loop). MOR-SPOTIT was stimulated with 10 µM fentanyl for 24 hours and CHRM2-SPOTall and all chimeric nanobody SENSIT were stimulated with 10 µM iperoxo for 24 hours. (C) Representative fluorescence images of CHRM2-SENSIT in HEK293T cells. Scale bar, 20 µm. Cells were stimulated with 50 µM iperoxo. Twenty-four hours after stimulation, cells were fixed and imaged at pH 11. GFP, cpGFP fluorescence. mCherry, protein expression level from ribosomal skip sequence P2A followed by mCherry. (D) Temporal kinetics study of CHRM2-SENSIT. Drug was washed away after a variable incubation time and then allowed to incubate for 24 hours before fixation. "s", seconds, "m", minutes, "h", hours. The numbers above each bracket are the SBRs between stimulated and unstimulated conditions. (E) Fluorescence images for (D) characterizing temporal kinetics of CHRM2-SENSIT stimulation. Each time point indicates how long drug was present before being washed away. (F) Dose response curve of iperoxo with CHRM2-SENSIT. EC_{50} displayed with the 95% confidence interval. For (B) (D) and (F): All significance was calculated using a two-tailed Welch's t-test. Stars indicate the degree of significance as follows *, P<0.05, **, P<0.01, ***, P<0.001, ****,

P<0.0001. Dots on the plot indicate the mean of three technical replicates. n = 3. The thick horizontal bar is the mean of the three technical replicates and the error bars are the SEM.

The temporal kinetics study showed that CHRM2-SENSIT performs best with long agonist stimulation time (Figure 3-4D and 3-4E), similar to B2AR-SENSIT. Dose-response characterization of CHRM2-SENSIT revealed a low sensitivity to iperoxo, a potent muscarinic receptor agonist (EC50 of 18.9 µM, Figure 3-4F and Appendix Figure A-8A) and negligible activation for acetylcholine (Appendix Figure A-8B and A-8C). The significantly reduced sensitivity of CHRM2-SENSIT likely stems from the chimeric nanobody destabilizing the overall sensor structure. Further engineering efforts could focus on stabilizing the nanobody framework to enhance expression level and stabilization of the activated-state complex of the sensor. Despite this limitation, CHRM2-SENSIT further demonstrated the chimeric nanobody design is generalizable beyond just Nb39 and Nb80. We have included the annotated amino acid sequence of all final SENSIT constructs in Appendix Figure A-9.

3.5 Design of Chimeric MiniG Protein SENSIT

To further expand the versatility of the SENSIT platform, we employed G-protein mimics as the bifunctional protein scaffold, to both inhibit the cpGFP fluorophore maturation and bind to the activated receptor. Unlike nanobodies, which require specific engineering for individual GPCRs, these mimics recognize a broad range of receptors upon agonist stimulation, offering a more universal approach to sensor design.[69]

As a proof-of-concept, we utilized the B2AR and the engineered alpha domain of the Gs protein, known as miniGs.[70] To develop the bifunctional miniGs, we selected three loop positions proximal to the GPCR-G protein interface for grafting the Nb39 sequences (Figure 3-5A). At each position, we evaluated the insertion of either Nb39 loop 2 or loop 8, designating the resulting sensors as B2AR-SENSIT2.0 (Figure 3-5A). Notably, several of these chimeric miniGs-variants yielded high SBRs comparable to that of B2AR-SENSIT1.1 (Figure 3-5B and 3-5C). B2AR-SENSIT2.0 exhibited lower overall activation than B2AR-SENSIT1.1, likely due to reduced stability of the chimeric protein, so future engineering efforts should focus on stabilizing the miniGs framework to enhance performance. Doing so would allow SENSIT design for any GPCR that binds the Gs-protein.

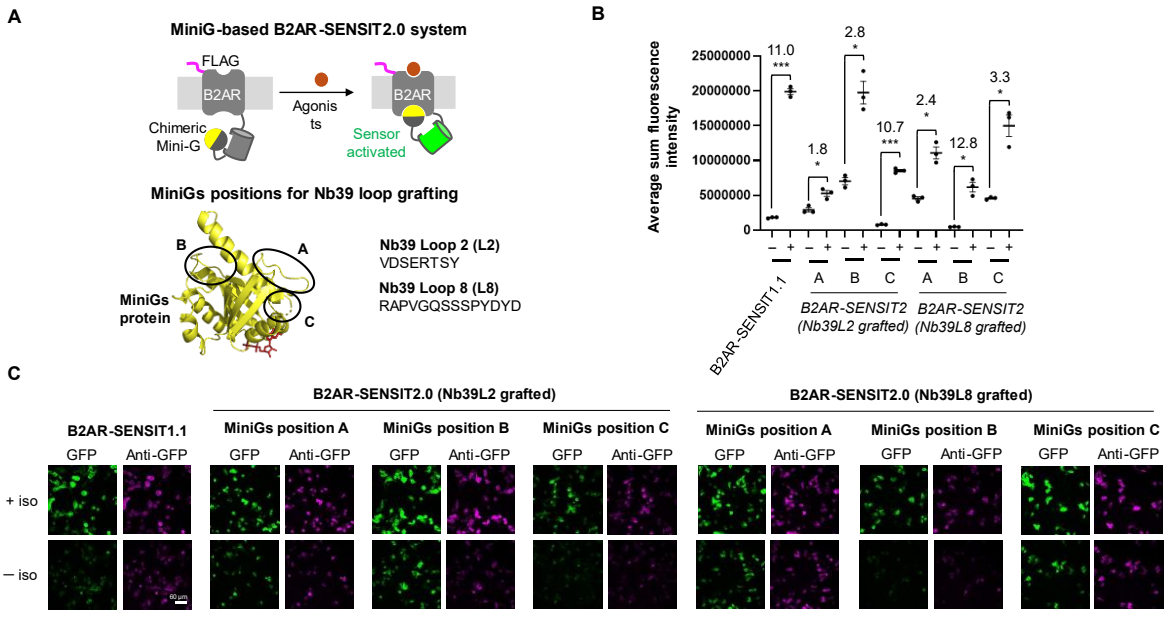


Figure 3-5: Design of the chimeric miniG protein B2AR-SENSIT2.0. (A) Schematic for the design strategy of miniGs based B2AR-SENSIT2.0. Three positions on miniG (A, B or C) were replaced with either Nb39 loop2 or Nb39 loop 8. PDB : 5G53. (B) Quantification of miniGs position (A, B, or C) replacement with Nb39 loop 2 or 8 in comparison to B2AR-SENSIT1.1. All sensors were stimulated with 10 µM isoproterenol for 24 hours. All significance was calculated using a two-tailed Welch's t-test. Stars indicate the degree of significance as follows *, P<0.05, **, P<0.01, ***, P<0.001, ****, P<0.0001. Dots on the plot indicate the mean of three technical replicates. n = 3. The thick horizontal bar is the mean of the three technical replicates and the error bars are the SEM. (C) Representative fluorescence images of B2AR-SENSIT2.0 from experiment described in prior figure panel (3-5B) in HEK293T cells. Scale bar, 60 µm. Cells were stimulated with 10 µM isoproterenol. Twenty-four hours after stimulation, cells were fixed, immunostained and imaged at pH 11. GFP, cpGFP fluorescence. Anti-GFP, protein expression level from immunostaining.

3.6 Discussion of the SENSIT platform

In this chapter I highlighted the properties of B2AR-SENSIT, selective for epinephrine (EC50 225 nM), and B1AR-SENSIT, selective for norepinephrine (EC50 959 nM). To our knowledge, these represent the first genetically encoded single-chain fluorescent integrator sensors capable of selectively detecting epinephrine and norepinephrine, two closely related catecholamines that have historically been difficult to distinguish in vivo. Together, these sensors provide a new opportunity to study the spatial organization and integration of adrenergic signaling.

Importantly, SENSIT is generalizable due to the robustness of the Nb39 loop insertion strategy. I demonstrate this by extending the platform to a muscarinic acetylcholine receptor sensor (CHRM2-SENSIT) and, more broadly, by converting mini-G proteins into SENSIT-style integrators. While the current CHRM2-SENSIT preferentially detects potent synthetic ligands, established directed evolution strategies—successfully applied here to B2AR-SENSIT—provide a clear path toward improving acetylcholine sensitivity. The demonstration of miniG-based SENSIT designs further suggests that this platform can be expanded across GPCR families using, miniGs, miniGi, and miniGq scaffolds, substantially broadening the repertoire of detectable ligands.

At present, SENSIT sensors require extended agonist stimulation and are not yet sensitive enough to detect endogenous ligand release in vivo. These limitations reflect engineering challenges rather than conceptual constraints and are well suited to iterative optimization through expanded mutational libraries, multi-site randomization, and refinement of GPCR–binder interactions. Improving sensitivity is expected to simultaneously reduce required stimulation times and enable endogenous neuromodulator detection. Another current limitation when applying SENSIT is the lack of temporal control, leading to the potential for high background accumulation and low temporal resolution. To address this B2AR-SENSIT could be incorporated into the MAPIT design, adding temporal control via doxycycline induced protease expression. An alternative approach could put B2AR-SENSIT expression under control of the tamoxifen-inducible Cre/loxP system.31 This would also allow integrator sensor signal accumulation under a specified experimental timeframe. A final consideration is the limitations of imaging at pH 11, as brain slices cannot be mounted and preserved, since the slices need to be imaged with high pH buffer. In addition, when using other fluorophores in conjunction with SENSIT, such as for immunostaining, it is important to understand their properties at pH 11.

In summary, SENSIT establishes a new, generalizable architecture for genetically encoded fluorescent integrator sensors, exemplified by an improved epinephrine integrator, B2AR-SENSIT. By designing modular conformation-specific binding proteins, SENSIT opens a path toward development of integrator sensors for diverse GPCR ligands. With continued optimization, this platform has the potential to enable large-volume mapping of neuromodulator localization and signaling integration across complex neural circuits.

3.7 Chapter 3 Bibliography

(62) Kroning, K.; Gannot, N.; Li, X.; Putansu, A.; Zhou, G.; Sescil, J.; Shen, J.; Wilson, A.; Fiel, H.; Li, P.; et al. Single-chain fluorescent integrators for mapping G-protein-coupled receptor agonists. *Proc Natl Acad Sci U S A* **2024**, *121* (18), e2307090121. DOI: 10.1073/pnas.2307090121 From NLM Medline.
(67) Baker, J. G. The selectivity of beta-adrenoceptor agonists at human beta1-, beta2- and beta3-adrenoceptors. *Br J Pharmacol* **2010**, *160* (5), 1048-1061. DOI: 10.1111/j.1476-5381.2010.00754.x From NLM Medline.
(68) Kruse, A. C.; Ring, A. M.; Manglik, A.; Hu, J.; Hu, K.; Eitel, K.; Hubner, H.; Pardon, E.; Valant, C.; Sexton, P. M.; et al. Activation and allosteric modulation of a muscarinic acetylcholine receptor. *Nature* **2013**, *504* (7478), 101-106. DOI: 10.1038/nature12735 From NLM Medline.
(69) Wan, Q.; Okashah, N.; Inoue, A.; Nehme, R.; Carpenter, B.; Tate, C. G.; Lambert, N. A. Mini G protein probes for active G protein-coupled receptors (GPCRs) in live cells. *J Biol Chem* **2018**, *293* (19), 7466-7473. DOI: 10.1074/jbc.RA118.001975 From NLM Medline.
(70) Carpenter, B.; Tate, C. G. Engineering a minimal G protein to facilitate crystallisation of G protein-coupled receptors in their active conformation. *Protein Eng Des Sel* **2016**, *29* (12), 583-594. DOI: 10.1093/protein/gzw049 From NLM Medline.

Chapter 4 Summary and Future Directions

The major results of my thesis work have been explained in detail in Chapters 2 and 3; here I would like to highlight the most important conclusions and findings. Then I'd like to discuss how SENSIT fits into the current need in our field, before expanding on necessary improvements, how to implement those improvements, and future applications.

4.1 Summary of Research Results

I designed a generalizable single-chain integrator sensor platform using chimeric nanobodies, reliant on disordered loop regions of Nb39 for cpGFP fluorophore maturation inhibition and started with replacing loop regions in Nb80. This led to an improved epinephrine sensor, B2AR-SENSIT1.0, compared to prior generation B2AR-SPOTall likely due to a simpler SPOTIT type activation mechanism. I used chimeric nanobodies to better inform design of other chimeric G-protein mimetics, through use of a TEVp cleavage system as well as mutating the chNb80/39. I also established a mammalian cell-based directed evolution platform for SENSIT evolution, wherein I evolved the chNb80/39 and developed B2AR-SENSIT1.1 with a higher SBR at lower agonist stimulation times than B2AR-SENSIT1.0.

To demonstrate the applicability, I characterized B2AR-SENSIT1.1 in HEK293T cells, rat neuronal culture, and mouse brain. I also developed B1AR-SENSIT using the evolved chNb80/39, which is selective for norepinephrine. Then, I illustrated the design strategy for other chimeric nanobodies, using Nb9-8 to develop CHRM2-SENSIT. Finally, I expanded beyond nanobody scaffolds to a structural distinct miniGs, a G-protein mimetic that can bind to Gs coupled receptors, and proved that the Nb39 loop replacement design for cpGFP inhibition is not limited to nanobodies. Together this work offers a unique strategy for single-chain integrator design based on modular chimeric conformation-specific binders.

4.2 Novelty and Expected Impact

The SPOTIT family of sensors has been extensively iterated on, as evidenced in my introduction chapter. The novelty of SENSIT lies in the design strategy, for the first time we

were able to remove the cpGFP inhibition feature from Nb39 and apply it to other conformation-specific binders. This contributed to the design of B2AR-SENSIT1.1 for epinephrine detection and B1AR-SENSIT for norepinephrine detection, which are too my knowledge the first integrator sensors capable of distinguishing these very structurally similar catecholamines. Then in the case of miniG proteins, which are active-state GPCR binders that interact with a class of GPCRs, SENSIT provides a truly generalizable and efficient engineering strategy to target many GPCR ligands of interest.

With further optimization that I will detail in the next section SENSIT can be applied for neurotransmitter localization mapping across large brain volumes. This will amplify our current understanding of the impacts of certain neurotransmitters signaling in complex neural circuits.

4.3 Future Directions

Currently SENSIT cannot detect endogenous neurotransmitters, and I believe the reason is two-fold. First, B2AR and B1AR-SENSIT have high nanomolar EC_{50}, while CHRM2-SENSIT cannot currently detect acetylcholine at biologically relevant concentrations. Therefore, sensitivity to the native ligand must be improved. Second, all SENSIT constructs show a preference for long agonist stimulation times, meaning the ligand must be continuously present for the best SBR. In mouse brains, an endogenous neurotransmitter will diffuse rapidly or undergo reuptake at the synapse, meaning it will not be present for extended amounts of time. This need for continual stimulation is most likely due to the instability of activation complex formed for SENSIT, because the affinity of the chimeric binders to the activated GPCR likely decreased due to the loop grafting. All components of SENSIT have been heavily modified from their native protein structure, consequently these proteins tend to be less stable as well.

I will discuss strategies for further improving sensitivity and reducing agonist stimulation time in the SENSIT platform, dividing the following sections by what protein component of SENSIT the strategy focuses on. In short, mammalian cell-based directed evolution would be critical for evolving the entire SENSIT construct for optimal protein folding and membrane trafficking. Finally, I will pivot to discuss what could be done to better understand the Nb39 cpGFP intramolecular interaction that results in fluorophore maturation inhibition.

4.3.1 Focusing on the GPCR

Sensitivity and agonist stimulation time may both be improved by evolving the GPCR in SENSIT for tighter binding of the agonist of interest to increase the stability of the active GPCR conformation. This can be done through targeted mutagenesis in the ligand binding pocket targeting residues that interact with the agonist. This targeted mutagenesis strategy will be benefited by available crystal or cryo-EM structures for the GPCR being evolved, in the case of B2AR there are currently many published, including bound to epinephrine.[65, 71-73] There are also published structures for B1AR and CHRM2.[68, 74, 75]

The binding pocket could also be targeted for random mutagenesis to create new interactions at specific positions to bind the agonist tighter. This approach would be most beneficial for GPCRs lacking a published structure. However, predictive structural software, such as AlphaFold for generating a structure prediction and Rosetta for predicting ligand binding, could help further inform either strategy though will be most beneficial in the case of a less characterized GPCR.[76, 77]

Another approach could focus on targeted mutagenesis of the conformation specific binder binding pocket. All the nanobodies I have used in designing SENSIT were developed for the purpose of stabilizing the active state for crystallization of GPCRs. However, in designing chimeric nanobodies some of that binding affinity was likely reduced. Then the intracellular binding pocket could be mutated to strengthen its binding to the chimeric nanobody.

For selection, I would follow a similar directed evolution strategy as described in Chapter 2, where I would stimulate the HEK cells expressing the SENSIT library for a shorter amount of time, such as 5 minutes, and select cells with higher fluorescence. In a separate experiment, we could sort the same libraries by decreasing the agonist concentration to increase selection pressure. Cells with higher fluorescence at lower agonist concentrations will be selected. This selection strategy could be used in the directed evolution of SENSIT libraries based on cpGFP and the chimeric binders as well.

Alternatively, with the introduction of chimeric miniG proteins, it would be possible to design sensors with a large array of GPCRs within the same agonist family to screen for improved sensitivity and agonist stimulation time. For example, with the design of a miniGi or miniGq, it would be possible to create an alpha-adrenergic receptor-based SENSIT. These would likely behave differently than B2AR-SENSIT1.1 or B1AR-SENSIT, and these new sensor variants could provide alternative starting points for directed evolution.

4.3.2 Focusing on the cpGFP

One unique property of cpGFP in SENSIT is the hours of time needed for fluorophore maturation. The parent protein of cpGFP, EGFP, takes around 25 minutes to form its fluorophore after expression.[78] This is likely due to the highly irregular environment cpGFP is expressed in, sandwiched between a GPCR and a chimeric GPCR binder. Additionally, the fluorophore in cpGFP is intentionally exposed to the environment through its circular permutation.

In chapter 2, our preliminary work towards evolving cpGFP we wanted to identify a cpGFP mutant that would have an improved SBR when stimulated with drug for shorter periods of time, to address the long agonist stimulation need in SENSIT. Unfortunately, the library design strategy targeting the N-terminal residues did not lead to identifying an improved variant. This was a matter of needing a different library design strategy. Rather than targeting N-terminal residues, it could be important to focus on internal facing beta-barrel residues that interact with the fluorophore for targeted mutagenesis. This could be informed by crystal structures of the genetically encoded calcium indicator GCaMP, as well as structural studies of EGFP.[79-81]

Finally, other FPs could be tested in SENSIT. There is already published work on red-SPOTIT, a red fluorescent protein integrator sensor. Intriguingly that design required the use of the entire calcium detecting O-Geco1, not just the red FP, circularly permuted mApple.[62] There is current work in the lab on a new red FP SPOTIT variant, as well. There is a precedent for exploring other FPs showing that fluorophore inhibition is not unique to Nb39 and cpGFP. It would be useful to find other FP variants that could be inhibited by Nb39 or the chimeric conformation specific GPCR binders described in this thesis. These could provide starting points for further engineering and expand the multiplexing options of SENSIT.

4.3.3 Focusing on the Chimeric Binder

The nanobodies I focused on, Nb39, Nb80, and Nb9-8 all bind to their receptor in a unique way. Targeted mutagenesis needs to be tailored to the binding surface of each nanobody. Nb9-8 and Nb80 bind similarly, so a similar targeted mutagenesis strategy could be applied to Nb9-8 loop 8. For targeting the most important nanobody loop for binding within the evolved chNb80/39, the Nb80 position 4, future work could generate randomized libraries of two positions rather than a single position.

Nb6B9, an engineered Nb80 mutant identified through directed evolution that was used for obtaining a crystal structure of epinephrine bound B2AR[71], could be used for chimeric

nanobody design for B2AR-SENSIT. This nanobody is reported to have a near tenfold binding affinity improvement over Nb80 due to its reduced dissociation rate and it could stabilize the activated complex formed in B2AR-SENSIT in the presence of agonists. Specifically, the reduction in dissociation rate could be critical, as longer chimeric nanobody binding would give cpGFP more time to begin fluorophore maturation leading to lower agonist stimulation time requirements for SENSIT.

One rational design approach I did not try was the incorporation of multiple loops of Nb39 into a scaffold, I believe this could improve inhibition but may further perturb the binder structure the loops are introduced into. It would be important to find the right balance between introducing Nb39 loops and maintaining desirable sensor properties. This approach may be even more important for the miniG scaffold because it is larger than a nanobody, and Nb39 loop positioning will be critical.

Thinking of Nb39 loop replacement, targeted mutagenesis of the chimeric Nb39 loop itself could be beneficial to balance the inhibition and conformation specific binding of the chimeric binders. This approach would not be limited to nanobodies but could be one potential starting point for the directed evolution of B2AR-SENSIT2.0 which uses chimeric miniGs.

In future work, one could also design chimeric miniG proteins for all reported miniG variants that cover all the major G protein families.[82] It will be important to identify the strongest chimeric miniG sensor starting point for further engineering efforts.

Finally, I believe random mutagenesis of the entire chimeric miniGs (or other potentially identified miniG) could be a strong starting library design strategy. However, the C-terminal region of Gα protein and miniG known as the α-5 helix, is extremely critical for GPCR binding. This region should most likely be excluded from random mutagenesis to avoid losing conformation specific binding altogether.

4.3.4 Further Elucidating the Nb39 cpGFP Fluorophore Maturation Inhibition Mechanism

Translating and evolving the Nb39 loop chimeric GPCR binders will be greatly enhanced by a more mechanistic understanding of how Nb39 and cpGFP interact. Currently AlphaFold cannot accurately predict a structure of SENSIT. Structural studies would be necessary for fully understanding how Nb39 and cpGFP interact in a single-chain sensor context. I would recommend using B2AR-SENSIT1.1 for X-ray crystallography or cryo-EM, however, it would

be necessary to develop a protein purification system. The purification could be guided by published B2AR purification methodologies which already include B2AR plus nanobody.

4.3.5 Future Applications

Throughout my work I have focused on SENSIT as a tool for neuroscience research and extensively discussed its limitations and need for further development to meet the demands for that application. However, SENSIT is not limited as a sensor for expression in the brain. Using a different promoter or expression system it could be introduced into an organ, such as the heart, to study the localization of epinephrine and norepinephrine.

Additionally, B2AR-SENSIT1.1 could be adapted for a high throughput screening platform for novel beta-adrenergic receptor agonists or antagonists since it maintains similar selectivity to the native receptor as shown in the characterization in Chapter 3. This would avoid a lot of the limitations of applying SENSIT in vivo as background accumulation would be on a shorter timescale during assay screening.

4.4 Chapter 4 Bibliography

(62) Kroning, K.; Gannot, N.; Li, X.; Putansu, A.; Zhou, G.; Sescil, J.; Shen, J.; Wilson, A.; Fiel, H.; Li, P.; et al. Single-chain fluorescent integrators for mapping G-protein-coupled receptor agonists. *Proc Natl Acad Sci U S A* **2024**, *121* (18), e2307090121. DOI: 10.1073/pnas.2307090121 From NLM Medline.
(65) Rasmussen, S. G.; Choi, H. J.; Fung, J. J.; Pardon, E.; Casarosa, P.; Chae, P. S.; Devree, B. T.; Rosenbaum, D. M.; Thian, F. S.; Kobilka, T. S.; et al. Structure of a nanobody-stabilized active state of the beta(2) adrenoceptor. *Nature* **2011**, *469* (7329), 175-180. DOI: 10.1038/nature09648 From NLM Medline.
(68) Kruse, A. C.; Ring, A. M.; Manglik, A.; Hu, J.; Hu, K.; Eitel, K.; Hubner, H.; Pardon, E.; Valant, C.; Sexton, P. M.; et al. Activation and allosteric modulation of a muscarinic acetylcholine receptor. *Nature* **2013**, *504* (7478), 101-106. DOI: 10.1038/nature12735 From NLM Medline.
(71) Ring, A. M.; Manglik, A.; Kruse, A. C.; Enos, M. D.; Weis, W. I.; Garcia, K. C.; Kobilka, B. K. Adrenaline-activated structure of beta2-adrenoceptor stabilized by an engineered nanobody. *Nature* **2013**, *502* (7472), 575-579. DOI: 10.1038/nature12572 From NLM Medline.
(72) Masureel, M.; Zou, Y.; Picard, L. P.; van der Westhuizen, E.; Mahoney, J. P.; Rodrigues, J.; Mildorf, T. J.; Dror, R. O.; Shaw, D. E.; Bouvier, M.; et al. Structural insights into binding specificity, efficacy and bias of a beta(2)AR partial agonist. *Nat Chem Biol* **2018**, *14* (11), 1059-1066. DOI: 10.1038/s41589-018-0145-x From NLM Medline.
(73) Guo, Q.; He, B.; Zhong, Y.; Jiao, H.; Ren, Y.; Wang, Q.; Ge, Q.; Gao, Y.; Liu, X.; Du, Y.; et al. A method for structure determination of GPCRs in various states. *Nat Chem Biol* **2024**, *20* (1), 74-82. DOI: 10.1038/s41589-023-01389-0 From NLM Medline.
(74) Xu, X.; Kaindl, J.; Clark, M. J.; Hubner, H.; Hirata, K.; Sunahara, R. K.; Gmeiner, P.; Kobilka, B. K.; Liu, X. Binding pathway determines norepinephrine selectivity for the human beta(1)AR over beta(2)AR. *Cell Res* **2021**, *31* (5), 569-579. DOI: 10.1038/s41422-020-00424-2 From NLM Medline.
(75) Suno, R.; Lee, S.; Maeda, S.; Yasuda, S.; Yamashita, K.; Hirata, K.; Horita, S.; Tawaramoto, M. S.; Tsujimoto, H.; Murata, T.; et al. Structural insights into the subtype-selective antagonist binding to the M(2) muscarinic receptor. *Nat Chem Biol* **2018**, *14* (12), 1150-1158. DOI: 10.1038/s41589-018-0152-y From NLM Medline.
(76) Abramson, J.; Adler, J.; Dunger, J.; Evans, R.; Green, T.; Pritzel, A.; Ronneberger, O.; Willmore, L.; Ballard, A. J.; Bambrick, J.; et al. Accurate structure prediction of biomolecular interactions with AlphaFold 3. *Nature* **2024**, *630* (8016), 493-500. DOI: 10.1038/s41586-024-07487-w From NLM Medline.
(77) Moretti, R.; Bender, B. J.; Allison, B.; Meiler, J. Rosetta and the Design of Ligand Binding Sites. *Methods Mol Biol* **2016**, *1414*, 47-62. DOI: 10.1007/978-1-4939-3569-7_4 From NLM Medline.
(78) Lambert, T. J. FPbase: a community-editable fluorescent protein database. *Nat Methods* **2019**, *16* (4), 277-278. DOI: 10.1038/s41592-019-0352-8 From NLM Medline.
(79) Akerboom, J.; Rivera, J. D.; Guilbe, M. M.; Malave, E. C.; Hernandez, H. H.; Tian, L.; Hires, S. A.; Marvin, J. S.; Looger, L. L.; Schreiter, E. R. Crystal structures of the GCaMP calcium sensor reveal the mechanism of fluorescence signal change and aid rational design. *J Biol Chem* **2009**, *284* (10), 6455-6464. DOI: 10.1074/jbc.M807657200 From NLM Medline.

(80) Wang, Q.; Shui, B.; Kotlikoff, M. I.; Sondermann, H. Structural basis for calcium sensing by GCaMP2. *Structure* **2008**, *16* (12), 1817-1827. DOI: 10.1016/j.str.2008.10.008 From NLM Medline.
(81) Myskova, J.; Rybakova, O.; Brynda, J.; Khoroshyy, P.; Bondar, A.; Lazar, J. Directionality of light absorption and emission in representative fluorescent proteins. *Proc Natl Acad Sci U S A* **2020**, *117* (51), 32395-32401. DOI: 10.1073/pnas.2017379117 From NLM Medline.
(82) Nehme, R.; Carpenter, B.; Singhal, A.; Strege, A.; Edwards, P. C.; White, C. F.; Du, H.; Grisshammer, R.; Tate, C. G. Mini-G proteins: Novel tools for studying GPCRs in their active conformation. *PLoS One* **2017**, *12* (4), e0175642. DOI: 10.1371/journal.pone.0175642 From NLM Medline.

Appendix A: Additional Data

A.1 Appendix Figures

A

wtNb80

```
QVQLQESGGGLVQAGGSLRL 20
SCAASGSIFSINTMGWYRQA 40
PGKQRELVAAIHSGGSTNYA 60
NSVKGRFTISRDNAANTVYL 80
QMNSLKPEDTAVYYCNVKDY 100
GAVLYEYDYWGQGTQVTVSS
```

Nb80 Position 1(S25 to N32) :
SGSIFSIN
Nb80 Position 2(H52 to T57) :
HSGGST
Nb80 Position 3(D72 to T77) :
DNAANT
Nb80 Position 4(D99 to Y107) :
DYGAVLYEY

B

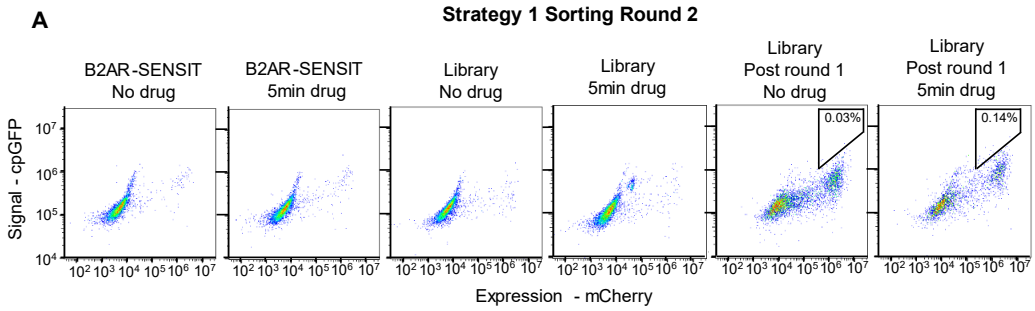
wtNb39

```
MAQVQLVESGGGLVRPGGSL 20
RLSCVDSERTSYPMGWFRRA 40
PGKEREFVASITWSGIDPTY 60
ADSVADRFTTSRDVANNTLY 80
LQMNSLKHEDTAVYYCAARA 100
PVGQSSSPYDYDYWGQGTQV 120
TVSS 124
```

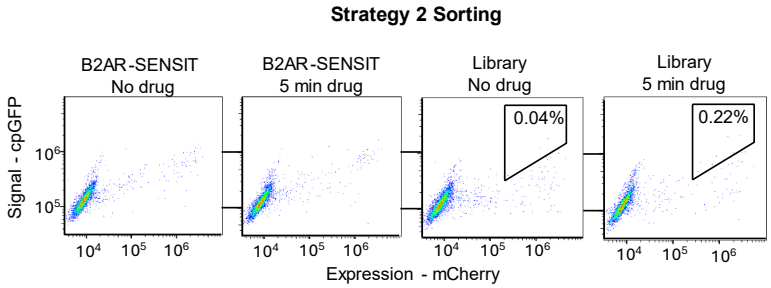
Nb39 Loop 1(V14 to L20) :
VRPGGSL
Nb39 Loop 2(V25 to Y32) :
VDSERTSY
Nb39 Loop 3(R39 to R45) :
RAPGKER
Nb39 Loop 4(I51 to P58) :
ITWSGIDP
Nb39 Loop 5(Y60 to F68) :
YADSVADRF
Nb39 Loop 6(D73 to T78) :
DVANNT
Nb39 Loop 7(M83 to A92) :
MNSLKHEDTA
Nb39 Loop 8(R99 to Y113) :
RAPVGSQSSSPYDYDY

Appendix Figure A-1: Defining the amino acids of the Nb80 positions and Nb39 loops. (A) Amino acid sequence of wtNb80 used in B2AR-SPOTall and basis of design of the chimeric nanobody. Listed positions and amino acids that were replaced with Nb39 loops. (B) Amino acid sequence of wtNb39 used in MOR-SPOTIT and basis of design of the chimeric nanobody. Listed amino acid sequences for loop 1 through 8.

A



B



C

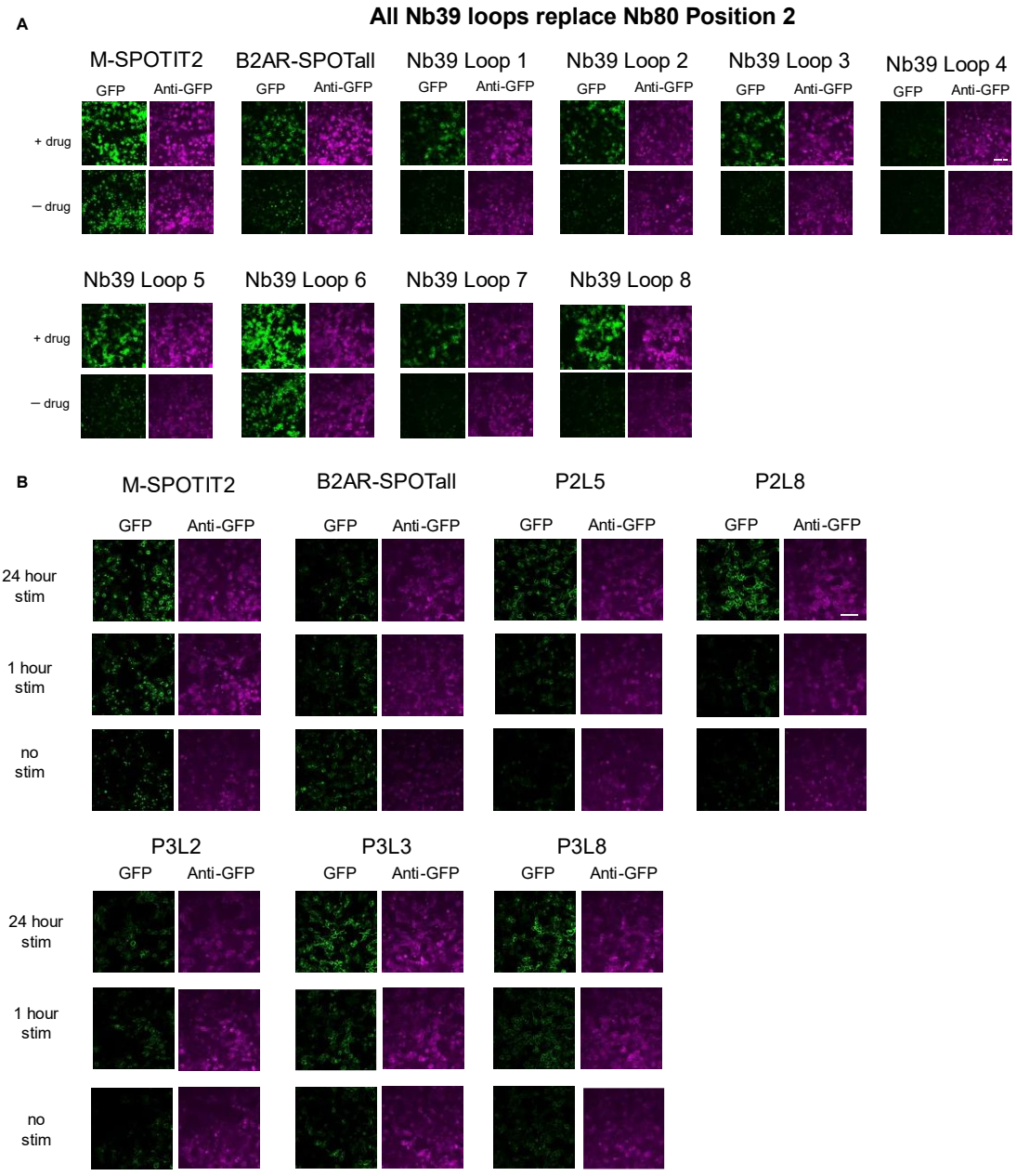
Strategy 1
Next Generation Sequencing
Top 10 Reads

Percent	Sequence
19.66	P3L7 WT
10.66	P3L8 WT
6.69	Silent mutation WT
6.67	DYGAVLYE R
3.7	DYGA L LYEY
3.58	DYGAVLY G Y
2.54	DYGAVLYE L
2.38	DYGAVLYE A
2.37	DYGAVLYE R
2.2	DYGAVLY S Y

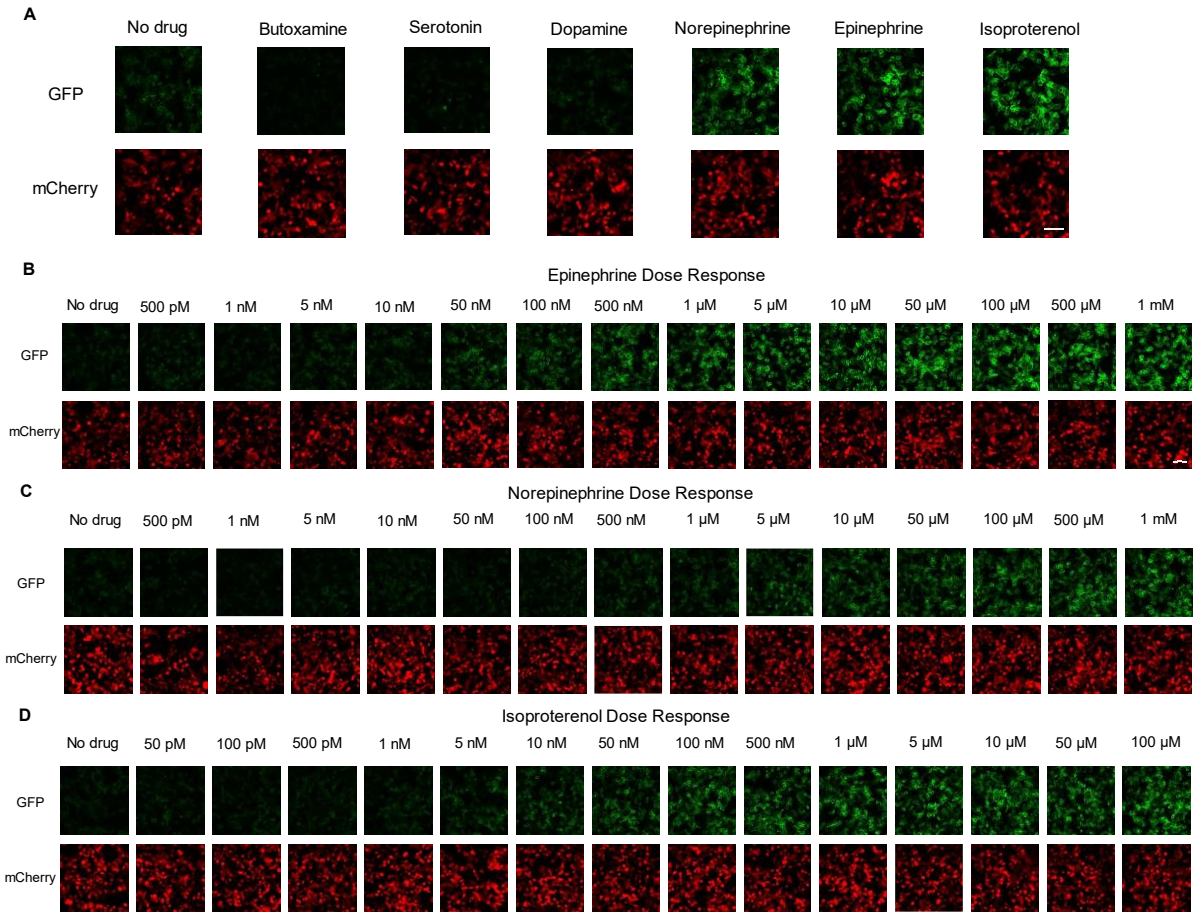
Strategy 2
Next Generation Sequencing
Top 10 Reads

Percent	Sequence
13.33	P3L7 WT
4.89	P3L8 WT
3.25	Silent mutation WT
2.92	Silent mutation WT
2.63	DY S AVLYEY
2.28	Deletion
1.86	Silent mutation WT
1.85	DY S AVLYEY
1.64	DYGAVLYE S
1.47	DYGAVLYE I

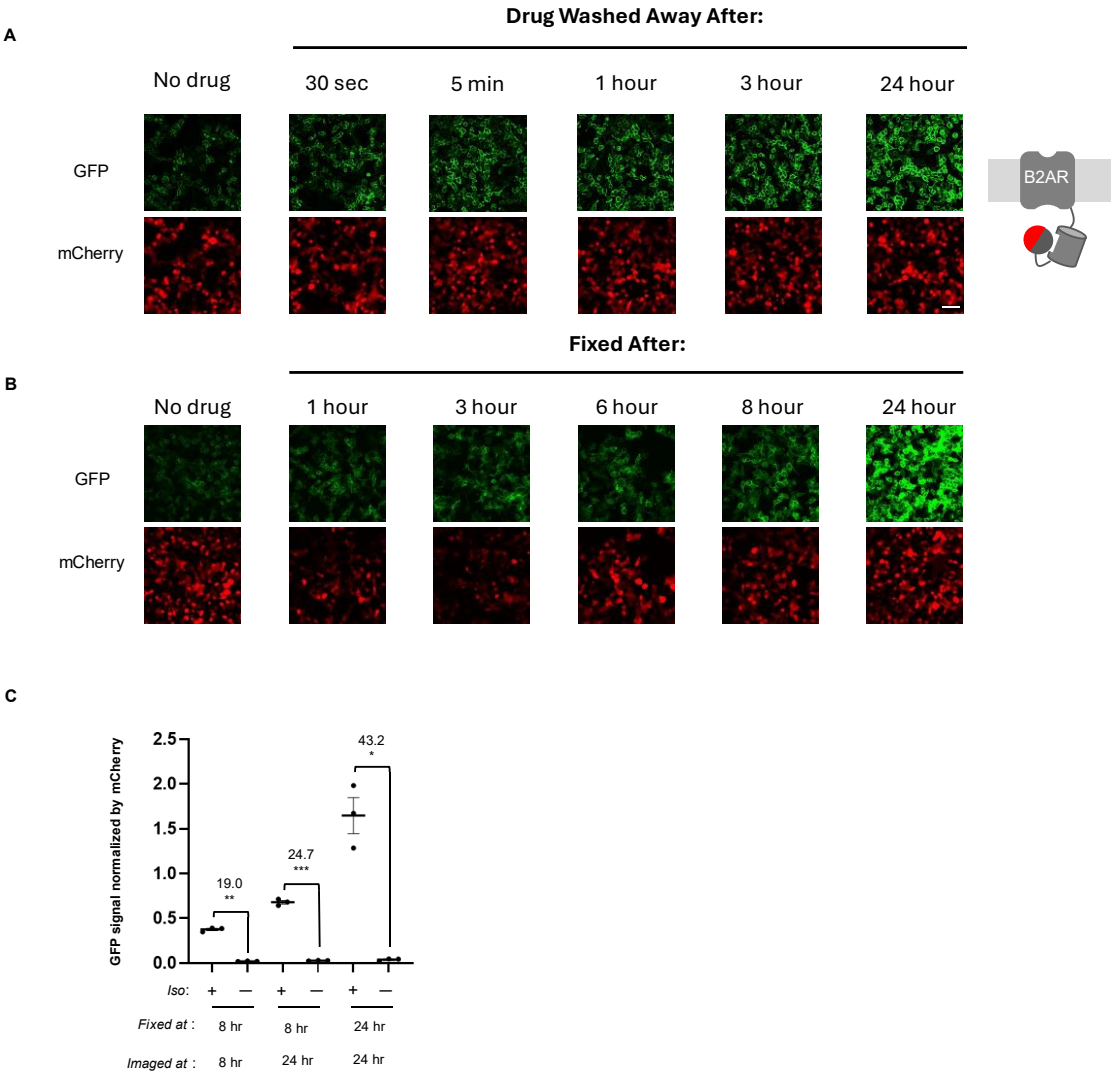
Appendix Figure A-2: Further information on the directed evolution of B2AR-SENSIT chimeric Nb80/39. (A) Gating strategy for the Strategy 1 second round of sorting. Strategy 1 involved an initial round of sorting where cells were stimulated with 10 µM isoproterenol for 24 hours then sorted. The second round of sorting using the cells from the first round were stimulated with 10 µM isoproterenol for 5 minutes then drug was washed away and cells were incubated for 24 hours before sorting. Numbers within the gate correspond to percent of total cell population present within the gate. (B) Gating strategy for the Strategy 2 sorting that was only one round. Cells were stimulated with 10 µM isoproterenol for 5 minutes then drug was washed away and cells were incubated for 24 hours before sorting. Numbers within the gate correspond to percent of total cell population present within the gate. (C) Tables summarizing next generation sequencing results for the top 10 reads from sorting Strategy 1 and 2. The first column is the percent of total reads corresponding to that base pair sequence. The second column is the amino acid sequence arising from the base pair sequence. Red corresponds to an amino acid mutation from the Nb80 position 4 sequence.



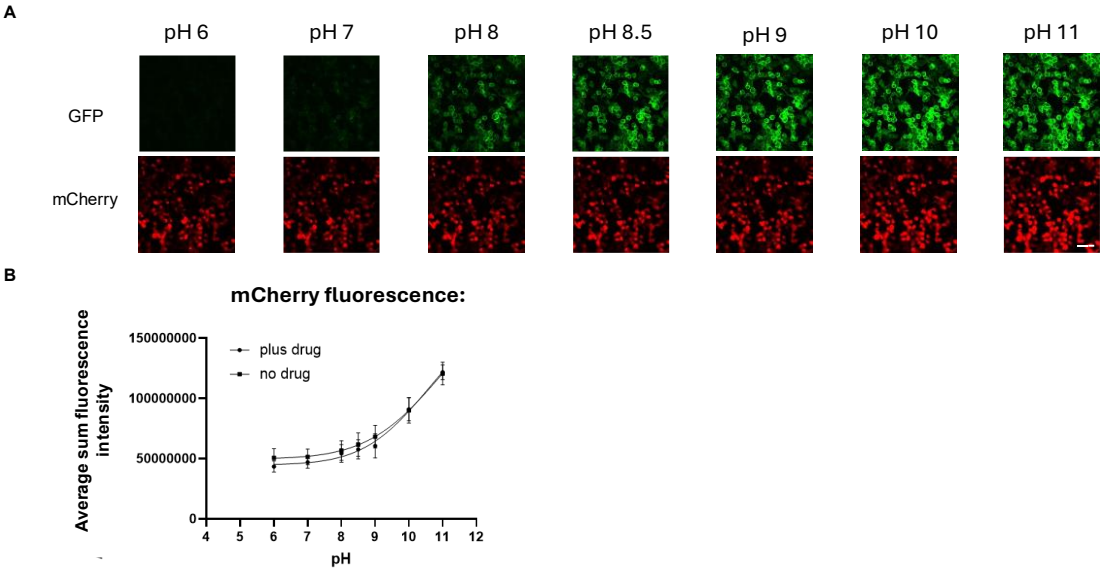
Appendix Figure A-3: Images from experiments found in Figure 2-7 selecting the best chimeric nanobody. (A) Representative fluorescence images of all Nb39 loops replacing Nb80 position 2, from experiment found in Figure 2-7A. (B) Representative fluorescence images of selecting the best chimeric Nb80/Nb39 considering position 2 and 3, from experiment found in Figure 2-7B. For (A) and (B) : 24 hours after stimulation, cells were fixed, immunostained, and imaged at pH 11. GFP, cpGFP fluorescence. Anti-GFP, protein expression level from immunostaining. Scale bar, 60 µm.



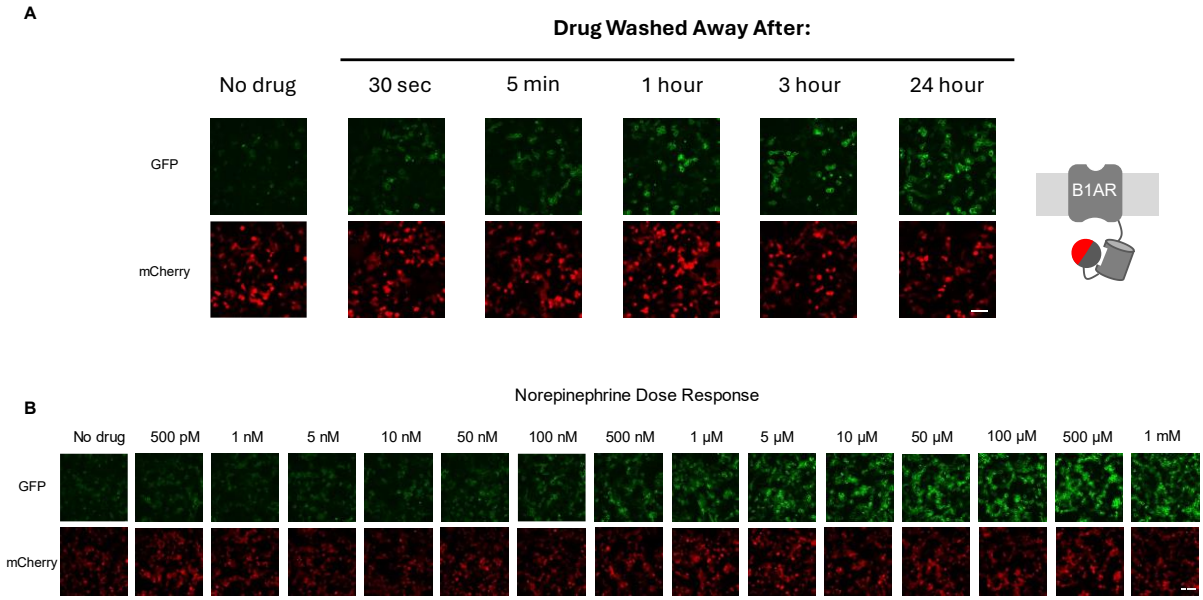
Appendix Figure A-4: Images from experiments found in Figure 3-1 characterizing B2AR-SENSIT1.1. (A) Fluorescence images for Figure 3C characterizing B2AR-SENSIT1.1 selectivity. Cells were stimulated with 10 µM of each indicated agonist. (B) Fluorescence images for Figure 3D characterizing B2AR-SENSIT1.1 sensitivity to epinephrine. Cells were stimulated with indicated concentration of epinephrine. (C) Fluorescence images for Figure 3D characterizing B2AR-SENSIT1.1 sensitivity to norepinephrine. Scale is same as images in (B). Cells were stimulated with indicated concentration of norepinephrine (D) Fluorescence images for Figure 3D characterizing B2AR-SENSIT1.1 sensitivity to isoproterenol. Scale is same as images in (B). Cells were stimulated with indicated concentration of norepinephrine. For (A-D): 24 hours after stimulation, cells were fixed and imaged at pH 11. GFP, cpGFP fluorescence. mCherry, protein expression level from ribosomal skip sequence P2A followed by mCherry. Scale bar, 60 µm.



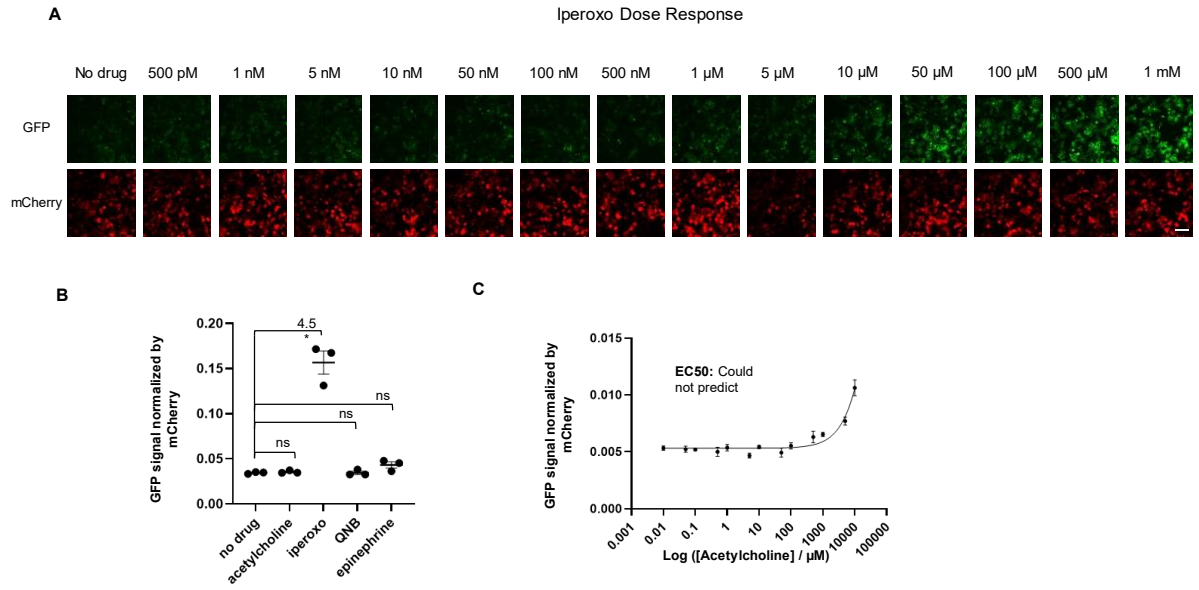
Appendix Figure A-5: Images from experiments found in Figure 3-1 characterizing B2AR-SENSIT1.1 Continued. (A) Fluorescence images for Figure 4E characterizing temporal kinetics of B2AR-SENSIT1.1 stimulation. Each time point indicates how long drug was present before being washed away. Cells were fixed 24 hours after stimulation and imaged at pH 11. (B) Fluorescence images for Figure 4F characterizing fluorophore maturation time of B2AR-SENSIT1.1. All samples were stimulated at the same time, but the time point refers to when the sample was fixed. All were imaged at pH 11. For (A and B): GFP, cpGFP fluorescence. mCherry, protein expression level from ribosomal skip sequence P2A followed by mCherry. Scale bar, 60 µm. (C) Quantification of an experiment to show how fixation impacts fluorophore maturation. One condition was imaged twice, immediately after fixation at 8 hours and again 24 hours later and compared to a condition that was fixed and imaged after 24 hours. The numbers above each bracket are the SBR between stimulated and unstimulated conditions. All significance was calculated using a two-tailed Welch's t-test. Stars indicate the degree of significance as follows *, P<0.05, **, P<0.01, ***, P<0.001, ****, P<0.0001. Dots on the plot indicate the mean of three technical replicates. n = 3. The thick horizontal bar is the mean of the three technical replicates and the error bars are the SEM.



Appendix Figure A-6: B2AR-SENSIT1.1 pKa characterization images and mCherry fluorescence. (A) Fluorescence images for Figure 4G characterizing B2AR-SENSIT1.1 cpGFP pKa. Cells were fixed 24 hours after stimulation, and imaged at varying pH. GFP, cpGFP fluorescence. mCherry, protein expression level from ribosomal skip sequence P2A followed by mCherry. Scale bar, 60 µm. (B) Fluorescence of B2AR-SENSIT1.1 mCherry. To monitor the same fluorophores over various pH ranges, we imaged one field of view at pH 6, 7, 8, 8.5, 9. 10 and 11. Dots on the plot indicate the mean of three replicates. n = 3, and the error bars are the SEM.



Appendix Figure A-7: Images from Figure 3-3 characterizing B1AR-SENSIT. (A) Fluorescence images for Figure 5B characterizing B1AR-SENSIT selectivity. Each time point indicates how long drug was present before being washed away. (B) Fluorescence images for Figure 5D characterizing B1AR-SENSIT sensitivity to norepinephrine. For (A) and (B): 24 hours after stimulation, cells were fixed and imaged at pH 11. GFP, cpGFP fluorescence. mCherry, protein expression level from ribosomal skip sequence P2A followed by mCherry. Scale bar, 60 µm.



Appendix Figure A-8: Expanded characterization of CHRM2-SENSIT. (A) Fluorescence images for Figure S10F characterizing CHRM2-SENSIT sensitivity to iperoxo. 24 hours after stimulation, cells were fixed and imaged at pH 11. GFP, cpGFP fluorescence. mCherry, protein expression level from ribosomal skip sequence P2A followed by mCherry. Scale bar, 60 µm. (B) Selectivity characterization of CHRM2-SENSIT. The numbers above each bracket are the SBRs between stimulated and unstimulated conditions. (C) Acetylcholine dose response characterization for CHRM2-SENSIT. EC_{50} displayed with the 95% confidence interval. For (B) and (C): All significance was calculated using a two-tailed Welch's t-test. Stars indicate the degree of significance as follows *, P<0.05, **, P<0.01, ***, P<0.001, ****, P<0.0001. Dots on the plot indicate the mean of three technical replicates. n = 3. The thick horizontal bar is the mean of the three technical replicates and the error bars are the SEM.

A

AAA – Lucy Tag
AAA – FLAG Tag
AAA – Receptor
AAA – Linker
AAA – cpGFP
AAA – chimeric protein
AAA – p2a

B – B2AR-SENSIT1.1 amino acid sequence

```
MRPQILLLLALLTLGLADYKDDDDAMGQPGNGSAFLLAPNRSHAPDHDVTQQRDEVWVVGMGIVMSLIVLAIVFGNVLVITAIAKFERLQTVTNYFITSL 100
ACADLVMGLAVVPFGAAHILMKMWTFGNFWCEFWTSIDVLCVTASIETLCVIAVDRYFAITSPFKYQSLLTKNKARVIILMVWIVSGLTSFLPIQMHWYR 200
ATHQEAINCYANETCCDFFTNQAYAIASSIVSFYVPLVIMVFVYSRVFQEAKRQLQKIDKSEGRFHVQNLSQVEQDGRTGHGLRRSSKFCLKEHKALKTL 300
GIIMGTFTLCWLPFFIVNIVHVIQDNLIRKEVYILLNWIGYVNSGFNPLIYCRSPDFRIAFQELLCFPLKMRMERQGAPNVYIKADKQKNGIKANFHIRH 400
NIEDGGVQLAYHYQQNTPIGDGPVLLPDNHYLSVQSKLSKDPNEKRDHMVLLEFVTAAGITLGMDELYKGGTGGSMVSKGEELFTGVVPILVELDGDVNG 500
HKFSVSGEGEGDATYGKLTLKFICTTGKLPVPWPTLVTTLTYGVQCFSRYPDHMKQHDFFKSAMPEGYIQERTIFFKDDGNYKTRAEVKFEGDTLVNRIE 600
LKGIDFKEDGNILGHKLEYNLKEDIQVQLQESGGGLVQAGGSLRLSCAASGSIFSINTMGWYRQAPGKQRELVAAIRAPVGQSSSPYDYDYNYANSVKGR 700
FTISRDNAANTVYLQMNSLKPEDTAVYYCNVKDYGAVLYSRDYWGQGTQVTVSSTGGSGATNFSLLKQAGDVEENPGPASMARDHPVATMVSKGEEDNMA 800
IIKEFMRFKVHMEGSVNGHEFEIEGEGEGRPYEGTQTAKLKVTKGGPLPFAWDILSPQFMYGSKAYVKHPADIPDYLKLSFPEGFKWERVMNFEDGGVVT 900
VTQDSSLQDGEFIYKVKLRGTNFPSDGPVMQKKTMGWEASSERMYPEDGALKGEIKQRLKLKDGGHYDAEVKTTYKAKKPVQLPGAYNVNIKLDITSHNE 1000
DYTIVEQYERAEGRHSTGGMDELYK* 1026
```

C – B1AR-SENSIT amino acid sequence

```
MRPQILLLLALLTLGLADYKDDDDAMNNSTNSSNNSLALTSPYKTFEVVFIVLVAGSLSLVTIIGNILVMVSIKVNRHLQTVNNYFLFSLACADLIIGVF 100
SMNLYTLYTVIGYWPLGPVVCDLWLALDYVVSNASVMNLLIISFDRYFCVTKPLTYPVKRTTKMAGMMIAAAWVLSFILWAPAILFWQFIVGVRTVEDGE 200
CYIQFFSNAAVTFGTAIAAFYLPVIIMTVLYWHISRASKSRIKKDKKEPVANQDPVSPSLVQGRIVKPNNNNMPSSDDGLEHNKIQNGKAPRDPVTENCV 300
QGEEKESSNDSTSVSAVASNMRDDEITQDENTVSTSLGHSKDENSKQTCIRIGTKTPKSDSCTPTNTTVEVVGSSGQNGDEKQNIVARKIVKMTKQPAKK 400
KPPPSREKKVTRTILAILLAFIITWAPYNVMVLINTFCAPCIPNTVWTIGYWLCYINSTINPACYALCNATFKKTFKHLLMCHYKNIGATRGAPNVYIKA 500
DKQKNGIKANFHIRHNIEDGGVQLAYHYQQNTPIGDGPVLLPDNHYLSVQSKLSKDPNEKRDHMVLLEFVTAAGITLGMDELYKGGTGGSMVSKGEELFT 600
GVVPILVELDGDVNGHKFSVSGEGEGDATYGKLTLKFICTTGKLPVPWPTLVTTLTYGVQCFSRYPDHMKQHDFFKSAMPEGYIQERTIFFKDDGNYKTR 700
AEVKFEGDTLVNRIELKGIDFKEDGNILGHKLEYNLKEDIQVQLQESGGGLVQAGDSLRLSCAASGFDFDNFDDYAIGWFRRAPVGQSSSPYDYDYEGVS 800
CIDPSDGSTIYADSAKGRFTISSDNAENTVYLQMNSLKPEDTAVYVCSAWTLFHSDEYWGQGTQVTVSSTGGSGATNFSLLKQAGDVEENPGPASMARDH 900
PVATMVSKGEEDNMAIIKEFMRFKVHMEGSVNGHEFEIEGEGEGRPYEGTQTAKLKVTKGGPLPFAWDILSPQFMYGSKAYVKHPADIPDYLKLSFPEGF 1000
KWERVMNFEDGGVVTVTQDSSLQDGEFIYKVKLRGTNFPSDGPVMQKKTMGWEASSERMYPEDGALKGEIKQRLKLKDGGHYDAEVKTTYKAKKPVQLPG 1100
AYNVNIKLDITSHNEDYTIVEQYERAEGRHSTGGMDELYK* 1141
```

D – CHRM2-SENSIT amino acid sequence

```
MRPQILLLLALLTLGLADYKDDDDAMGAGVLVLGASEPGNLSSAAPLPDGAATAARLLVPASPPASLLPPASESPEPLSQQWTAGMGLLMALIVLLIVAG 100
NVLVIVAIAKTPRLQTLTNLFIMSLASADLVMGLLVVPFGATIVVWGRWEYGSFFCELWTSVDVLCVTASIETLCVIALDRYLAITSPFRYQSLLTRARA 200
RGLVCTVWAISALVSFLPILMHWWRAESDEARRCYNDPKCCDFVTNRAYAIASSVVSFYVPLCIMAFVYLRVFREAQKQVKKIDSCERRFLGGPARPPSP 300
SPSPVPAPAPPPGPPRPAAAAATAPLANGRAGKRRPSRLVALREQKALKTLGIIMGVFTLCWLPFFLANVVKAFHRELVPDRLFVFFNWLGYANSAFNPI 400
IYCRSPDFRKAFQGLLCFPLKMRMERQGAPNVYIKADKQKNGIKANFHIRHNIEDGGVQLAYHYQQNTPIGDGPVLLPDNHYLSVQSKLSKDPNEKRDHM 500
VLLEFVTAAGITLGMDELYKGGTGGSMVSKGEELFTGVVPILVELDGDVNGHKFSVSGEGEGDATYGKLTLKFICTTGKLPVPWPTLVTTLTYGVQCFSR 600
YPDHMKQHDFFKSAMPEGYIQERTIFFKDDGNYKTRAEVKFEGDTLVNRIELKGIDFKEDGNILGHKLEYNLKEDIQVQLQESGGGLVQAGGSLRLSCAA 700
SGSIFSINTMGWYRQAPGKQRELVAAIRAPVGQSSSPYDYDYNYANSVKGRFTISRDNAANTVYLQMNSLKPEDTAVYYCNVKDYGAVLYSRDYWGQGTQ 800
VTVSSTGGSGATNFSLLKQAGDVEENPGPASMARDHPVATMVSKGEEDNMAIIKEFMRFKVHMEGSVNGHEFEIEGEGEGRPYEGTQTAKLKVTKGGPLP 900
FAWDILSPQFMYGSKAYVKHPADIPDYLKLSFPEGFKWERVMNFEDGGVVTVTQDSSLQDGEFIYKVKLRGTNFPSDGPVMQKKTMGWEASSERMYPEDG 1000
ALKGEIKQRLKLKDGGHYDAEVKTTYKAKKPVQLPGAYNVNIKLDITSHNEDYTIVEQYERAEGRHSTGGMDELYK* 1077
```

Appendix Figure A-9: Annotated amino acid sequences for B2AR-, B1AR-, and CHRM2-SENSIT. (A) Key for color annotation on amino acid sequences. (B) B2AR-SENSIT1.1 amino acid sequence. (C) B1AR-SENSIT amino acid sequence. (D) CHRM2-SENSIT amino acid sequence.

Bibliography

(1) Yang, D.; Zhou, Q.; Labroska, V.; Qin, S.; Darbalaei, S.; Wu, Y.; Yuliantie, E.; Xie, L.; Tao, H.; Cheng, J.; et al. G protein-coupled receptors: structure- and function-based drug discovery. *Signal Transduct Target Ther* **2021**, *6* (1), 7. DOI: 10.1038/s41392-020-00435-w From NLM Medline.

(2) Sriram, K.; Insel, P. A. G Protein-Coupled Receptors as Targets for Approved Drugs: How Many Targets and How Many Drugs? *Mol Pharmacol* **2018**, *93* (4), 251-258. DOI: 10.1124/mol.117.111062 From NLM Medline.

(3) Wu, Z.; Lin, D.; Li, Y. Pushing the frontiers: tools for monitoring neurotransmitters and neuromodulators. *Nat Rev Neurosci* **2022**, *23* (5), 257-274. DOI: 10.1038/s41583-022-00577-6 From NLM Medline.

(4) Jiang, H.; Galtes, D.; Wang, J.; Rockman, H. A. G protein-coupled receptor signaling: transducers and effectors. *Am J Physiol Cell Physiol* **2022**, *323* (3), C731-C748. DOI: 10.1152/ajpcell.00210.2022 From NLM Medline.

(5) Liu, S.; Anderson, P. J.; Rajagopal, S.; Lefkowitz, R. J.; Rockman, H. A. G Protein-Coupled Receptors: A Century of Research and Discovery. *Circ Res* **2024**, *135* (1), 174-197. DOI: 10.1161/CIRCRESAHA.124.323067 From NLM Medline.

(6) Gilman, A. G. G proteins and dual control of adenylate cyclase. *Cell* **1984**, *36* (3), 577-579. DOI: 10.1016/0092-8674(84)90336-2 From NLM Medline.

(7) Simon, M. I.; Strathmann, M. P.; Gautam, N. Diversity of G proteins in signal transduction. *Science* **1991**, *252* (5007), 802-808. DOI: 10.1126/science.1902986 From NLM Medline.

(8) Berridge, M. J. The Inositol Trisphosphate/Calcium Signaling Pathway in Health and Disease. *Physiol Rev* **2016**, *96* (4), 1261-1296. DOI: 10.1152/physrev.00006.2016 From NLM Medline.

(9) Chen, Z.; Singer, W. D.; Sternweis, P. C.; Sprang, S. R. Structure of the p115RhoGEF rgRGS domain-Galpha13/i1 chimera complex suggests convergent evolution of a GTPase

activator. *Nat Struct Mol Biol* **2005**, *12* (2), 191-197. DOI: 10.1038/nsmb888 From NLM Medline.

(10) Ford, C. E.; Skiba, N. P.; Bae, H.; Daaka, Y.; Reuveny, E.; Shekter, L. R.; Rosal, R.; Weng, G.; Yang, C. S.; Iyengar, R.; et al. Molecular basis for interactions of G protein betagamma subunits with effectors. *Science* **1998**, *280* (5367), 1271-1274. DOI: 10.1126/science.280.5367.1271 From NLM Medline.

(11) Benovic, J. L.; Strasser, R. H.; Caron, M. G.; Lefkowitz, R. J. Beta-adrenergic receptor kinase: identification of a novel protein kinase that phosphorylates the agonist-occupied form of the receptor. *Proc Natl Acad Sci U S A* **1986**, *83* (9), 2797-2801. DOI: 10.1073/pnas.83.9.2797 From NLM Medline.

(12) Lohse, M. J.; Benovic, J. L.; Codina, J.; Caron, M. G.; Lefkowitz, R. J. beta-Arrestin: a protein that regulates beta-adrenergic receptor function. *Science* **1990**, *248* (4962), 1547-1550. DOI: 10.1126/science.2163110 From NLM Medline.

(13) Zhang, M.; Chen, T.; Lu, X.; Lan, X.; Chen, Z.; Lu, S. G protein-coupled receptors (GPCRs): advances in structures, mechanisms, and drug discovery. *Signal Transduct Target Ther* **2024**, *9* (1), 88. DOI: 10.1038/s41392-024-01803-6 From NLM Medline.

(14) Hikino, K.; Kobayashi, S.; Ota, E.; Mushiroda, T.; Kobayashi, T. The Influence of Beta-2 Adrenergic Receptor Gene Polymorphisms on Albuterol Therapy for Patients With Asthma: Protocol for a Systematic Review and Meta-Analysis. *JMIR Res Protoc* **2019**, *8* (9), e14759. DOI: 10.2196/14759 From NLM PubMed-not-MEDLINE.

(15) Frishman, W. H. Cardiology patient page. Beta-adrenergic blockers. *Circulation* **2003**, *107* (18), e117-119. DOI: 10.1161/01.CIR.0000070983.15903.A2 From NLM Medline.

(16) Azam, S.; Haque, M. E.; Jakaria, M.; Jo, S. H.; Kim, I. S.; Choi, D. K. G-Protein-Coupled Receptors in CNS: A Potential Therapeutic Target for Intervention in Neurodegenerative Disorders and Associated Cognitive Deficits. *Cells* **2020**, *9* (2). DOI: 10.3390/cells9020506 From NLM Medline.

(17) Sudhof, T. C.; Malenka, R. C. Understanding synapses: past, present, and future. *Neuron* **2008**, *60* (3), 469-476. DOI: 10.1016/j.neuron.2008.10.011 From NLM Medline.

(18) Burrows, M. Neurotransmitters, neuromodulators and neurohormones. In *The Neurobiology of an Insect Brain*, Oxford University Press, 1996; pp 168-228.

(19) Fuller, R. W. Pharmacology of brain epinephrine neurons. *Annu Rev Pharmacol Toxicol* **1982**, *22*, 31-55. DOI: 10.1146/annurev.pa.22.040182.000335 From NLM Medline.

(20) O'Donnell, J.; Zeppenfeld, D.; McConnell, E.; Pena, S.; Nedergaard, M. Norepinephrine: a neuromodulator that boosts the function of multiple cell types to optimize CNS performance. *Neurochem Res* **2012**, *37* (11), 2496-2512. DOI: 10.1007/s11064-012-0818-x From NLM Medline.

(21) Holland, N.; Robbins, T. W.; Rowe, J. B. The role of noradrenaline in cognition and cognitive disorders. *Brain* **2021**, *144* (8), 2243-2256. DOI: 10.1093/brain/awab111 From NLM Medline.

(22) Wong, D. L.; Tai, T. C.; Wong-Faull, D. C.; Claycomb, R.; Meloni, E. G.; Myers, K. M.; Carlezon, W. A., Jr.; Kvetnansky, R. Epinephrine: a short- and long-term regulator of stress and development of illness : a potential new role for epinephrine in stress. *Cell Mol Neurobiol* **2012**, *32* (5), 737-748. DOI: 10.1007/s10571-011-9768-0 From NLM Medline.

(23) Kim, M. H.; Gorouhi, F.; Ramirez, S.; Granick, J. L.; Byrne, B. A.; Soulika, A. M.; Simon, S. I.; Isseroff, R. R. Catecholamine stress alters neutrophil trafficking and impairs wound healing by beta2-adrenergic receptor-mediated upregulation of IL-6. *J Invest Dermatol* **2014**, *134* (3), 809-817. DOI: 10.1038/jid.2013.415 From NLM Medline.

(24) Wood, S. K.; Valentino, R. J. The brain norepinephrine system, stress and cardiovascular vulnerability. *Neurosci Biobehav Rev* **2017**, *74* (Pt B), 393-400. DOI: 10.1016/j.neubiorev.2016.04.018 From NLM Medline.

(25) Chandley, M. J.; Ordway, G. A. Noradrenergic Dysfunction in Depression and Suicide. In *The Neurobiological Basis of Suicide*, Dwivedi, Y. Ed.; Frontiers in Neuroscience, 2012.

(26) Buck, K.; Voehringer, P.; Ferger, B. Rapid analysis of GABA and glutamate in microdialysis samples using high performance liquid chromatography and tandem mass spectrometry. *J Neurosci Methods* **2009**, *182* (1), 78-84. DOI: 10.1016/j.jneumeth.2009.05.018 From NLM Medline.

(27) Kao, C. Y.; Anderzhanova, E.; Asara, J. M.; Wotjak, C. T.; Turck, C. W. NextGen Brain Microdialysis: Applying Modern Metabolomics Technology to the Analysis of Extracellular Fluid in the Central Nervous System. *Mol Neuropsychiatry* **2015**, *1* (1), 60-67. DOI: 10.1159/000381855 From NLM PubMed-not-MEDLINE.

(28) Westerhout, J.; Ploeger, B.; Smeets, J.; Danhof, M.; de Lange, E. C. Physiologically based pharmacokinetic modeling to investigate regional brain distribution kinetics in rats. *AAPS J* **2012**, *14* (3), 543-553. DOI: 10.1208/s12248-012-9366-1 From NLM Medline.

(29) Flik, G.; Folgering, J. H.; Cremers, T. I.; Westerink, B. H.; Dremencov, E. Interaction Between Brain Histamine and Serotonin, Norepinephrine, and Dopamine Systems: In Vivo Microdialysis and Electrophysiology Study. *J Mol Neurosci* **2015**, *56* (2), 320-328. DOI: 10.1007/s12031-015-0536-3 From NLM Medline.

(30) Yoshitake, T.; Kehr, J.; Todoroki, K.; Nohta, H.; Yamaguchi, M. Derivatization chemistries for determination of serotonin, norepinephrine and dopamine in brain microdialysis samples by liquid chromatography with fluorescence detection. *Biomed Chromatogr* **2006**, *20* (3), 267-281. DOI: 10.1002/bmc.560 From NLM Medline.

(31) Folkesson, K. T.; Samuelsson, A.; Tesselaar, E.; Dahlstrom, B.; Sjoberg, F. A human vascular model based on microdialysis for the assessment of the vasoconstrictive dose-response effects of norepinephrine and vasopressin in skin. *Microcirculation* **2012**, *19* (4), 352-359. DOI: 10.1111/j.1549-8719.2012.00170.x From NLM Medline.

(32) Devoto, P.; Sagheddu, C.; Santoni, M.; Flore, G.; Saba, P.; Pistis, M.; Gessa, G. L. Noradrenergic Source of Dopamine Assessed by Microdialysis in the Medial Prefrontal Cortex. *Front Pharmacol* **2020**, *11*, 588160. DOI: 10.3389/fphar.2020.588160 From NLM PubMed-not-MEDLINE.

(33) Hascup, E. R.; af Bjerken, S.; Hascup, K. N.; Pomerleau, F.; Huettl, P.; Stromberg, I.; Gerhardt, G. A. Histological studies of the effects of chronic implantation of ceramic-based microelectrode arrays and microdialysis probes in rat prefrontal cortex. *Brain Res* **2009**, *1291*, 12-20. DOI: 10.1016/j.brainres.2009.06.084 From NLM Medline.

(34) Puthongkham, P.; Venton, B. J. Recent advances in fast-scan cyclic voltammetry. *Analyst* **2020**, *145* (4), 1087-1102. DOI: 10.1039/c9an01925a From NLM Medline.

(35) Vickrey, T. L.; Condron, B.; Venton, B. J. Detection of endogenous dopamine changes in Drosophila melanogaster using fast-scan cyclic voltammetry. *Anal Chem* **2009**, *81* (22), 9306-9313. DOI: 10.1021/ac901638z From NLM Medline.

(36) Nicolai, E. N.; Trevathan, J. K.; Ross, E. K.; Lujan, J. L.; Blaha, C. D.; Bennet, K. E.; Lee, K. H.; Ludwig, K. A. Detection of Norepinephrine in Whole Blood via Fast Scan Cyclic

Voltammetry. *IEEE Int Symp Med Meas Appl* **2017**, *2017*, 111-116. DOI: 10.1109/MeMeA.2017.7985859 From NLM PubMed-not-MEDLINE.

(37) Park, J.; Takmakov, P.; Wightman, R. M. In vivo comparison of norepinephrine and dopamine release in rat brain by simultaneous measurements with fast-scan cyclic voltammetry. *J Neurochem* **2011**, *119* (5), 932-944. DOI: 10.1111/j.1471-4159.2011.07494.x From NLM Medline.

(38) Samels, S. B., Yuksel, P., Espana, R.A. Monoamine Transporters in Drugs of Abuse : Insights from Fast Scan Cyclic Voltammetry. In *Monoamine Transporters, Advances in Neurobiology*, Mortensen, O. V. Ed.; Vol. 46; Springer, Cham, 2025.

(39) Ou, Y.; Buchanan, A. M.; Witt, C. E.; Hashemi, P. Frontiers in Electrochemical Sensors for Neurotransmitter Detection: Towards Measuring Neurotransmitters as Chemical Diagnostics for Brain Disorders. *Anal Methods* **2019**, *11* (21), 2738-2755. DOI: 10.1039/c9ay00055k From NLM PubMed-not-MEDLINE.

(40) Vilardaga, J. P.; Bunemann, M.; Krasel, C.; Castro, M.; Lohse, M. J. Measurement of the millisecond activation switch of G protein-coupled receptors in living cells. *Nat Biotechnol* **2003**, *21* (7), 807-812. DOI: 10.1038/nbt838 From NLM Medline.

(41) Nakanishi, J.; Takarada, T.; Yunoki, S.; Kikuchi, Y.; Maeda, M. FRET-based monitoring of conformational change of the beta2 adrenergic receptor in living cells. *Biochem Biophys Res Commun* **2006**, *343* (4), 1191-1196. DOI: 10.1016/j.bbrc.2006.03.064 From NLM Medline.

(42) Muller, A.; Joseph, V.; Slesinger, P. A.; Kleinfeld, D. Cell-based reporters reveal in vivo dynamics of dopamine and norepinephrine release in murine cortex. *Nat Methods* **2014**, *11* (12), 1245-1252. DOI: 10.1038/nmeth.3151 From NLM Medline.

(43) Nguyen, Q. T.; Schroeder, L. F.; Mank, M.; Muller, A.; Taylor, P.; Griesbeck, O.; Kleinfeld, D. An in vivo biosensor for neurotransmitter release and in situ receptor activity. *Nat Neurosci* **2010**, *13* (1), 127-132. DOI: 10.1038/nn.2469 From NLM Medline.

(44) Martin, J. R. In vivo brain imaging: fluorescence or bioluminescence, which to choose? *J Neurogenet* **2008**, *22* (3), 285-307. DOI: 10.1080/01677060802298517 From NLM Medline.

(45) Masuho, I.; Ostrovskaya, O.; Kramer, G. M.; Jones, C. D.; Xie, K.; Martemyanov, K. A. Distinct profiles of functional discrimination among G proteins determine the actions of G

protein-coupled receptors. *Sci Signal* **2015**, *8* (405), ra123. DOI: 10.1126/scisignal.aab4068 From NLM Medline.

(46) Hall, M. P.; Unch, J.; Binkowski, B. F.; Valley, M. P.; Butler, B. L.; Wood, M. G.; Otto, P.; Zimmerman, K.; Vidugiris, G.; Machleidt, T.; et al. Engineered luciferase reporter from a deep sea shrimp utilizing a novel imidazopyrazinone substrate. *ACS Chem Biol* **2012**, *7* (11), 1848-1857. DOI: 10.1021/cb3002478 From NLM Medline.

(47) Laschet, C.; Dupuis, N.; Hanson, J. A dynamic and screening-compatible nanoluciferase-based complementation assay enables profiling of individual GPCR-G protein interactions. *J Biol Chem* **2019**, *294* (11), 4079-4090. DOI: 10.1074/jbc.RA118.006231 From NLM Medline.

(48) Patriarchi, T.; Cho, J. R.; Merten, K.; Howe, M. W.; Marley, A.; Xiong, W. H.; Folk, R. W.; Broussard, G. J.; Liang, R.; Jang, M. J.; et al. Ultrafast neuronal imaging of dopamine dynamics with designed genetically encoded sensors. *Science* **2018**, *360* (6396). DOI: 10.1126/science.aat4422 From NLM Medline.

(49) Feng, J.; Zhang, C.; Lischinsky, J. E.; Jing, M.; Zhou, J.; Wang, H.; Zhang, Y.; Dong, A.; Wu, Z.; Wu, H.; et al. A Genetically Encoded Fluorescent Sensor for Rapid and Specific In Vivo Detection of Norepinephrine. *Neuron* **2019**, *102* (4), 745-761 e748. DOI: 10.1016/j.neuron.2019.02.037 From NLM Medline.

(50) Barnea, G.; Strapps, W.; Herrada, G.; Berman, Y.; Ong, J.; Kloss, B.; Axel, R.; Lee, K. J. The genetic design of signaling cascades to record receptor activation. *Proc Natl Acad Sci U S A* **2008**, *105* (1), 64-69. DOI: 10.1073/pnas.0710487105 From NLM Medline.

(51) Lee, D.; Creed, M.; Jung, K.; Stefanelli, T.; Wendler, D. J.; Oh, W. C.; Mignocchi, N. L.; Lüscher, C.; Kwon, H. B. Temporally precise labeling and control of neuromodulatory circuits in the mammalian brain. *Nature Methods* **2017**, *14* (5), 495-+. DOI: 10.1038/Nmeth.4234.

(52) Kim, M. W.; Wang, W.; Sanchez, M. I.; Coukos, R.; von Zastrow, M.; Ting, A. Y. Time-gated detection of protein-protein interactions with transcriptional readout. *Elife* **2017**, *6*. DOI: 10.7554/eLife.30233 From NLM Medline.

(53) (53) Zhou, G.; Wan, W. W.; Wang, W. Modular Peroxidase-Based Reporters for Detecting Protease Activity and Protein Interactions with Temporal Gating. *J Am Chem Soc* **2022**, *144* (50), 22933-22940. DOI: 10.1021/jacs.2c08280 From NLM Medline.

(54) Han, Y.; Branon, T. C.; Martell, J. D.; Boassa, D.; Shechner, D.; Ellisman, M. H.; Ting, A. Directed Evolution of Split APEX2 Peroxidase. *ACS Chem Biol* **2019**, *14* (4), 619-635. DOI: 10.1021/acschembio.8b00919 From NLM Medline.

(55) Kerppola, T. K. Bimolecular fluorescence complementation (BiFC) analysis as a probe of protein interactions in living cells. *Annu Rev Biophys* **2008**, *37*, 465-487. DOI: 10.1146/annurev.biophys.37.032807.125842 From NLM Medline.

(56) Cabantous, S.; Terwilliger, T. C.; Waldo, G. S. Protein tagging and detection with engineered self-assembling fragments of green fluorescent protein. *Nat Biotechnol* **2005**, *23* (1), 102-107. DOI: 10.1038/nbt1044 From NLM Medline.

(57) Feinberg, E. H.; Vanhoven, M. K.; Bendesky, A.; Wang, G.; Fetter, R. D.; Shen, K.; Bargmann, C. I. GFP Reconstitution Across Synaptic Partners (GRASP) defines cell contacts and synapses in living nervous systems. *Neuron* **2008**, *57* (3), 353-363. DOI: 10.1016/j.neuron.2007.11.030 From NLM Medline.

(58) Shao, S.; Zhang, H.; Zeng, Y.; Li, Y.; Sun, C.; Sun, Y. TagBiFC technique allows long-term single-molecule tracking of protein-protein interactions in living cells. *Commun Biol* **2021**, *4* (1), 378. DOI: 10.1038/s42003-021-01896-7 From NLM Medline.

(59) Huppertz, M. C.; Wilhelm, J.; Grenier, V.; Schneider, M. W.; Falt, T.; Porzberg, N.; Hausmann, D.; Hoffmann, D. C.; Hai, L.; Tarnawski, M.; et al. Recording physiological history of cells with chemical labeling. *Science* **2024**, *383* (6685), 890-897. DOI: 10.1126/science.adg0812 From NLM Medline.

(60) Kroning, K. E.; Li, M.; Shen, J.; Fiel, H.; Nassar, M.; Wang, W. A Modular Fluorescent Sensor Motif Used to Detect Opioids, Protein-Protein Interactions, and Protease Activity. *ACS Chem Biol* **2022**, *17* (8), 2212-2220. DOI: 10.1021/acschembio.2c00364 From NLM Medline.

(61) Sescil, J.; Fiel, H.; Havens, S. M.; Fu, E.; Li, X.; Kroning, K. E.; Solowiej, I.; Li, P.; Wang, W. Functionalization of a versatile fluorescent sensor for detecting protease activity and temporally gated opioid sensing. *RSC Chem Biol* **2025**, *6* (4), 555-562. DOI: 10.1039/d4cb00276h From NLM PubMed-not-MEDLINE.

(62) Kroning, K.; Gannot, N.; Li, X.; Putansu, A.; Zhou, G.; Sescil, J.; Shen, J.; Wilson, A.; Fiel, H.; Li, P.; et al. Single-chain fluorescent integrators for mapping G-protein-coupled

receptor agonists. *Proc Natl Acad Sci U S A* **2024**, *121* (18), e2307090121. DOI: 10.1073/pnas.2307090121 From NLM Medline.

(63) Havens, S. M.; Georgis, B.; Weng, J.; Rodriguez, J.; Rivett, H.; Alrawi, S.; Li, P.; Wang, W. SPLICEIT Fluorescent Sensor for Integrating Dopamine Release with Cellular Resolution. *Angew Chem Int Ed Engl* **2025**, *64* (33), e202511186. DOI: 10.1002/anie.202511186 From NLM Medline.

(64) Huang, W.; Manglik, A.; Venkatakrishnan, A. J.; Laeremans, T.; Feinberg, E. N.; Sanborn, A. L.; Kato, H. E.; Livingston, K. E.; Thorsen, T. S.; Kling, R. C.; et al. Structural insights into mu-opioid receptor activation. *Nature* **2015**, *524* (7565), 315-321. DOI: 10.1038/nature14886 From NLM Medline.

(65) Rasmussen, S. G.; Choi, H. J.; Fung, J. J.; Pardon, E.; Casarosa, P.; Chae, P. S.; Devree, B. T.; Rosenbaum, D. M.; Thian, F. S.; Kobilka, T. S.; et al. Structure of a nanobody-stabilized active state of the beta(2) adrenoceptor. *Nature* **2011**, *469* (7329), 175-180. DOI: 10.1038/nature09648 From NLM Medline.

(66) Mitchell, L. S.; Colwell, L. J. Comparative analysis of nanobody sequence and structure data. *Proteins* **2018**, *86* (7), 697-706. DOI: 10.1002/prot.25497 From NLM Medline.

(67) Baker, J. G. The selectivity of beta-adrenoceptor agonists at human beta1-, beta2- and beta3-adrenoceptors. *Br J Pharmacol* **2010**, *160* (5), 1048-1061. DOI: 10.1111/j.1476-5381.2010.00754.x From NLM Medline.

(68) Kruse, A. C.; Ring, A. M.; Manglik, A.; Hu, J.; Hu, K.; Eitel, K.; Hubner, H.; Pardon, E.; Valant, C.; Sexton, P. M.; et al. Activation and allosteric modulation of a muscarinic acetylcholine receptor. *Nature* **2013**, *504* (7478), 101-106. DOI: 10.1038/nature12735 From NLM Medline.

(69) Wan, Q.; Okashah, N.; Inoue, A.; Nehme, R.; Carpenter, B.; Tate, C. G.; Lambert, N. A. Mini G protein probes for active G protein-coupled receptors (GPCRs) in live cells. *J Biol Chem* **2018**, *293* (19), 7466-7473. DOI: 10.1074/jbc.RA118.001975 From NLM Medline.

(70) Carpenter, B.; Tate, C. G. Engineering a minimal G protein to facilitate crystallisation of G protein-coupled receptors in their active conformation. *Protein Eng Des Sel* **2016**, *29* (12), 583-594. DOI: 10.1093/protein/gzw049 From NLM Medline.

(71) Ring, A. M.; Manglik, A.; Kruse, A. C.; Enos, M. D.; Weis, W. I.; Garcia, K. C.; Kobilka, B. K. Adrenaline-activated structure of beta2-adrenoceptor stabilized by an

engineered nanobody. *Nature* **2013**, *502* (7472), 575-579. DOI: 10.1038/nature12572 From NLM Medline.

(72) Masureel, M.; Zou, Y.; Picard, L. P.; van der Westhuizen, E.; Mahoney, J. P.; Rodrigues, J.; Mildorf, T. J.; Dror, R. O.; Shaw, D. E.; Bouvier, M.; et al. Structural insights into binding specificity, efficacy and bias of a beta(2)AR partial agonist. *Nat Chem Biol* **2018**, *14* (11), 1059-1066. DOI: 10.1038/s41589-018-0145-x From NLM Medline.

(73) Guo, Q.; He, B.; Zhong, Y.; Jiao, H.; Ren, Y.; Wang, Q.; Ge, Q.; Gao, Y.; Liu, X.; Du, Y.; et al. A method for structure determination of GPCRs in various states. *Nat Chem Biol* **2024**, *20* (1), 74-82. DOI: 10.1038/s41589-023-01389-0 From NLM Medline.

(74) Xu, X.; Kaindl, J.; Clark, M. J.; Hubner, H.; Hirata, K.; Sunahara, R. K.; Gmeiner, P.; Kobilka, B. K.; Liu, X. Binding pathway determines norepinephrine selectivity for the human beta(1)AR over beta(2)AR. *Cell Res* **2021**, *31* (5), 569-579. DOI: 10.1038/s41422-020-00424-2 From NLM Medline.

(75) Suno, R.; Lee, S.; Maeda, S.; Yasuda, S.; Yamashita, K.; Hirata, K.; Horita, S.; Tawaramoto, M. S.; Tsujimoto, H.; Murata, T.; et al. Structural insights into the subtype-selective antagonist binding to the M(2) muscarinic receptor. *Nat Chem Biol* **2018**, *14* (12), 1150-1158. DOI: 10.1038/s41589-018-0152-y From NLM Medline.

(76) Abramson, J.; Adler, J.; Dunger, J.; Evans, R.; Green, T.; Pritzel, A.; Ronneberger, O.; Willmore, L.; Ballard, A. J.; Bambrick, J.; et al. Accurate structure prediction of biomolecular interactions with AlphaFold 3. *Nature* **2024**, *630* (8016), 493-500. DOI: 10.1038/s41586-024-07487-w From NLM Medline.

(77) Moretti, R.; Bender, B. J.; Allison, B.; Meiler, J. Rosetta and the Design of Ligand Binding Sites. *Methods Mol Biol* **2016**, *1414*, 47-62. DOI: 10.1007/978-1-4939-3569-7_4 From NLM Medline.

(78) Lambert, T. J. FPbase: a community-editable fluorescent protein database. *Nat Methods* **2019**, *16* (4), 277-278. DOI: 10.1038/s41592-019-0352-8 From NLM Medline.

(79) Akerboom, J.; Rivera, J. D.; Guilbe, M. M.; Malave, E. C.; Hernandez, H. H.; Tian, L.; Hires, S. A.; Marvin, J. S.; Looger, L. L.; Schreiter, E. R. Crystal structures of the GCaMP calcium sensor reveal the mechanism of fluorescence signal change and aid rational design. *J Biol Chem* **2009**, *284* (10), 6455-6464. DOI: 10.1074/jbc.M807657200 From NLM Medline.

(80) Wang, Q.; Shui, B.; Kotlikoff, M. I.; Sondermann, H. Structural basis for calcium sensing by GCaMP2. *Structure* **2008**, *16* (12), 1817-1827. DOI: 10.1016/j.str.2008.10.008 From NLM Medline.

(81) Myskova, J.; Rybakova, O.; Brynda, J.; Khoroshyy, P.; Bondar, A.; Lazar, J. Directionality of light absorption and emission in representative fluorescent proteins. *Proc Natl Acad Sci U S A* **2020**, *117* (51), 32395-32401. DOI: 10.1073/pnas.2017379117 From NLM Medline.

(82) Nehme, R.; Carpenter, B.; Singhal, A.; Strege, A.; Edwards, P. C.; White, C. F.; Du, H.; Grisshammer, R.; Tate, C. G. Mini-G proteins: Novel tools for studying GPCRs in their active conformation. *PLoS One* **2017**, *12* (4), e0175642. DOI: 10.1371/journal.pone.0175642 From NLM Medline.